Title
Modeling and Stochastic Analysis of Contaminant Transport in Soils and Aquifers

Authors
Hantush, Mohamed M
Marino, Miguel A
Shumway, Robert H

Publication Date
1996-08-30

Iodeling and Stochastic Analysis of Contaminant Transport in Soils and Aquifers

By

Mohamed M. Hantush
Department of Land, Air and Water Resources

Miguel A. Mariño, Professor
Department of Land, Air and Water Resources
Department of Civil and Environmental Engineering

Robert H. Shumway, Professor
Division of Statistics

University of California, Davis
Davis, CA 95616

TECHNICAL COMPLETION REPORT

Project Number UCAL-WRC-W-832

August 30, 1996

University of California Water Resources Center

The research leading to this report was supported by the University of California Water Resources Center, as part of Water Resources Center Project UCAL-WRC-W-832

TABLE OF CONTENTS

LIST OF TABLES

LIST OF FIGURES

ABSTRACT

The effort that led to this report is twofold. First, it deals with the development of fundamental transport equations and their solutions; they describe the effect of low-permeability zones on the motion and spread of contaminant plumes in high-permeability porous layers. Second, it concerns the development of an analytical multiphase-transport model that describes leaching of pesticides in soils and their fate and transport in groundwater. Using Monte Carlo simulations, the effect of stochastic precipitation, random adsorption, and random (bio)chemical reaction, on the probability distributions of the herbicide Simazine, is investigated under conditions typical to the City of Fresno in California.

The transport equations that are developed in Chapter 2 describe the capacitance of low-permeability layers to store and release reactive constituents by diffusion and mechanical mixing. It is shown that under quasi-steady conditions and a mean flow parallel to the bedding, lateral solute transfer between thin layers is governed by the phenomenological first-order rate model, with a uniquely defined mass transfer rate coefficient, modified to account for reactive constituents. Two-dimensional analytical solutions are obtained in Chapter 3 for the first-order rate model in an infinite porous medium, using the methods of Fourier and Laplace transforms, and superposition. The solutions consider a rectangular area at the source with (1) an instantaneous release of a contaminant mass, and (2) an exponentially-decaying source concentration, applied at a fixed rate. Comparison of the theory with tracer chloride levels at the Borden aquifer indicates that the first-order rate model can describe adequately the dispersion process, on the basis of lateral or transverse diffusive mass transfer between layers.

In the second effort (Chapter 4), a multiphase transport model is developed with the objective of investigating the impact of soil environment, physical and (bio)chemical processes, especially, volatilization, crop uptake, and agricultural practices on long-term vulnerability of groundwater to contamination by pesticides. The soil is separated into root and intermediate vadose zones, each with uniform properties. Transport in each soil zone is modeled on the basis of complete mixing, by spatial averaging the related point multiphase-transport partial differential equation (i.e., linear-reservoir models). Transport in the aquifer, however, is modeled by a two-dimensional advection-dispersion transport equation, considering adsorption and first-order decay rate. Vaporization in the soil is accounted for by assuming liquid-vapor phase partitioning using Henry's law, and vapor flux (volatilization) from the soil surface is modeled by diffusion through an air boundary layer. Sorption of liquid-phase solutes by crops is described by a linear relationship that is valid for first-order (passive) crop uptake. The model is applied to five pesticides (Atrazine, Bromacil, Chlordane, Heptachlor, and Lindane), and the potential for pesticides contamination of groundwater is investigated for sandy and clayey soils. Simulation results show that groundwater contamination can be substantially reduced for clayey soil environments, where bio(chemical) degradation and volatilization are most efficient as natural loss pathways for the pesticides. Also, uptake by crops can be a significant mechanism for attenuating exposure levels in groundwater, especially in a sandy soil environment, and for relatively persisting pesticides. Further, simulations indicate that changing agricultural practices can have a profound effect on vulnerability of groundwater to mobile and relatively persisting pesticides.

The deterministic model is integrated with the Monte Carlo method in Chapter 5, to obtain the probability density function, mean, and standard deviation of the concentrations in groundwater, due to random adsorption and stochastic precipitation. The distribution coefficient, which is used to calculate the retardation factor for equilibrium adsorption, is assumed to be normally distributed, and the precipitation is modeled by fitting an ARIMA model to an observed time series. Consequently, the results of the analysis are also probability distribution functions for the concentration of the contaminant, which are useful representations for regulation and management purposes. The stochastic model is applied to data typical to the Fresno area in California, to assess the impact of herbicide Simazine on groundwater quality. The results show that predicted concentrations exhibit non-Gaussian probability distributions and standard deviations of the order of magnitude of the estimated means. Further, predictions made on the basis of averaged values of input parameters may substantially overestimate in transient, and later underestimate, the actual mean (ensemble) of the contaminant levels in groundwater. The results also highlight the importance of accounting for the mechanism of preferential flow.

Keywords: Aquifers; Agriculture; Contaminant transport; Ground water and ground water hydrology; Hydrogeology; Hydrology and hydrologic models; Mathematical models; Migration; Environmental contamination; Ground water modeling; Ground water quality; Stochastic hydrology, processes, and models; Solute transport and exchanges; Water pollution, non-point source; Water quality modeling; Herbicides; Pesticides and applications; Soil pollution; Time-series analysis; Rain and rainfall; Precipitation; Roots; Biodegradation; Chemical movement through soil; Decays; Evapotranspiration; Fractured rock hydrology; Leaching; Weather prediction.

CHAPTER 1

INTRODUCTION

1.1 Problem

Agricultural activities in California constitute a major environmental concern to the public, due to vulnerability of groundwater to toxic substances applied on farmlands. Chemicals, such as pesticides, leach through soils by the forces of infiltrating water (precipitation and return flow) and threaten to contaminate shallow water tables and pollute nearby drinking-water wells. Mobility and persistence of pesticides in soils are influenced by physical and (bio)chemical processes such as degradation, volatilization, adsorption, and crop-root uptake. These processes interact in a complex fashion and describe mobility and persistence of pesticides in soils and their potential to contaminate groundwater. Uncertainty associated with precipitation and spatial variability of the (bio)chemical parameters may limit the use of deterministic models for predicting exposure levels of chemicals in soils and groundwater. Hence, an alternative methodology is needed in order to account for the effect of uncertainty on reliability of prediction models.

The geohydrology of a subsurface environment (e.g., heterogeneity) plays a significant role in controlling the fate of chemicals and their exposure levels in groundwater. In specific, dispersion in layered aquifers can be enhanced by the existence of zones of stagnant water or layers of low hydraulic conductivity. Diffusive mass transfer of solute, between layers of contrasting permeability, results in a portion of a migrating contaminant's plume being retained, hence, delayed in pockets and layers of stagnant water. The net effect being the attenuation of concentrations and extensive tailing of concentrations profiles in the high-permeability layers.

Understanding of the physical processes in the underlying groundwater system is an important step toward conducting risk assessment against pollutant exposure levels in groundwater.

1.2 Objectives

The major theme of the study is to investigate the interaction among the physical processes, (bio)chemical processes, and heterogeneity, and their integrated effect on transport of contaminants in soils and groundwater. The specific objectives of the research are: (1) to investigate the effect of low-permeability porous layers on the dispersion of migrating contaminant plumes, at the local scale and the formation scale; (2) to predict long-term impacts of agricultural activities on exposure levels of pesticides in groundwater, in environments and climatic conditions typical to the Sacramento and San Joaquin Valleys in California; and (3) to investigate the effect of random physical and chemical processes on the predictions of contaminants concentrations in the subsurface environment, and to develop the probability density of the exposure levels of pesticides in soils and groundwater, with the aim of determining the risks in exceeding their hazardous levels.

1.3 Present Work

This effort deals with: (1) the development, based on physical principles, of an aquifer-scale transport model that describes, on average, the capacitance of low-permeability layers to store and release solute mass; (2) the development of a transport model that accounts for different physical and (bio)chemical processes in the root zone, intermediate-vadose zone, and aquifer; (3) the development of a stochastic model capable of characterizing the probability of solute

concentrations in groundwater, due to random precipitation and (bio)chemical processes; and (4) the verification and application of the theory to real data.

CHAPTER 2

CONTAMINANT TRANSPORT IN A LAYERED FORMATION

2.1 Abstract

This chapter deals with the development of two-dimensional reactive-solute transport equations in a two-layer system. The transport equations describe the capacitance of low-permeability layers to store and release reactive constituents by diffusive and transverse-dispersive mixing mechanisms. Vertical averaging of the governing point three-dimensional equations, over the layers' thicknesses, introduces a coupling mass flux term that describes solute exchange between mobile and immobile water phases. It is shown that under quasi-steady conditions, for thin layers, and a mean flow parallel to the bedding, the interlayer solute exchange process is governed by the phenomenological first-order rate model, modified to account for reactive constituents and with a uniquely defined mass transfer coefficient α. The derived coefficient of mass transfer α takes into account the effect of a convective mixing mechanism, attributed to transverse-vertical dispersion, as well as the effect of the conventional diffusive transfer mechanism. For a small capacity ratio parameter $\beta < 1$, the coefficient α shows a linear dependence on the flow velocity, and a linearized expression is obtained which shows that such relationship is governed by the magnitude of the transverse-vertical dispersivity of the high-permeability layer. Application of the theory is demonstrated by three examples using previously developed solutions and published experimental data, and the results are discussed. An asymptotic effective mass transfer coefficient α_{eff} is obtained for a stratified formation and is shown to be equal to the arithmetic mean of α defined for an invidual two-layer system. The

effective coefficient of mass transfer and the effective longitudinal dispersivity are estimated for a hypothetical stratified formation.

2.2 Introduction

Dispersion is a scale-dependent process that causes spreading of contaminant plumes and the ever decreasing peak concentrations. It is largely attributed to scale-dependent pore-water velocity variations in a heterogeneous porous medium, which displays spatial variability of its hydraulic properties. At the local scale, dispersion is caused by effective molecular diffusion and velocity variations due to the statistical distribution of flow path and pore size (*Saffman*, 1960). At a larger scale, which spans numerous layers of a stratified formation, macrodispersion is realized and is dominated by velocity variations across the strata (*Bear*, 1977; *Gelhar et al.*, 1979; *Matheron and DeMarsily*, 1980; *Güven et al.*, 1984; *Gupta and Bhattacharya*, 1986; *and Neuman et al.*, 1987). Regardless of the adopted framework, stochastic averaging (e.g., *Gelhar et al.*, 1979; and *Neuman et al.*, 1987) or deterministic averaging (*Bear*, 1977; and *Güven et al.*, 1984), the developed models were successful in capturing the asymptotic behavior of a contaminant plume, i.e., after a large displacement. In general, those models fail to capture the non-Fickian behavior during the early development of the plumes. The early non-Fickian behavior may be attributed either to the initial plume being overwhelmed by the much greater scale of heterogeneity (e.g., *Gelhar et al.*, 1979), or to rate-limited diffusive sorption into zones of stagnant water and the subsequent desorption process (*Gillham et al.*, 1984; *Tang and Aral*, 1992; *Piquemal*, 1993; and *Haggerty and Gorelick*, 1995). The concept of diffusive sorption (matrix diffusion in fractured rocks) of solutes between zones of mobile and immobile water is

not new, especially its application to transport in aggregated soils, unsaturated soils, and fractured rocks (*Coats and Smith*, 1964; *Passioura,* 1971; *Skopp and Warrick,* 1974; *Van Genuchten and Wierenga,* 1976; *Rao et al.*, 1980a; *Rasmuson and Neretnieks*, 1980; *Grisak and Pickens*, 1980; *Tang et al.*, 1981; *Valocchi*, 1985; *Goltz and Roberts*, 1986; and *Bond and Wierenga*, 1990). Slow diffusive transfer continuously removes mass from high-permeability layers (mobile phase) to low-permeability layers (immobile phase) and causes a significant decrease in peak concentration and extensive tailing (asymmetric breakthrough profiles), due to reversed mass transfer from the immobile to the mobile phase. The implication of the concept of rate-limited mass transfer between mobile and immobile zones to aquifer remediation or cleanup, has been considered by *Goltz and Oxley* (1991), *Harvey et al.* (1994), and *Haggerty and Gorelick* (1995).

In this chapter, we develop, from pore-scale three-dimensional transport equations, two-dimensional transport equations of a reactive constituent that relate vertically-averaged concentrations in a two-layer system composed of a high-permeability layer (e.g., sand) and a low-permeability layer (e.g., sand and silt). The development shows that, on average, the capacitance of low-permeability layers to store and release solute mass can be described by the phenomenological first-order rate model, however, under slow groundwater flow and after some displacement. The results indicate that in addition to diffusive transfer, a convective mixing mechanism can play a role in the mass transfer process. The latter is attributed to mechanical mixing or a transverse-vertical dispersive flux across the interface between the low- and high permeability layers. Because dispersion is produced by the statistical distribution of pore-water velocities, in magnitude and direction, this may partially explain the observed dependence of the

mass transfer coefficient on relatively large pore-water velocity in laboratory experiments (*Bennet and Goodridge*, 1970; *Coats and Smith*, 1964; *Baker*, 1977; *Van Genuchten and Wierenga*, 1977; *Rao et al.*, 1980b; and *De Smedt and Wierenga*, 1984). In the analysis, we also consider a partitioning relationship between the concentrations at the interface between the low- and high-permeability layers, which may account for unmodeled (bio)chemical processes there. Based on that, the derived expression for the mass transfer coefficient is shown to be dependent on the partitioning, too. The analysis presented here is valid for thin layers (i.e., lateral dimensions greater than the thickness) and slow groundwater flow. *Coats and Smith* (1964) indicated that first-order rate models fail at large velocities, and that diffusive-like transfer remains the mechanism in question, however, it obeys a transfer law other than the linear form. A more rigorous approach is needed in order to account for large velocities.

2.3 Theory

2.3.1 Development of Transport Equations

In this section, we develop coupled two-dimensional transport equations that can be applied to a layered formation made up of conductive and impervious layers similar to the ones conceptualized in Figure 2.1. It is assumed that convective transport is parallel to the bedding, under steady flow, and that the exchange mechanism of contaminant mass between the layers of contrasting conductivity (e.g. sand and clay) is dominated by a diffusive transfer. Also, we assume that longitudinal and lateral extent of the individual layers are much greater than their thicknesses. Figure 2.1 shows two adjacent and relatively thin conductive and impervious layers from the conceptualized strata in Figure 2.1. Starting with a point three-dimensional advection-

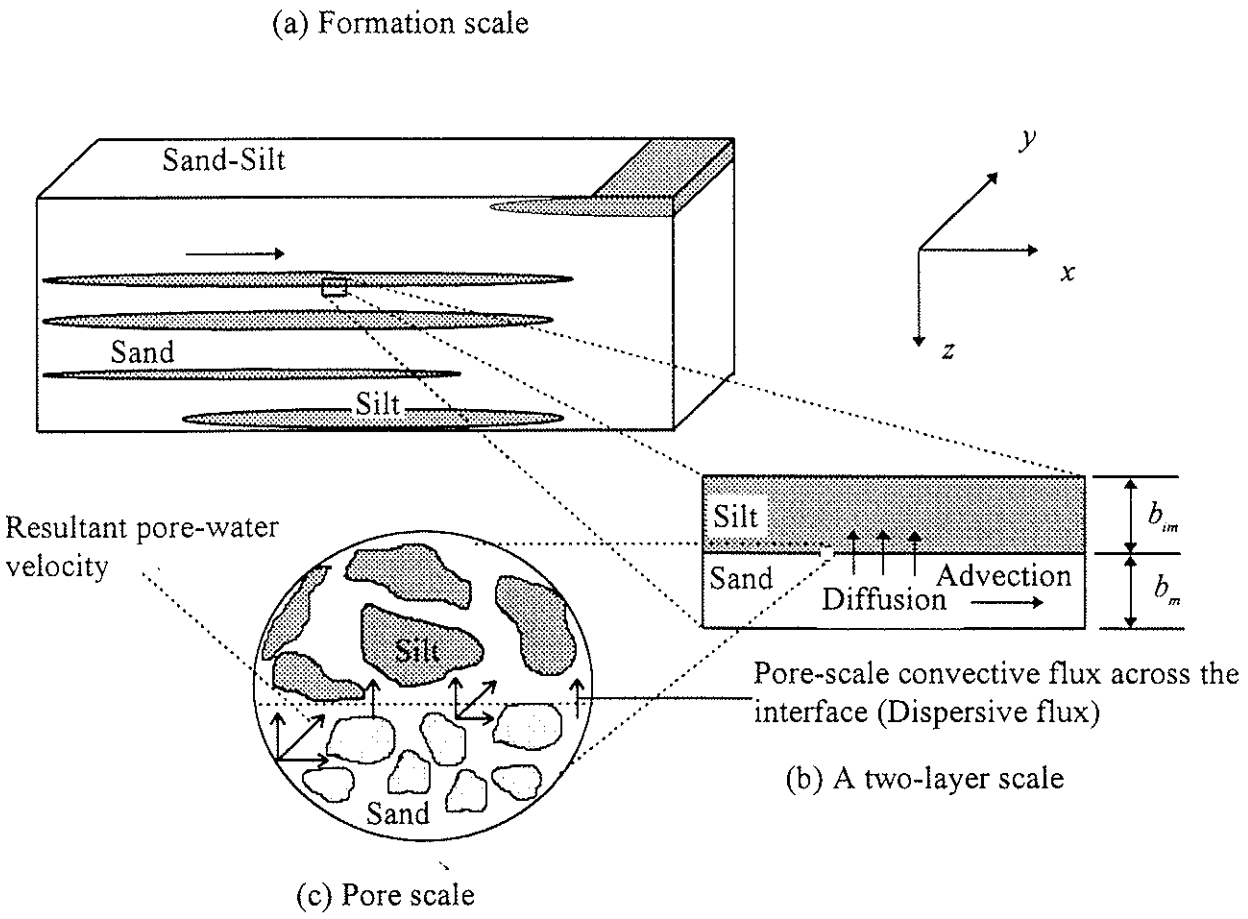

Figure 2.1 Schematic representation of: (a) a layered porous formation; (b) a two-layer system; and (c) pore-scale dispersive flux of a convective nature across the interface between high- and low-permeability layers.

dispersion equation in the permeable layer and a three-dimensional diffusion equation in the impervious layer, we develop a two-dimensional transport system in which the point concentration is averaged vertically over each layer (i.e., along the z direction in Figure 2.1). The governing transport equations in the impervious layer can be written as

$$\theta_{im} \frac{\partial C_{im}}{\partial t} = \nabla \cdot \left(\theta_{im} \mathbf{D}_{im} \cdot \nabla C_{im}\right) - \theta_{im} k C_{im} \tag{2.1}$$

in which C_{im} is the point concentration in an impervious layer [M/L^3]; θ_{im} is the porosity of the impervious layer; $\mathbf{D}_{im}$ is three-dimensional and symmetric diffusion tensor [L^2/T]; and k is the (bio)chemical-decay rate constant [T^{-1}]. In the permeable layer,

$$\theta_{m} \frac{\partial C_{m}}{\partial t} = \nabla \cdot \left(\theta_{m} \mathbf{D}_{m} \cdot \nabla C_{m}\right) - \nabla \cdot \mathbf{U} C_{m} - \theta_{m} k C_{m} \tag{2.2}$$

in which C_m is the point concentration in a the permeable layer [M/L^3]; θ_m is the porosity of the high-permeability layer; $\mathbf{D}_m$ is three-dimensional dispersion tensor, assumed isotropic; $\mathbf{U}$ is the specific discharge vector; and k_{im} is the (bio)chemical-decay rate constant [T^{-1}]. Assuming a zero mass flux at the exterior boundaries of the layered system, and accounting for the continuity of mass flux across the interface between the two layers (Figure 2.1), we introduce the following interfacial boundary conditions:

$$\theta_m D_z \frac{\partial C_m}{\partial z} = 0 \qquad z = b_{im} + b_m \tag{2.3a}$$

$$\theta_m D_z \frac{\partial C_m}{\partial z} = \theta_{im} D^* \frac{\partial C_{im}}{\partial z} \qquad z = b_{im} \tag{2.3b}$$

$$C_m = k^* C_{im} \qquad z = b_{im} \tag{2.3c}$$

$$\theta_{im} D^* \frac{\partial C_{im}}{\partial z} = 0 \qquad z = 0 \qquad (2.3d)$$

in which D_z and D^* are transverse vertical dispersion and effective molecular diffusion parameters, respectively [L^2/T]; b_{im} and b_m are some average characteristic thickness of the impermeable and conductive layers, respectively [L]; and k^* is a partition coefficient.

Boundary condition (2.3c) allows for a jump in solute concentration across the interfacial boundary so that unmodeled (bio)chemical processes that are prevailing at the pore scale can be accounted for in a lumped fashion. *Jury and Utermann* (1992) argued that averaged resident concentration is not necessarily continuous across the interface between two layers, unless the local concentration or porosity (moisture content in unsaturated flow) is constant there.

For a steady and unidirectional (horizontal) flow, we have $\nabla \cdot \mathbf{U} = 0$, in which $\mathbf{U} = u(x,z)$ **i**. Hence,

$$\frac{\partial}{\partial x}\left(b_m \bar{u}\right) = 0 \qquad (2.4)$$

in which $\bar{u}$ is $u(x,z)$ averaged in the z direction. We start by defining the following averaging relationships:

$$\overline{\overline{\psi}}_{im}(x,y,t) = \frac{1}{b_{im}} \int_{z=0}^{z=b_{im}} \psi(\mathbf{x},t)\, dz \qquad (2.5)$$

in the impermeable layer, and

$$\overline{\overline{\psi}}_{m}(x,y,t) = \frac{1}{b_m} \int_{z=b_{im}}^{z=b_{im}+b_m} \psi(\mathbf{x},t)\, dz \qquad (2.6)$$

in the conductive layer. Applying the averaging operator (2.6) to (2.2), we obtain

$$\overline{\theta_m \frac{\partial C_m}{\partial t}} = \overline{\nabla \cdot \left(\theta_m \mathbf{D}_m \cdot \nabla C_m\right)} - \overline{u(x,z) \frac{\partial C_m}{\partial x}} - \overline{k \theta_m C_m} \qquad (2.7)$$

The average of the left-hand-side term is given by

$$\overline{\theta_m \frac{\partial C_m}{\partial t}} = \theta_m \frac{\partial \overline{C_m}}{\partial t} \tag{2.8}$$

in which it is assumed that the porosity is locally constant and that the limits of integration in (2.6) are time-invariant. For locally-constant b_m and b_{im},, the average of the dispersive mass flux term on the left-hand side of (2.7) is given by

$$\overline{\nabla \cdot (\theta_m \mathbf{D}_m \cdot \nabla C_m)} = \frac{1}{b_m} \int_{b_{im}}^{b_{im}+b_m} \nabla \cdot (\theta_m \mathbf{D}_m \cdot \nabla C_m) dz$$

$$= \frac{1}{b_m} \nabla' \cdot \int_{b_{im}}^{b_{im}+b_m} (\theta_m \mathbf{D}'_m \cdot \nabla' C_m) dz - \frac{1}{b_m} \theta_m D_z \frac{\partial C_m}{\partial z}\bigg|_{z=b_{im}} \tag{2.9}$$

in which the primed notation denotes a two-dimensional vector (dependence on z is eliminated by the integration along the z axis) and a two-dimensional gradient operator, i.e., $\nabla' = \partial/\partial x\ \mathbf{i} + \partial/\partial y\ \mathbf{j}$. The second term on the right-hand side of (2.9) represents the z-components of the solute mass flux evaluated at the interfacial boundary. Equation (2.9) can be simplified further to yield

$$\overline{\nabla \cdot (\theta_m \mathbf{D}_m \cdot \nabla C_m)} = \nabla' \cdot (\theta_m \mathbf{D}'_m \cdot \nabla' \overline{C_m}) - \frac{1}{b_m} \theta_m D_z \frac{\partial C_m}{\partial z}\bigg|_{z=b_{im}} \tag{2.10}$$

The convective term in (2.7) can be evaluated as

$$\overline{u(x,z) \frac{\partial C_m}{\partial x}} = \overline{(\bar{u} + \tilde{u}) \frac{\partial}{\partial x} (\overline{C_m} + \tilde{c}_m)} = \bar{u} \frac{\partial \overline{C_m}}{\partial x} + \overline{\tilde{u} \frac{\partial \tilde{c}_2}{\partial x}} \tag{2.11}$$

where we used the following perturbations

$$C_m(x,y,z,t) = \overline{C_m}(x,y,t) + \tilde{c}_m(x,y,z,t) \quad , \qquad \overline{\tilde{c}_m} = 0 \tag{2.12a}$$

$$u(z) = \bar{u} + \tilde{u}(z) \quad , \qquad \overline{\tilde{u}} = 0 \tag{2.12b}$$

The closure conditions appearing on the right-hand sides of (2.12a) and (2.12b) follow immediately after applying the average operator (2.6) to the left- and right-hand sides of these equations. In (2.11) we used the fact that the average of the product of an average and a perturbation is zero. If the region that is accessible to subsurface flow displays spatial variability of hydraulic conductivity in the z direction, e.g., layered formations, then the average of the perturbed convective term in (2.11) gives rise to the phenomenon of macrodispersion which has been addressed extensively using deterministic and stochastic frameworks. Macrodispersion is mainly the product of subsurface velocity variations attributed to the spatial variability of hydraulic conductivity (*Bear, 1977; Matheron and De Marsily, 1980; Dagan, 1984; Gelhar and Axness, 1983; and Neuman et al., 1987*)

$$\overline{\tilde{u}\,\frac{\partial \tilde{c}_m}{\partial x}} = -D_{x,eff}\,\frac{\partial \overline{C}_m}{\partial x} \tag{2.13}$$

in which $D_{x,eff}$ is the effective longitudinal dispersion parameter that takes into account the spatial variability of the hydraulic conductivity. Because (2.13) represents a Fickian behavior, it is additive to the contribution of local dispersion that is produced by velocity variations at the pore scale. Since the scope of our work is diffusive transfer at the scale of individual layers with slightly variable hydraulic conductivity along the z-direction, we therefore drop the second term on the right-hand side of (2.11). The substitution of (2.8), (2.10), (2.11), and (2.12a) into (2.7) yields

$$b_m \theta_m \frac{\partial \overline{C}_m}{\partial t} = b_m \nabla' \cdot \left(\theta_m \mathbf{D}'_m \cdot \nabla' \overline{C}_m\right) - b_m \overline{u}\,\frac{\partial \overline{C}_m}{\partial x} - k\theta_m b_m \overline{C}_m - \theta_m D_z \frac{\partial \tilde{c}_m}{\partial z}\Big|_{z=b_m} \tag{2.14}$$

Note that the diffusive flux of the perturbation $\tilde{c}_m$ across (normal to) the interfacial boundary acts as a distributed source/sink which influences the longitudinal and transverse-lateral distributions

$$b_{im}\theta_{im}\frac{\partial \overline{C_{im}}}{\partial t} = b_{im}\nabla'\cdot\left(\theta_{im}\mathbf{D}'_{im}\cdot\nabla'\overline{C_{im}}\right) - k\theta_{im}b_{im}\overline{C_{im}} + \theta_{im}D\cdot\frac{\partial \tilde{c}_{im}}{\partial z}\bigg|_{z=b_{im}} \tag{2.15}$$

in which the point concentration is expressed as

$$C_{im}(x,y,z,t) = \overline{C_{im}}(x,y,t) + \tilde{c}_{im}(x,y,z,t) \quad , \qquad \overline{\tilde{c}_i} = 0 \tag{2.16}$$

The diffusive flux term which is evaluated at the interface (i.e., $z = b_{im}$) couples (2.15) with (2.14) through the continuity relation (2.3b); it accounts for diffusive-type solutes mass exchange between the two layers. In the next section, we develop coupled equations and obtain approximate solutions for the perturbation fields, $\tilde{c}_1$ and $\tilde{c}_2$.

2.3.2 Closure Problem

The substitution of (2.12a) into (2.2) yields

$$\begin{aligned}\theta_m\frac{\partial \overline{C_m}}{\partial t} + \theta_m\frac{\partial \tilde{c}_m}{\partial t} = {} & \nabla'\cdot\left(\theta_m\mathbf{D}'_m\cdot\nabla'\overline{C_m}\right) + \nabla\cdot\left(\theta_m\mathbf{D}_m\cdot\nabla\tilde{c}_m\right) \\ & - u\frac{\partial \overline{C_m}}{\partial x} - u\frac{\partial \tilde{c}_m}{\partial x} - \theta_m k\overline{C_m} - \theta_m k\tilde{c}_m\end{aligned} \tag{2.17}$$

in which, as mentioned earlier, the variation of u is assumed negligible along the thickness of the conductive layer and, thus, we dropped the over-bar notation. The subtraction of (2.14) from (2.17) multiplied by b_m yields

$$b_m\theta_m\frac{\partial \tilde{c}_m}{\partial t} = b_m\nabla\cdot\left(\theta_m\mathbf{D}_m\cdot\nabla\tilde{c}_m\right) - b_m u\frac{\partial \tilde{c}_m}{\partial x} - b_m\theta_m k\tilde{c}_m + \theta_m D_z\frac{\partial \tilde{c}_m}{\partial z}\bigg|_{z=b_{im}} \tag{2.18a}$$

Similarly, the substitution of (2.16) into (2.1) after multiplying by b_{im} and subtracting (2.15) from the resulting equation yields a partial differential equation for $\tilde{c}_{im}$,

$$b_{im}\theta_{im}\frac{\partial \tilde{c}_{im}}{\partial t} = b_{im}\nabla\cdot\left(\theta_{im}\,\mathbf{D}_{im}\cdot\nabla\tilde{c}_{im}\right) - b_{im}\theta_{im}k\,\tilde{c}_{im} - \theta_{im}D^{*}\frac{\partial \tilde{c}_{im}}{\partial z}\bigg|_{z=b_{im}} \tag{2.18b}$$

Now, if we define the new variables $\tilde{c}_{m}' = e^{kt}\tilde{c}_{m}$ and $\tilde{c}_{im}' = e^{kt}\tilde{c}_{im}$, then in terms of $\tilde{c}_{m}'$ and $\tilde{c}_{im}'$, (2.18a) and (2.18b) can be transformed to the following partial differential equations:

$$b_{m}\theta_{m}\frac{\partial \tilde{c}_{m}'}{\partial t} = b_{m}\nabla\cdot\left(\theta_{m}\,\mathbf{D}_{m}\cdot\nabla\tilde{c}_{m}'\right) - b_{m}\,u\frac{\partial \tilde{c}_{m}'}{\partial x} + \theta_{m}D_{z}\frac{\partial \tilde{c}_{m}'}{\partial z}\bigg|_{z=b_{m}} \tag{2.19a}$$

$$b_{im}\theta_{im}\frac{\partial \tilde{c}_{im}'}{\partial t} = b_{im}\nabla\cdot\left(\theta_{im}\,\mathbf{D}_{im}\cdot\nabla\tilde{c}_{im}'\right) - \theta_{im}D^{*}\frac{\partial \tilde{c}_{im}'}{\partial z}\bigg|_{z=b_{im}} \tag{2.19b}$$

Using order of magnitude analysis, we obtain analytical solutions for (2.19a) and (2.19b) valid for thin porous layers and under quasi-steady conditions of the perturbation fields, $\tilde{c}_{im}'$ and $\tilde{c}_{m}'$. An order of magnitude of a variable can be defined as the average of its absolute value over a characteristic length which is usually the domain of the variable (*Whitaker*, 1977). In general, an exact order of magnitude cannot be obtained since the variable in question is to be solved for; instead, we rely on an estimate of the order of magnitude. In the analysis presented below, we use l_x, l_y, and l_z as characteristic lengths associated with the variations of C_m and C_{im} along the x, y, and z directions.

For the term that involves the partial derivative with respect to time in (2.19a), we make the following order of magnitude estimate

$$b_m \theta_m \frac{\partial \tilde{c}_m'}{\partial t} = \mathrm{O}\left[\frac{b_m \theta_m}{t^*}\right] \tilde{c}_m', \tag{2.20}$$

and for the transverse vertical diffusive term, we have

$$b_m \theta_m \frac{\partial}{\partial z}\left(D_z \frac{\partial \tilde{c}_m'}{\partial z}\right) = \mathrm{O}\left[\frac{b_m \theta_m D_z}{l_z^2}\right] \tilde{c}_m' \tag{2.21}$$

Thus, it can be asserted that

$$\frac{\partial \tilde{c}_m'}{\partial t} << \frac{\partial}{\partial z}\left(D_z \frac{\partial \tilde{c}_m'}{\partial z}\right) \tag{2.22}$$

if the following quasi-steady constraint is satisfied

$$\frac{D_z t^*}{b_m^2} >> 1 \tag{2.23}$$

in which l_z is considered to be O[b_m] and t^* is a characteristic time, associated with the plume length, and can be estimated as $l_x / (u/\theta_m)$. Also, the longitudinal and transverse (i.e., in the x and y directions) dispersion terms have the order of magnitude estimates

$$b_m \theta_m \frac{\partial}{\partial x}\left(D_x \frac{\partial \tilde{c}_m'}{\partial x}\right) = \mathrm{O}\left[\frac{b_m \theta_m D_x}{l_x^2}\right] \tilde{c}_m' \tag{2.24}$$

$$b_m \theta_m \frac{\partial}{\partial y}\left(D_y \frac{\partial \tilde{c}_m'}{\partial y}\right) = \mathrm{O}\left[\frac{b_m \theta_m D_y}{l_y^2}\right] \tilde{c}_m' \tag{2.25}$$

Hence, transverse molecular diffusion of $\tilde{c}_m'$ dominates over its longitudinal and transverse (lateral) dispersions, i.e.,

$$b_m \theta_m \frac{\partial}{\partial x}\left(D_x \frac{\partial \tilde{c}_m{}'}{\partial x} \right), \quad b_m \theta_m \frac{\partial}{\partial y}\left(D_y \frac{\partial \tilde{c}_m{}'}{\partial y} \right) << b_m \theta_m \frac{\partial}{\partial z}\left(D_z \frac{\partial \tilde{c}_m{}'}{\partial z} \right) \tag{2.26}$$

if

$$\frac{l_x{}^2}{b_m{}^2}\frac{\alpha_T}{\alpha_L}, \quad \frac{l_y{}^2}{b_m{}^2} >> 1 \tag{2.27}$$

in which mechanical mixing is assumed to be the dominant hydrodynamic dispersion mechanism, i.e., $D_x \approx \alpha_L u/\theta_2$, $D_y \approx \alpha_T u/\theta_2$ (*Bear*, 1972), and α_L , α_T are the longitudinal and transverse local dispersivities [L]. In (2.27) it is assumed that α_T in the y direction is equal to that in the z direction; this is not the case in general.

Finally, for the advection term in (2.18), we have

$$b_m u \frac{\partial \tilde{c}_m{}'}{\partial x} = O\left[\frac{b_m u}{l_x} \right] \tilde{c}_m{}' \tag{2.28}$$

Thus,

$$b_m u \frac{\partial \tilde{c}_m{}'}{\partial x} << b_m \theta_m \frac{\partial}{\partial z}\left(D_z \frac{\partial \tilde{c}_m{}'}{\partial z} \right) \tag{2.29}$$

if

$$\frac{b_m{}^2 (u/\theta_m)}{D_z l_x} << 1 \tag{2.30}$$

Likewise, for the impervious layer, one may conclude that

$$\frac{D^* t^*}{b_{im}{}^2} >> 1 \tag{2.31}$$

in which D^* is the effective molecular diffusion parameter [L^2/T]. Under condition (2.31), $\tilde{c}_{im}'$ is quasi-steady and the partial derivative term in (2.29) can be neglected. Similarly, if

$$\frac{l_x^2}{b_{im}^2}, \quad \frac{l_y^2}{b_{im}^2} >> 1 \tag{2.32}$$

Under this condition, transverse dispersion of $\tilde{c}_{im}'$ dominates over the longitudinal and lateral dispersions and (2.26), rewritten for $\tilde{c}_{im}'$ instead of $\tilde{c}_m'$, is valid in this case. Using conditions (2.23), (2.27), (2.30), (2.31), and (2.32), equations (2.18) and (2.19), after retaining the dominant terms, reduce to the following coupled boundary-value problem:

Boundary-Value Problem:

$$b_m \theta_m D_z \frac{\partial^2 \tilde{c}_m'}{\partial z^2} = -\theta_m D_z \frac{\partial \tilde{c}_m'}{\partial z}\bigg|_{z=b_m} \tag{2.33}$$

$$b_{im} \theta_{im} D^* \frac{\partial^2 \tilde{c}_{im}'}{\partial z^2} = \theta_{im} D^* \frac{\partial \tilde{c}_{im}'}{\partial z}\bigg|_{z=b_m} \tag{2.34}$$

Boundary Conditions:

$$\theta_m D_z \frac{\partial \tilde{c}_m'}{\partial z} = 0 \qquad z = b_{im} + b_m \tag{2.35a}$$

$$\theta_m D_z \frac{\partial \tilde{c}_m'}{\partial z} = \theta_{im} D^* \frac{\partial \tilde{c}_{im}'}{\partial z}\bigg|_{z=b_m} \qquad z = b_{im} \tag{2.35b}$$

$$\tilde{c}_m' = k^* e^{kt} \overline{C_{im}} - e^{kt} \overline{C_m} + k^* \tilde{c}_{im}' \qquad z = b_{im} \tag{2.35c}$$

$$\theta_{im} D^* \frac{\partial \tilde{c}_{im}'}{\partial z} = 0 \qquad z = 0 \tag{2.35d}$$

2.3.3 Solution

Although they appear with partial derivatives, equations (2.33) and (2.34) are essentially second-order ordinary differential equations whose solutions involve four unknown constants in addition to the unknown and coupling diffusive-flux terms. The use of (2.35b) leaves us with a total of five unknowns and three boundary conditions. In order to obtain a unique solution, two more boundary conditions are needed, and we make use of the following closure conditions that were stated earlier:

$$\overline{\tilde{c}_{im}} = \overline{e^{-kt}\tilde{c}_{im}}' = e^{-kt}\frac{1}{b_{im}}\int_0^{b_{im}} \tilde{c}_{im}'(x,y,z,t)\,dz = 0 \tag{2.35e}$$

$$\overline{\tilde{c}_{m}} = \overline{e^{-kt}\tilde{c}_{m}}' = e^{-kt}\frac{1}{b_{m}}\int_{b_{im}}^{b_{im}+b_m} \tilde{c}_{m}'(x,y,z,t)\,dz = 0 \tag{2.35f}$$

The integration of (2.33) from $z = z$ to $z = b_{im} + b_m$ and using (2.35a) yields

$$-b_m\theta_m D_z\frac{\partial\tilde{c}_m'}{\partial z} = -\theta_m D_z\frac{\partial\tilde{c}_m'}{\partial z}\bigg|_{z=b_{im}}(b_{im}+b_m-z) \tag{2.36}$$

in which the partial derivative notation is retained because $\tilde{c}_m'$ is a function of x and y as well. Integrating (2.36) once more,

$$\tilde{c}_m' = -\frac{1}{2b_m}\frac{\partial\tilde{c}_m'}{\partial z}\bigg|_{z=b_{im}}(b_{im}+b_m-z)^2 + a_0 \tag{2.37}$$

and the use of the closure condition (2.35f) leads to

$$\overline{\tilde{c}_m'} = \frac{1}{2b_m^{\,2}}\frac{\partial\tilde{c}_m'}{\partial z}\bigg|_{z=b_{im}}\frac{1}{3}(-b_m^{\,3}) + \frac{1}{b_m}a_0(b_m) = 0 \tag{2.38}$$

which can be solved for a_0,

$$a_0 = \frac{b_m}{6}\frac{\partial \tilde{c}_m'}{\partial z}\bigg|_{z=b_{im}} \tag{2.39}$$

Similarly, the solution of (2.34) is obtained by integrating twice with respect to z and imposing the boundary condition (2.35d),

$$\tilde{c}_{im} = \frac{1}{2b_{im}}\frac{\partial \tilde{c}_{im}'}{\partial z}\bigg|_{z=b_{im}} z^2 + b_0 \tag{2.40}$$

The imposition of the closure requirement (2.35e) results in

$$\overline{\tilde{c}_{im}'} = \frac{1}{2b_{im}^{\ 2}}\frac{\partial \tilde{c}_{im}'}{\partial z}\bigg|_{z=b_{im}} \frac{1}{3}(b_{im}^{\ 3}) + \frac{1}{b_{im}}(b_0 b_{im}) = 0 \tag{2.41}$$

Hence,

$$b_0 = -\frac{b_{im}}{6}\frac{\partial \tilde{c}_{im}'}{\partial z}\bigg|_{z=b_{im}} \tag{2.42}$$

After evaluating (2.37) and (2.40) at $z = b_{im}$ and using (2.35c), (2.39), and (2.42), one obtains

$$-\frac{1}{2b_m}\frac{\partial \tilde{c}_m'}{\partial z}\bigg|_{z=b_{im}} b_m^{\ 2} + \frac{b_m}{6}\frac{\partial \tilde{c}_m'}{\partial z}\bigg|_{z=b_{im}} = \frac{k^*}{2b_{im}}\frac{\partial \tilde{c}_{im}'}{\partial z}\bigg|_{z=b_{im}} b_{im}^{\ 2} - k^*\frac{b_{im}}{6}\frac{\partial \tilde{c}_{im}'}{\partial z}\bigg|_{z=b_{im}} + k^* e^{kt}\overline{C_{im}} - e^{kt}\overline{C_m} \tag{2.43}$$

which can be solved for either of the boundary flux terms after imposing the continuity of the flux boundary condition (2.35b),

$$\theta_{im} D^* \frac{\partial \tilde{c}_{im}'}{\partial z}\bigg|_{z=b_{im}} = \theta_m b_m \alpha e^{kt}(\overline{C_m} - k^*\overline{C_{im}}) \tag{2.44}$$

where

$$\alpha = \frac{3\theta_{im}^{\ 2} D^*}{\theta_m^{\ 2} b_m^{\ 2} (k^* \beta + \nu)} \tag{2.45}$$

$$\beta = \frac{\theta_{im} b_{im}}{\theta_m b_m} \tag{2.46}$$

$$\nu = \frac{\theta_{im}^{\ 2} D^*}{\theta_m^{\ 2} D_z} \tag{2.47}$$

Thus, for continuous concentrations at the interface, we have $k^* = 1$, and (2.45) reduces to the simple expression

$$\alpha = \frac{3D^* \beta^2}{b_{im}^{\ 2} (\beta + \nu)} \tag{2.48}$$

in which α is commonly referred to as the mass transfer coefficient [T^{-1}], and *Haggerty and Gorelick* (1995) refer to β as the capacity ratio for phenomenological first-order rate processes. By assuming locally uniform θ_m and θ_{im}, then substituting (2.44) into (2.15), after the use of the fact $\tilde{c}_{im} = e^{-k t} \tilde{c}_{im}'$, and dividing both sides by $\theta_m b_m$, yields the following transport equation in the low-permeability layer

$$\beta \frac{\partial \overline{C_{im}}}{\partial t} + \beta k \overline{C_{im}} = \beta \nabla' \cdot \left(\mathbf{D}'_{im} \cdot \nabla' \overline{C_{im}} \right) + \alpha (\overline{C_m} - k^* \overline{C_{im}}) \tag{2.49}$$

By adding (2.14) to (2.15) and dividing both sides of the resulting equation by $\theta_m b_m$, one obtains the governing transport equation in the conductive layer

$$\frac{\partial \overline{C_m}}{\partial t} + \beta \frac{\partial \overline{C_{im}}}{\partial t} + \beta k \overline{C_{im}} = \beta \nabla' \cdot \left(\mathbf{D}'_{im} \cdot \nabla' \overline{C_{im}} \right) + \nabla' \cdot \left(\mathbf{D}'_m \cdot \nabla' \overline{C_m} \right) - \frac{u}{\theta_m} \frac{\partial \overline{C_m}}{\partial x} - k \overline{C_m} \tag{2.50}$$

Equations (2.49) and (2.50) describe the effect of interlayer diffusive mass transfer on contaminant concentrations averaged over high-permeability and low-permeability thin layers. The combined effect of transverse vertical dispersion (mechanical mixing) and effective molecular diffusion, capacity ratio β, porosities, and partition coefficient k^*, are lumped into the mass transfer coefficient α The latter and the capacity ratio parameter β describe in an average sense the capacitance effect of low-conductivity layers to store and release solute mass into the high-conductivity layers. Also, note that a reactive chemical produces a sink term for the mobile phase, which is proportional to the product of the capacity ratio β and concentrations in the immobile phase. This is shown by the third term on the left-hand side of (2.50).

2.4 Application and Discussion

The developed expression for α in (2.45) is interesting and constitutes a new element of this effort, because it explicitly relates the rate of mass transfer to processes other than the conventional diffusion transfer. Equations (2.45)-(2.47) show how (bio)chemical processes through k^*, and mechanical mixing through the term v, affect the rate of mass transfer between zones of mobile and immobile water. It would have been too difficult to realize these results without the recognition of the information contained in the perturbations about average concentrations, and solving for $\bar{c}_m$ and $\bar{c}_{im}$. Figure 2.2 compares the relationship between the dimensionless α and the capacity ratio β for different values of flow velocities, using (2.45) and the relationship (2.52) suggested by *Van Genuchten* (1985) and *Parker and Valocchi* (1986). The results show that the expression suggested by the above investigators is close to (2.45) for $\beta > 4$. Also, the dimensionless α varies significantly for a small capacity ratio β; $\beta < 1$.

While the dependence of the rate coefficient α on the magnitude of pore-water velocity has been observed in laboratory experiments (*Bennet and Goodridge*, 1970; *Coats and Smith*, 1964; *Baker*, 1977; *Van Genuchten and Wierenga*, 1977; *Rao et al.*, 1980b; and *De Smedt and Wierenga*, 1984), *Coats and Smith* (1964), *Baker* (1977), *Van Genuchten and Wierenga* (1977), and *Raven et al.* (1988) attributed the increase in the mass transfer coefficient α with the pore-water velocity to convective mixing coming into play as a dominant mechanism other than diffusive exchange only between flowing and immobile solute zones. *De Smedt and Wierenga* (1984) explained the increase in α with flow velocity due to increase in the water content which may result in a larger cross-sectional area and thus higher values of α. *Van Genuchten and Wierenga* (1977) provided another explanation on the basis of an increase in the amount of immobile water, and hence by an increase in the diffusion length for the solute from the mobile phase to the center of the immobile phase. By conducting a laboratory experiment under unsaturated flow conditions, *Gaudet et al.* (1977) observed that the amount of stagnant water increased with decreasing water content; however, estimated values of α showed no apparent dependence on the water content. The relation developed here for α (2.45) confirms that the mass transfer coefficient α increases with the flow velocity under saturated conditions also, especially for $\beta < 1.0$. Over the range of values of u/θ_m shown in Figure 2.3, the dimensionless α showed approximately a linear relationship for $\beta < 0.05$, while it is increasingly less dependent on u/θ_m for greater capacity ratios, $\beta \geq 1$. In the case of nonreactive constituents, if we expand (2.45), using Taylor series, in terms of the transverse vertical dispersivity α_{Tv} around zero and retain the leading two terms, we obtain the approximation:

$$\alpha(u/\theta_m) \approx \frac{3\theta_{im}^{\ 2} D^*}{\theta_m^{\ 2} b_m^{\ 2}\left(\frac{\theta_{im}^{\ 2}}{\theta_m^{\ 2}} + \beta\right)} + \frac{3}{b_m^{\ 2}} \frac{\theta_{im}^{\ 4} \alpha_{Tv}}{\theta_m^{\ 4}\left(\frac{\theta_{im}^{\ 2}}{\theta_m^{\ 2}} + \beta\right)^2} \frac{u}{\theta_m} \tag{2.51}$$

in which the first term (zero-order) represents the contribution of diffusive mixing while the second term represents the effect of mechanical mixing or the convective dispersive mechanism across the interface between the high-permeability and low-permeability layers. Thus, on the basis of Figure 2.3 and equation (2.51), we may conclude that velocity variations due to pore-scale heterogeneity, produce a convective flux across the interfacial boundary which augments diffusive flux, and whose contribution to the mass transfer is dependent on the magnitude of the average pore-water velocity. The greater the average flow velocity, the greater the flow velocities across the interface; hence, the greater their net effect being described in an average sense by transverse vertical dispersion. *Baker* (1977) observed that α depends on velocity to the 0.84 power, and *De Smedt and Wierenga* (1984) noted a proportional dependence and they fitted a linear relationship between the average pore-water velocity and α.

In the case of high flow rates (e.g., flow toward wells), transverse vertical dispersion may dominate over effective molecular diffusion; thus, we have $\nu \rightarrow 0$, and (2.45) reduces to

$$\alpha = \frac{3D^*\beta}{b_{im}^{\ 2}} \tag{2.52}$$

For small flow velocities (e.g., natural gradient conditions), transverse vertical dispersion is negligible and diffusive transfer dominates; thus, $\nu = 1$. In the case of thick low-permeability layers, we have $\beta >> 1$, and (2.45) also reduces to (2.52), which was suggested by *Van Genuchten* (1985), *Parker and Valocchi* (1986), and *Goltz and Roberts* (1987). Implicit in (2.52) is the fact that the characteristic time for transverse dispersion in the mobile phase $b_m^{\ 2}/D_{TV}$ is

much less than that in the immobile phase b_{im}^2 / D^*. Thus, any transverse vertical concentration gradients in the high-permeability layer should be negligible compared with those in the low-permeability layer. For inert solutes, equation (2.45) is general in the sense that it is also applicable under small flow velocities in a heterogeneous formation whereby relatively thin clay, or silt, sheets are embedded into the more permeable sandy material. There, the characteristic time for transverse dispersion in a sand layer may be of the same order of magnitude of that in the surrounding clay layer, and (2.45) should be used to estimate the mass transfer coefficient.

Although the analysis here is based on a time-invariant capacity ratio β (i.e., b_{im} is independent on time), this, however, may not be the case during the early development of a contaminant plume where the solute is invading a semi-infinite low-permeability layer. This is, also, analogous to solute transport in fractured rocks where fractures are separated by large distances. In spite of numerous efforts to derive analytical solutions for diffusive transfer into semi-infinite immobile regions (or matrix in fractured rocks) (see, e.g.; *Tang et al.*, 1981; *Grisak and Pickens*, 1981; *Gillham et al.*, 1984; and *Sudicky et al.*, 1985), they, however, are impractical for describing interlayer transfer at a scale where uncertainty regarding local information prevails. The ability to define global values for β, and from which α can be defined uniquely through the relation (2.45), may render capacitance models, in whatever form (e.g., first-order rate models), more practical to describe the interlayer transfer at a scale whereby uncertainties play a prominent role. Figure 2.4 compares the longitudinal variance of a real contaminant plume of tracer chloride (adapted from *Gillham et al.*, 1984) to that estimated on the basis of a first-order rate model. The latter is calculated based on a formula for the second longitudinal moment developed by *Goltz and Roberts* (1987) (the third in Table 3 under first-order rate model, *Goltz*

and Roberts, 1987), modified to account for an initial plume length L_1 by adding an additional term of the form $L_1^2(1+\beta)/12(1+\beta A)$, in which $A = \exp\left[-(\alpha/\beta)(1+\beta)t\right]$. The best fit between the first-order rate model and the experimental data is obtained by adjusting the initial plume length L_1 to 1.5 m and the capacity ratio β to 0.5. The value for the effective diffusion parameter $D^* = 3 \times 10^{-5}$ cm^2/day is chosen based on *Gillham et al.* (1984), while the fitted mean groundwater velocity value is based on that measured by *Sudicky et al.* (1985). Inserting the fitted β and $k^* = 1$ into (2.45) yields the following estimate for the mass transfer coefficient, α = 0.052 day^{-1}. The close agreement between the variances predicted by the first-order rate model (see, Figure 2.4) and the experimental results indicates that early dispersion of the tracer chloride in fluvial deposits can be interpreted, on the basis of local dispersion as well as interlayer-diffusive transfer. Further, it shows that a first-order rate model can be used to account for diffusive transfer, even in a semi-infinite setup. Because the experimental data in Figure 2.4 is based on a forced injection through a thin permeable layer surrounded by much thicker (i.e., semi-infinite) low-permeability layers (*Gillham et al., 1984*), the fitted value for the capacity ratio β = 0.5 should be understood as being related approximately to some time-averaged immobile-phase thickness b_{im} (recall (2.46) and refer to Figure 2.1) during the development of the plume; hence, an effective value in that sense. It is anticipated that advection dominates at later stages as the main dispersive mechanism, when the tracer plume spreads out to encompass different layers of different hydraulic conductivities.

Figure 2.5 displays chloride breakthrough data from an experiment conducted by *Grisak et al.* (1980) on transport through fractured till with matrix diffusion. The measured chloride relative concentrations are made at the end of a 0.76 m cylindrical column of fractured till, and

they are marked by the empty circles. The dotted line represents predictions of the breakthrough curve using an analytical solution of *Grisak and Pickens* (equations (8) and (9), 1981) for diffusion into a semi-infinite matrix. The solid line predicts relative concentrations on the basis of a first-order rate model using an analytical solution given by equation (12) of *Lindstrom and Stone* (1974). The data concerning the velocity in the fracture, longitudinal dispersivity, matrix porosity, half-aperture size, and distance are shown in Figure 2.5, and they simulate the conditions during the experiment (*Grisak et al.*, 1980). The fit between the above theoretical models and measured concentrations is obtained with an effective matrix diffusion coefficient of $D^* = 7.58 \times 10^{-7}$ cm^2/day. If we consider the free-solution diffusion coefficient D to be 1.5×10^{-5} cm^2/day, then we may estimate, based on the fitted D^*, the apparent tortuosity factor to be 0.05. The effective value of β for the first-order rate fit is estimated to be 50, from which the mass transfer coefficient α is calculated from the relationship (2.46) as 79 day^{-1}. The first-order rate model predicted earlier breakthrough when compared to the matrix-diffusion model; however, it overestimates the measured concentrations after 1.8 days, while the latter underestimates the concentrations after 1.5 days. This is anticipated because the first-order rate model predicts less diffusive sorption of solute mass, while it predicts a greater bleeding rate (i.e., diffusive-transfer back into the mobile region) than the matrix-diffusion model with a semi-infinite low-permeability zone. There is more room for solute mass to spread over by molecular diffusion in a semi-infinite immobile region, and the net effect is reduced capacity for releasing mass back into the mobile phase.

Figure 2.6 shows sodium chloride breakthrough adapted from *Sudicky et al.* (1985). The solution is forced through a thin layer of coarse-grained sand which is sandwiched between thick

silt layers (i.e., semi-infinite). Also shown in Figure 2.6 are predicted relative concentrations using a first-order rate one-dimensional solution of *Lindstrom and Stone* (1974) and a thin-layer diffusion model of *Sudicky et al.* (1985). The predictions are based on a parameter set that simulates the conditions during the experiment: u = 0.5 m/day; α_L = 0.5 cm; θ_{im} = 0.36; θ_m = 0.33; b_m = 1.5 cm; and the duration of the pulse, t_0 = 7 days. Using D^* = 1.21× 10^{-9} m^2/s based on *Sudicky et al.* (1985), the best fit for β by trial-and-error is found to be 2.0, which yielded α = 0.52 day^{-1}. The first-order rate model predicted earlier breakthrough and overestimated the measured concentrations, especially during the rising and falling (elution) parts of the breakthrough curve. The first-order rate model exaggerated the magnitude of tailing produced by the reversed concentration gradient between the sand and silt layers, during the falling part. Thus, it overestimated the solute mass that reentered the sand layer (i.e., overestimated the bleeding rate). The thin-layer diffusion model, on the other hand, predicted later breakthrough and compared relatively better to the measurements; however, it underestimated the concentrations during the rising part of the curve and overestimated them during the falling part. In the thin-layer model, the vertical transverse dispersion is ignored in the sand layer; nevertheless, *Sudicky et al.* (1985) developed a solution for a thick-layer diffusion model and the results compared relatively better than the thin-layer one. This is because the characteristic time for vertical transverse dispersion in the sand is given by b_m^2/D^*= $(0.015)^2$ /0.0001045= 2.2 days, which is of the same order of magnitude of the time at which measurements are made, 2-13 days. Thus, assuming complete mixing in the sand layer, when in fact vertical gradients in concentrations may have been significant, resulted in the discrepancy of the thin-layer model with the observations (Figure 2.6). It is worth noting that in the first-order rate model, the effect of

vertical transverse dispersion is lumped into the mass transfer coefficient α through the parameter v in (2.47). Hence, we may conclude that the relatively poor fit presented by the first-order rate model can be attributed to the following reasons. First, as we pointed out earlier, the first-order rate model is applicable to the case of a semi-infinite immobile phase, only in an approximate sense. Second, the constraint given by (2.30) for disregarding the effect of the convective term of the mobile-phase perturbation $\tilde{c}_m'$, is severely violated in the fractured media example (Figure 2.5), where the magnitude of the velocity in the fracture was large u = 29.7 m/day. The same constraint, however, is violated to a lesser extent in the following example of the sand-silt porous media (Figure 2.6). Furthermore, in the latter example, the quasi-steady condition is also somewhat violated, because, as explained earlier, the time scale of the experiment was of the same order of magnitude of the characteristic time associated with vertical transverse diffusion in the sand layer.

As demonstrated by the above examples, interpretation of the dispersion of solutes on the basis of diffusive-type interlayer mass transfer is indisputable; however, in doubt is the strict validity of the linear first-order rate model under general conditions. Although diffusive transfer remains the mechanism for mass exchange between the mobile and immobile phases, *Coats and Smith* (1964) pointed out that linear models fail at large velocities. Since it was demonstrated earlier that a first-order rate process prevails under quasi-steady conditions, then it is natural to believe that prior to this state (i.e., in transient) some other mechanism, perhaps different in form, may describe the mass transfer phenomenon.

Notwithstanding the discrepancies shown in the above examples between the first-order rate approximation and the experimental results, we may assert that first-order rate models

remain useful tools for describing interlayer diffusive-type mass transfer, especially at larger scales where uncertainties dominate.

2.5 Formation-Scale Mass Transfer Rate Coefficient, α_{eff}

2.5.1 Development of an Effective Property

In this section we develop an estimate for mass transfer coefficient α of a formation made of layers of two distinct conductivities, K_1 and K_2, and $K_1 >> K_2$ (e.g., sand and silt, Figure 2.7 a). We define the formation-mass transfer coefficient as an effective property α_{eff} for an equivalent formation composed of two layers; one is conductive (e.g., sand) and maintain the groundwater flux of the original formation and the other is semipervious through which the diffusive mass flux of the actual formation is conserved. If the layers display spatial variation of their thicknesses in space (e.g., clay lenses dispersed in sand), then we associate α_{eff} with a given section of the formation; hence, averaged over the depth of the formation rather than the entire formation. In this case, α_{eff} displays also spatial variations. Figure 2.7 shows the actual and equivalent formation. Note that the thickness d of the equivalent conductive layer, of conductivity K_1, is equal to the sum of the thicknesses of the individual conductive layers of the actual formation. In contrast, the thickness b of the equivalent layer of conductivity $K_2 << K_1$, is equal to the sum of the thicknesses of the individual semipervious layers of conductivity K_2. The total inter-layer diffusive contaminant-mass flux Q_T per area for the layered system in Figure 2.7 is given by

$$Q_T = \sum_{i=1}^{3} \left\{ Q''_i + Q'_i \right\} \tag{2.53}$$

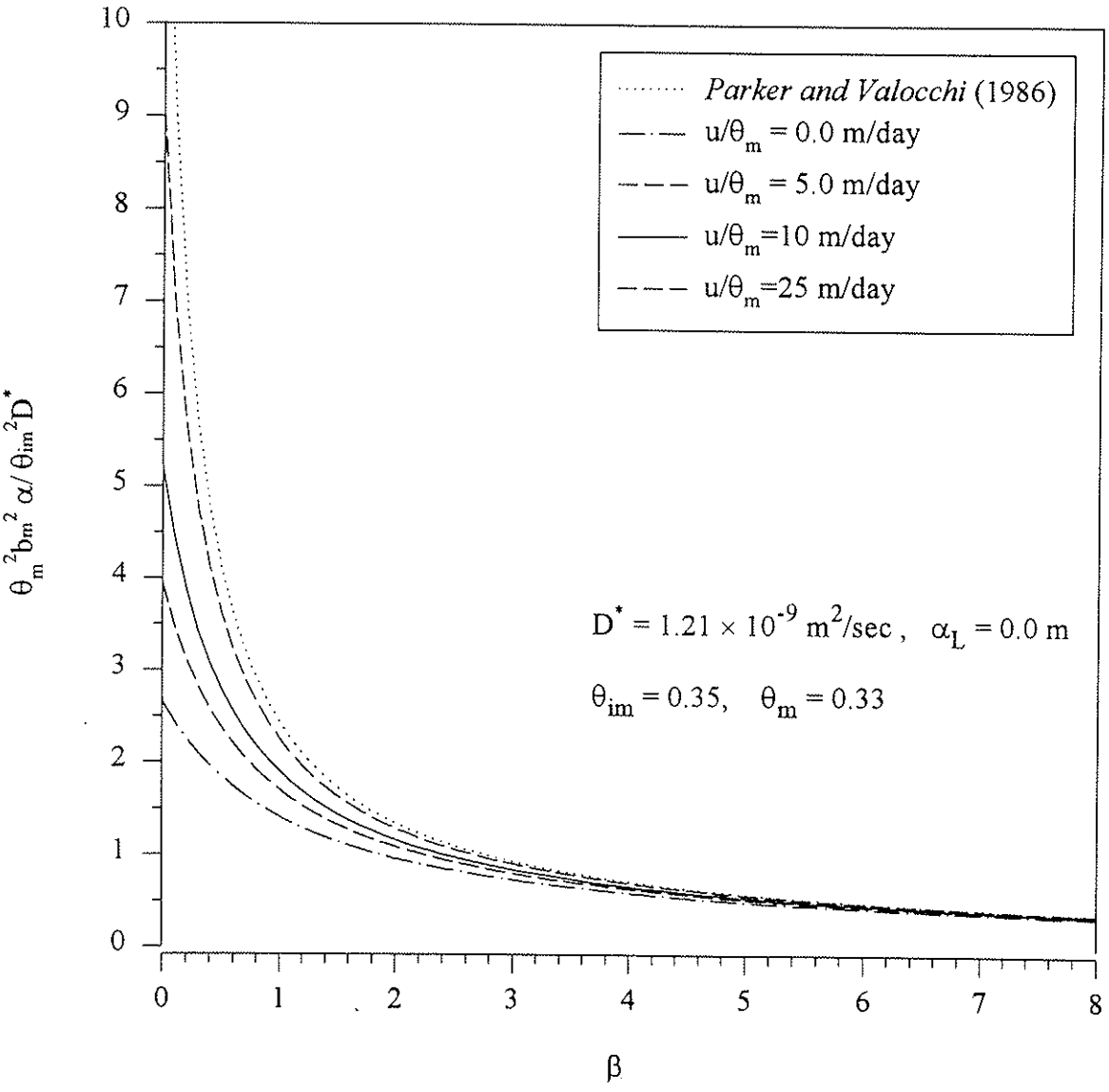

Figure 2.2 Relation between dimensionless transfer rate coefficient and capacity ratio coefficient, for different values of pore-water velocity.

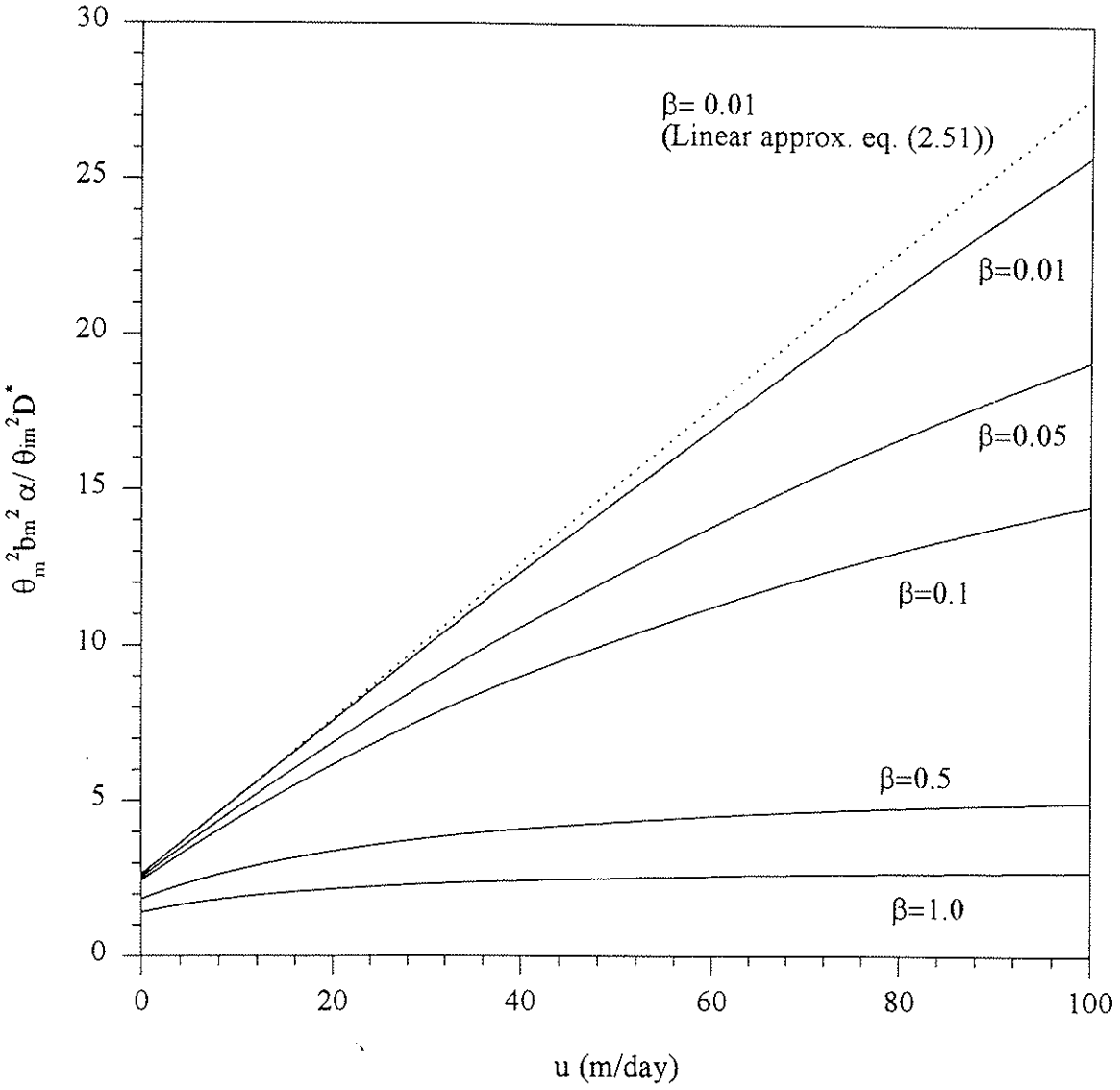

Figure 2.3 Relation between dimensionless transfer rate coefficient and pore-water velocity, for different values of capacity ratio.

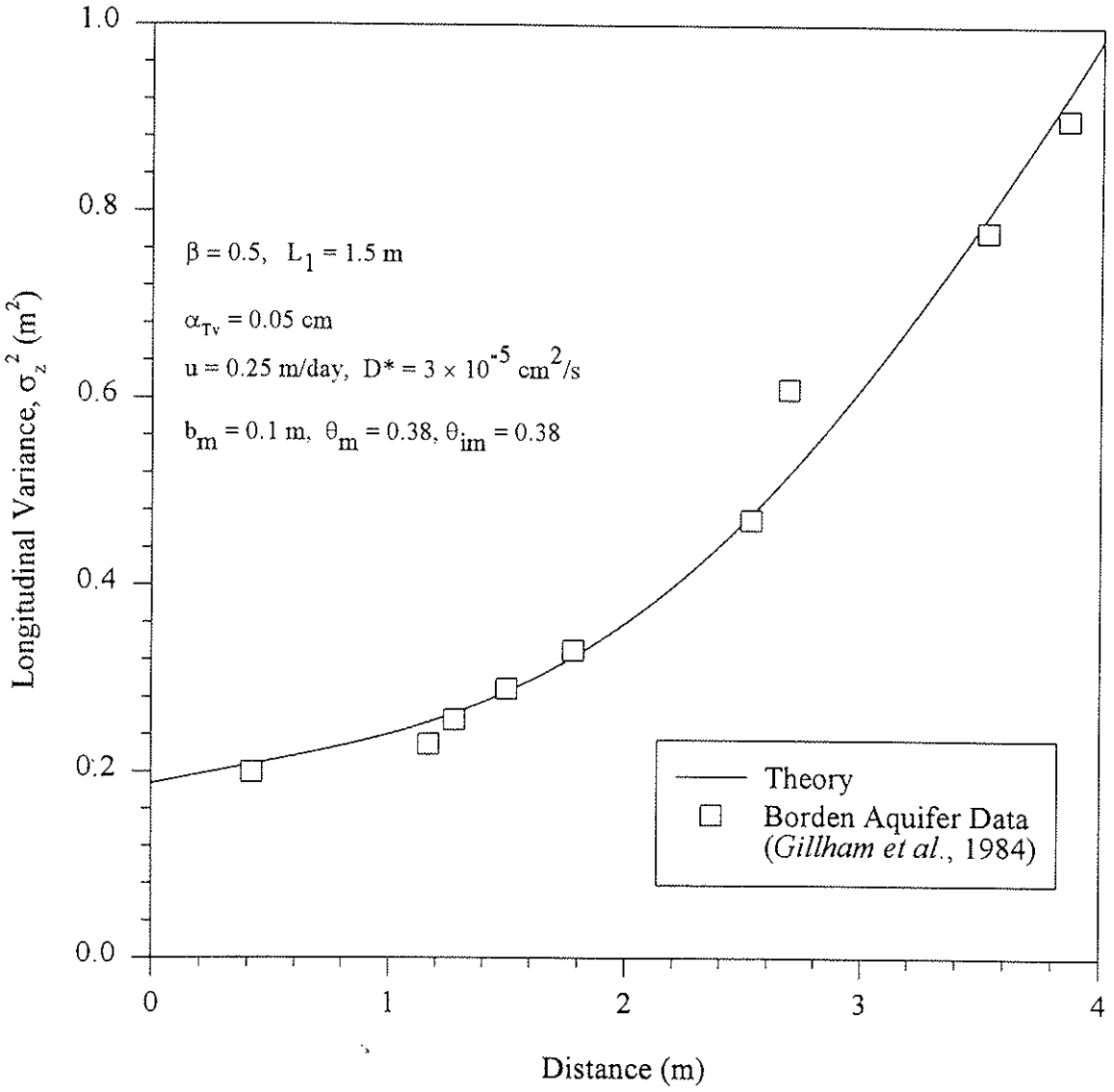

Figure 2.4 Relation between longitudinal variance and displacement: Comparison between first-order rate model and experimental measurements.

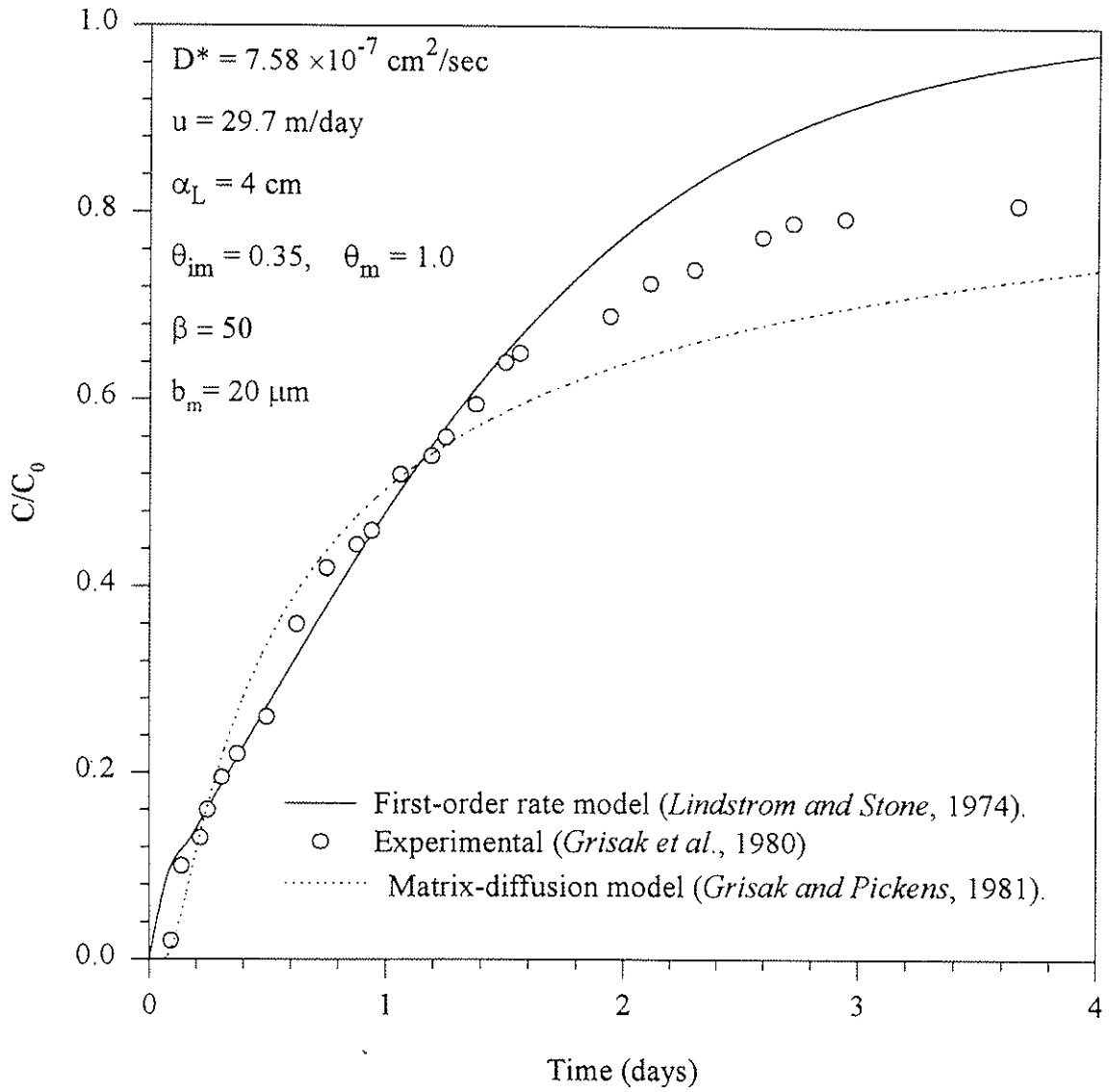

Figure 2.5 Chloride breakthrough at x = 0.76 m in a fractured system: Comparison between theoretical models and experimental measurements.

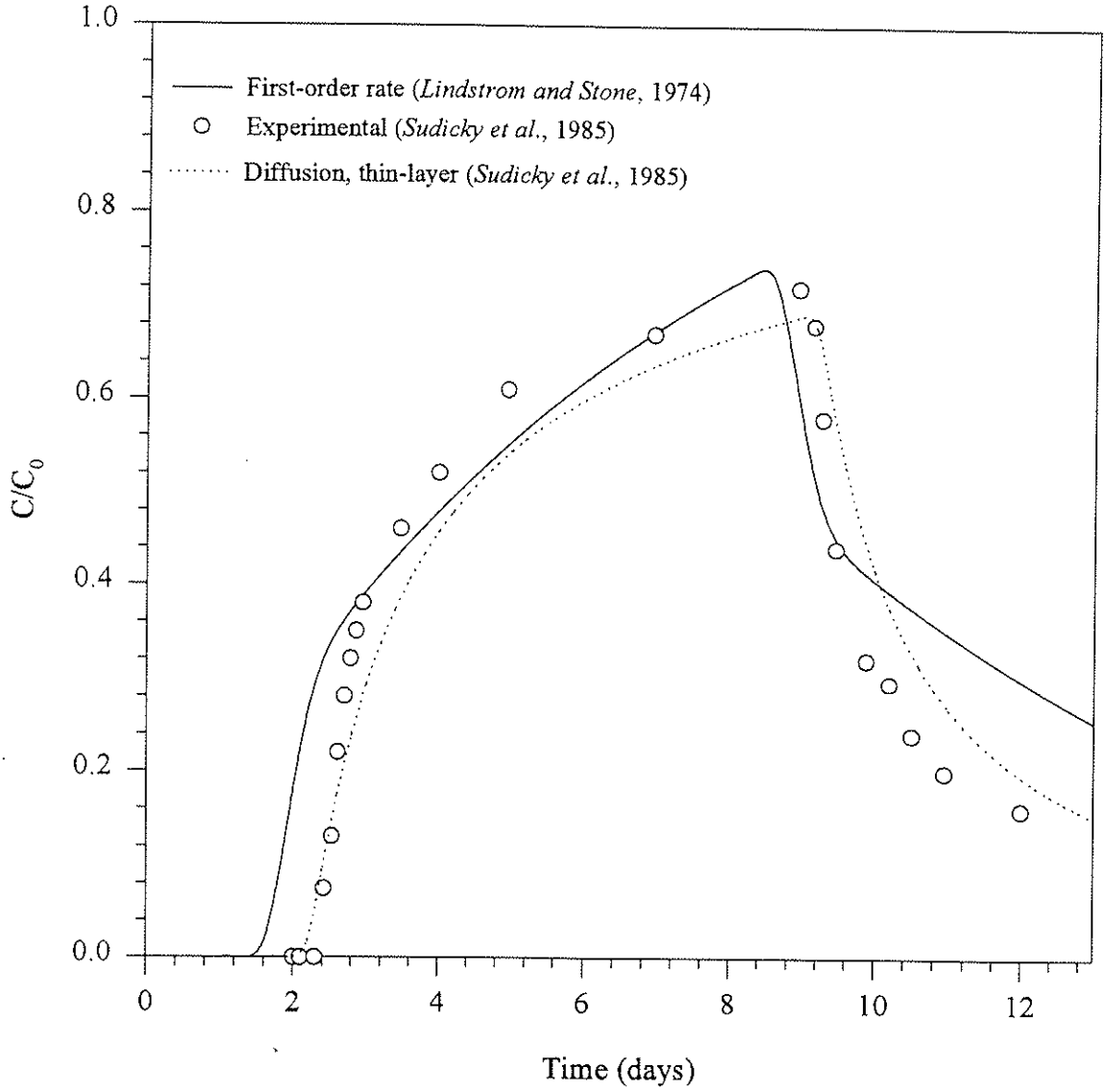

Figure 2.6 Sodium chloride breakthrough at x = 1.0 m in a sand layer situated between two layers of silt; comparison between theoretical models and experimental data: u = 0.5 m/day; α_L = 0.5 cm; θ_{im} = 0.36; θ_m = 0.33; b_m = 1.5 cm; and t_0 = 7 days.

where

$$Q''_j = d''_j \alpha''_j (C_m^j - C_{im}^j) \tag{2.54a}$$

$$Q^l_j = d^l_j \alpha^l_j (C_m^j - C_{im}^{j+1}) \tag{2.54b}$$

$$d_j = d''_j + d^l_j \tag{2.54c}$$

in which Q''_j and Q^l_j are the upward and downward diffusive mass flux per area (M/T/L^2) (see, Figure 2.7), respectively; d_j is the thickness of the jth high-permeability layer [L]; d''_j is the thickness of a portion of the high-permeability layer j that is contributing a diffusive-mass flux to the upper semipervious layer [L]; d^l_j is the thickness of a remaining portion of the jth high-permeability layer that is contributing a diffusive-mass flux to the lower semipervious layer [L]; α''_j is the mass-transfer coefficient associated with the upper interfacial boundary of the jth high-permeability layer [T^{-1}]; α^l_j is the mass-transfer coefficient associated with the lower interfacial boundary of the jth high-permeability layer [T^{-1}]; C_m^j is the concentration of the mobile contaminant in the jth layer [M/L^3]; and C_{im}^j is the concentration of the immobile contaminant in the jth semipervious layer [M/L^3]. In the manner we defined α_{eff} above, we have

$$Q_T = d\alpha_{eff} (\overline{C}_m - \overline{C}_{im}) \tag{2.55}$$

where $d = \sum_{j=1}^{4} d_j$; $\overline{C}_m$ is the concentration of the mobile contaminant averaged over the high-permeability layers of the strata (Figure 2.7) [M/L^3]; and $\overline{C}_{im}$ is the concentration of the immobile contaminant averaged over the semipervious layers of the strata [M/L^3].

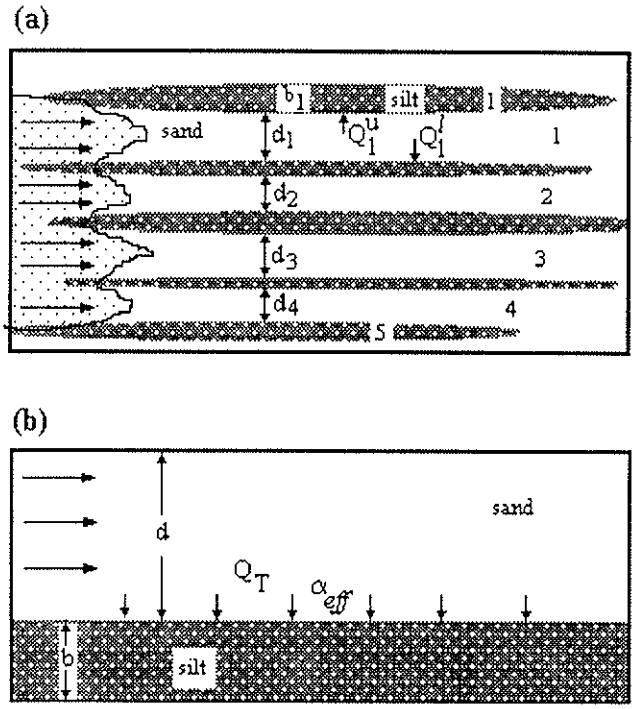

Figure 2.7 Schematic representation of: (a) a stratified formation; and (b) an equivalent two-layer system.

The substitution of (2.54a), (2.54b), and (2.55) into (2.53) yields

$$d\alpha_{eff}(\overline{C}_m - \overline{C}_{im}) = \sum_{j=1}^{4} \left\{ d''_j \alpha''_j (C_m^{\,j} - C_{im}^{\,j}) + d'_j \alpha'_j (C_m^{\,j} - C_{im}^{\,j+1}) \right\} \tag{2.56}$$

Asymptotically (i.e., after large displacement), we may assume that $C_m^{\,j} \approx \overline{C}_m$ and $C_{im}^{\,j} \approx \overline{C}_{im}$; hence, (2.56) reduces to

$$d\alpha_{eff}(\overline{C}_m - \overline{C}_{im}) = \sum_{j=1}^{4} \left\{ d''_j \alpha''_j + d'_j \alpha'_j \right\} (\overline{C}_m - \overline{C}_{im}) \tag{2.57}$$

from which we obtain the following expression for the effective coefficient of mass transfer,

$$\alpha_{eff} = \frac{\sum_{j=1}^{4} \left\{ d''_j \alpha''_j + d'_j \alpha'_j \right\}}{\sum_{j=1}^{4} d_j} \tag{2.58}$$

Equation (2.58) states that after large displacement, the formation mass-transfer coefficient is the arithmetic mean of the coefficient values of the individual two-layer system. Implicit in (2.58), diffusive mixing between layers produces phase-averaged vertical concentration profiles after large displacement in the direction of horizontal flow. For N high-permeability layers, (2.58) becomes

$$\alpha_{eff} = \frac{\sum_{j=1}^{N} \left\{ d''_j \alpha''_j + d'_j \alpha'_j \right\}}{\sum_{j=1}^{N} d_j} \tag{2.59}$$

Note that as an estimate, $d''_j \approx d'_j \approx d_j / 2$.

In the following section, we use representative values for the geohydrologic parameters to demonstrate the estimation of effective mass-transfer coefficient, and asymptotic dispersivity in a hypothetical stratification.

2.5.2 Application

Table 2.1 shows representative values for the geohydrologic parameters. The values used for d^* and seepage velocities are similar to those used by *Gillham et al.* (1984), and based on Borden aquifer data; the high-permeability layer and low-permeability layers are assumed to be sand and silt, respectively, and values assigned for their porosities in Table 2.1 are obtained from *Domenico and Schwartz* (1990, p.26, Table 2.1). The assumed dispersivities values however are attributed to the statistical variations of pore-water velocity in each layer. b_1 and b_2 are half the average thicknesses of silt and sand layers in the stratified system depicted in Figure 2.7, repectively, and whose values are displayed in Table 2.2a. Tables 2.2-2.4 show numerical evaluations of α_{eff} for a hypothetical stratified system of thickness 2.5 m shown in Figure 2.7 (four sand layers and five silt layers). For each case, thicknesses of the silt and sand layers are varied while maintaining the thickness of the stratification at 2.5 m. Figure 2.7 also shows the equivalent two-layered system with α_{eff} defined by (2.59), and β defined as the volume fraction of fillable voids in the silt layers to that in the sand layers; $\beta = b/d$. In the first case (Table 2.2a), the average thicknesses of the sand and silt layers in the hypothetical stratified system are 40 cm and 18 cm, respectively. For the equivalent two-layer system in this case (recall Figure 2.7), we have $\beta \approx 0.63$. Values of α at an individual two-layered subsystem are calculated from (2.48) and the effective α is estimated as $\alpha_{eff} \approx 1.7 \times 10^{-7}$ sec^{-1}. Using the result of *Van Genuchten and*

Table 2.1
Typical values for geohydrological parameters

Property		Property	
b_1 (cm)	9	θ_m	0.3
b_2 (cm)	20	α_L (cm)	4
D^* (cm^2/sec)	10^{-5}	α_T (cm)	0.25
u/θ_m (cm/sec)	3×10^{-4}	$\beta = \theta_1 b_1 / \theta_2 b_2$	0.64
θ_{im}	0.4	k	1.0

Table 2.2
Numerical evaluation of α_{eff} (case 1, $\beta = 0.625$)

j	d_j (cm)	b_j (cm)	α^u 10^{-7}(sec^{-1})	$d^u_j \alpha^u$ * 10^{-7}(sec^{-1})	α^l 10^{-7}(sec^{-1})	$d^l_j \alpha^l$ * 10^{-7}(sec^{-1})	α_{eff} 10^{-7}(sec^{-1})
1	50	20	1.108	27.7	1.694	42.35	
2	40	10	2.34	46.76	1.475	29.5	
3	40	20	1.475	29.5	1.078	21.56	
4	30	30	1.509	22.64	3.478	52.17	
5		10					
			$\sum d^u_j \alpha^u$ =	126.6	$\sum d^l_j \alpha^l$ =	145.58	1.7

* $d^l_j = d^u_j = d_j / 2$
$d = \sum d_j = d_1 + d_2 + d_3 + d_4$
$b = \sum b_j = b_1 / 2 + b_2 + b_3 + b_4 + b_5/2$

Table 2.3
Numerical evaluation of α_{eff} (case 2, $\beta = 1.12$)

j	d_j (cm)	b_j (cm)	α^u $10^{-7}(sec^{-1})$	$d^u_j \alpha^u$ * $10^{-7}(sec^{-1})$	α^l $10^{-7}(sec^{-1})$	$d^l_j \alpha^l$ * $10^{-7}(sec^{-1})$	α_{eff} $10^{-7}(sec^{-1})$
1	40	30	1.078	21.56	1.475	29.5	
2	30	20	2.105	31.58	1.758	26.37	
3	35	25	1.464	25.62	0.989	17.31	
4	20	40	1.837	18.37	5.902	59.02	
5		10					
			$\sum d^u_j \alpha^u$ =	97.13	$\sum d^l_j \alpha^l$ =	132.2	1.83

Table 2.4
Numerical evaluation of α_{eff} (case 3, $\beta = 2.33$)

j	d_j (cm)	b_j (cm)	α^u $10^{-7}(sec^{-1})$	$d^u_j \alpha^u$ * $10^{-7}(sec^{-1})$	α^l $10^{-7}(sec^{-1})$	$d^l_j \alpha^l$ * $10^{-7}(sec^{-1})$	α_{eff} $10^{-7}(sec^{-1})$
1	20	50	1.494	14.94	1.837	18.37	
2	10	40	3.83	19.15	3.83	19.15	
3	20	40	1.837	18.37	2.384	23.84	
4	30	30	1.509	22.64	3.478	52.17	
5		10					
			$\sum d^u_j \alpha^u$ =	75.1	$\sum d^l_j \alpha^l$ =	113.53	2.36

Dalton (1986) and *Goltz and Roberts* (1986) we may estimate the effective longitudinal-dispersion parameter for the equivalent two-layer system from the relationship

$$D_{x_{eff}} = \frac{1}{1+\beta} D_x \left(1 + \frac{\beta^2}{\alpha_{eff} D_x} \frac{u^2}{\theta_2^2 (1+\beta)^2} \right) \tag{2.60}$$

Equation (2.60) is useful only after large displacement in the mean flow direction. For α_{eff} = 1.7×10^{-7} sec^{-1} and $\beta = 0.63$, we have from (2.60):

$$D_{x_{eff}} \approx (12\times10^{-4}/1.63)(1 + [(0.63)^2\times(3\times10^{-4})^2)]/(1.7\times 10^{-7}\times12\times10^{-4}\times(1.63)^2) = 0.049 \text{ cm}^2/\text{sec}$$

for which the apparent longitudinal dispersivity is given by $\alpha_L^* = D_{x_{eff}} /(u/\theta_2) = 0.049/(3\times10^{-4})$ $\approx$ 163 cm (1.63 m). At this value of dispersivity, if we use the simple relation $\alpha_L^* = 0.1\ x$, based on field measurements (*Fetter*, 1993, Figure 2.17, p 72), the depth-averaged plume would have traveled a distance of 16 m in the direction of horizontal flow and spread out over a distance of order $3.625\sqrt{\alpha_L^* x} = 3.625 \times (1.63\times163)^{1/2} \approx 18.7$ m. The average thicknesses of the silt and sand layers in the second case (see, Table 2.2b) are 25 cm and 31.25 cm, respectively. In this case, we have $\beta \approx 1.1$ and α_{eff} = 1.83×10^{-7} sec^{-1}; similarly, $D_{x_{eff}} \approx 0.065$ cm^2/sec, and $\alpha_L^* \approx 218$ cm (2.2 m). The volume fraction of the silt is greater than that of the sand in the third case, and the average thicknesses are 34 cm and 20 cm, respectively (Table 2.2c). In this case, we have $\beta \approx$ 2.33, α_{eff} = 2.36×10^{-7} sec^{-1} ; $D_{x_{eff}} \approx 0.056$ cm^2 / sec, and $\alpha_L^* \approx 188$ cm (1.88 m).

The results of three cases above showed apparent longitudinal dispersivities an order of magnitude greater than the local longitudinal dispersivity shown in Table 1. Increasing the average thickness of silt layers relative to that of sand layers, increased slightly the values of α_{eff}, as Tables 2.2-2.4 indicate, and to a greater extent the values of β for the equivalent two-layer

system. Comparison between cases 1 and 2 indicates that as the value of β increased from 0.63 to 1.1, α_{eff} increased only slightly, and the apparent longitudinal dispersivity α_L^* increased significantly from 1.6 m to 2.2 m. However, as the volume fraction of silt layers increased significantly in case 3, β = 2.33, the apparent longitudinal dispersivity decreased considerably from 2.33 m (case 3) to 1.88 m, while α_{eff} increased slightly. With little inspection, equation (2.60) reveals that $D_{x_{eff}}$ is monotonically decreasing with α_{eff}; however, it increases with β for small values, up to a certain value and decreases thereafter. The increased apparent dispersivity in the sand layers is produced by the rate-limited sorption and desorption; when at a given section the contaminant mass being sorbed into the silt layers by transverse diffusion is released back, rather gradually, to the sand layers, as the plume passes that section, hence, resulting in the spreading of mobile-contaminant mass over a larger area. Such a phenomenon manifests itself in the often observed tailing (bleeding) of breakthrough curves in laboratory experiments (see, e.g., *Van Genuchten and Wierenga*, 1976); it occurs at relatively small values of β. For greater β, more space is available for the sorbed contaminant mass to diffuse inside the silt layers (zones of immobile contaminant), hence reducing the capacitance of these layers to release back the contaminant. The net effect being a reduced fraction of the contaminant-mass in the sand layers; consequently, a decrease in the apparent dispersivity of the mobile contaminant.

Although the local longitudinal dispersivity chosen here (see Table 2.1) is somewhat higher than observed values based on column experiments (0.01-0.51 cm), the calculations above, however, clearly indicate that field-scale mixing may be interpreted on the basis of a long-term transverse-diffusive-dispersive mixing in stratified systems.

2.6 Summary and Conclusions

Transport of contaminants in a stratified porous formation is modeled by averaging the governing local three-dimensional transport equations over the thickness of a two-layer system. The developed two-dimensional equations describe the capacitance effect of a low-permeability layer to store and release a reactive solute mass from and to a high-permeability layer. The development shows that the phenomenological first-order rate process prevails when the elapsed time is much greater than the characteristic time for diffusion (quasi-steady condition), and under small pore-water velocity. For reactive constituents, the first-order rate process is modified by introducing a sink/source, which is the product of the capacity ratio β multiplied by the solute concentration averaged over the thickness of the low-permeability layer. An explicit expression is obtained for the mass transfer coefficient α in terms of geometric properties, porosities of the layers, effective diffusion parameter, transverse-vertical dispersion in the high-permeability layer, and the capacity ratio β. In addition to molecular diffusion, the dependence of the coefficient of mass transfer α on transverse dispersion indicates that diffusive-like convective mixing can be another mechanism responsible for the solute exchange process. The results showed that the coefficient of mass transfer increases significantly with the magnitude of the flow velocity for small capacity ratio $\beta < 1$. Further, α showed approximately a linear dependence on the velocity for smaller values of the pore-water velocity, and a linear expression was obtained which relates the rate of increase of α with the flow velocity to the lateral dispersivity.

Application of the first-order rate model to interpret previously published experimental data showed some discrepancies; however, the results were consistent in describing the

mechanism of interlayer diffusive solute transfer. Further, the results were promising toward larger-scale applications whereby heterogeneities limit the use of available analytical solutions.

Application of the concept of diffusional transfer to larger scales is discussed in the context of a formation mass transfer coefficient, α_{eff}. The concept of effective mass transfer coefficient allows for the interpretation of field-scale dispersion in stratified formations.

Future efforts may be twofold. First, directed toward developing models applicable: (1) under large pore-water velocities, and (2) prior to a quasi-steady condition, where the time-scale of observations is smaller than the characteristic time of vertical transverse dispersion. Second, of practical significance, especially for pump-and-treat methods, is to attempt to describe the capacitance effect at the scale of strata that encompasses numerous layers. Such an effort is better rewarded if a stochastically-based averaging technique is implemented, because of uncertainties regarding the geometric properties and expected discontinuities of the low-permeability layers.

CHAPTER 3

ANALYTICAL SOLUTIONS

3.1 Abstract

Transverse diffusive transfer of solute mass between regions of mobile and immobile water is a key mechanism causing extensive tailing and reduced peak concentrations. In Chapter 2, we developed a two-dimensional first-order rate model that describes reactive solute transport averaged across the thickness of a two-layer system. The model describes the capacitance effect of low-permeability layers to store and release solute by diffusive-type mass transfer. In this chapter, we develop two-dimensional analytical solutions for the first-order rate model in an infinite porous medium, using the methods of Fourier and Laplace transforms, and superposition. The solutions consider a rectangular area at the source with (1) an instantaneous release of a contaminant mass, and (2) an exponentially-decaying source concentration applied at a fixed rate. Comparison of the theory with tracer chloride levels at the Borden aquifer indicates that first-order rate model can describe adequately the dispersion process on the basis of lateral or transverse diffusive mass transfer between layers.

3.2 Introduction

Prediction of spatial and temporal patterns of solute concentrations in a subsurface environment is hampered by natural heterogeneity of the porous media. While it is conventional to use advection-dispersion models to predict toxic levels in groundwater, there is overwhelming evidence in the literature that these models are strictly valid after an asymptotic state is achieved, and when the Fickian behavior prevails with uniquely defined effective dispersion parameters

(see, e.g., *Bear, 1977* and *Gelhar and Axness, 1983).* Until the asymptotic state is achieved, a non-Fickian behavior dominates and a unique dispersion parameter ceases to be meaningful. Because achieving this state is a slow process (usually after a large displacement), it is of primary interest to hydrologists to identify and model the mechanisms that are at work during the early development of the dispersion process.

In Chapter 2, a theory was presented whereby the non-Fickian behavior is explained on the basis of solute mass exchange between layers of contrasting permeability. A perfectly stratified two-layer system is considered in the analysis, and two-dimensional transport equations are derived by an averaging technique that describes transport of a reactive solute in a high- and low-permeability layer. The phenomenological first-order rate process is shown to prevail under a quasi-steady condition, and a uniquely defined porous-media coefficient of mass transfer is developed. The developed equations describe solute transfer into and out of low-permeability zones by a diffusive-type mass transfer, produced by the combined effect of mechanical mixing (transverse vertical dispersion) and molecular diffusion. The findings complement the vast literature in the area of solute transport in mobile-immobile phase, soils, fractured rocks, and stratified porous formations (see, e.g., *Passioura, 1971; Skopp and Warrick, 1974; Van Genuchten and Wierenga, 1976; Rao et al., 1980; Grisak and Pickens, 1980; Tang et al., 1981; Sudicky et al.*, 1985; *Gillham et al., 1984; Bond and Wierenga, 1990; and Piquemal, 1993*). These efforts attribute early dispersion of inert toxic material to diffusive mass transfer between zones of mobile and immobile water, and that slow exchange of material between these zones is the main mechanism responsible for the observed decrease in peak concentration and considerable tailing.

In this chapter, we solve the two-dimensional and coupled equations in an infinite-domain, analytically. The solution considers a reactive constituent emanating from a rectangular source at: (1) an instantaneous rate, and (2) an exponentially-decaying rate, and the specific case of a uniform application during a finite period of time follows as a specific case of the exponentially-decaying rate. The solutions are obtained using the approach of *Goltz and Roberts* (1986) and *Lindstrom and Narasimhan* (1973), and the method of superposition to integrate the point-source solution in space and time, in order to account for a nonpoint source and a continuous injection in time. The former investigators developed a three-dimensional analytical solution for the linear first-order rate model, in an infinite domain for an instantaneous point source. *Carnahan and Remer* (1984) obtained three-dimensional solutions for various initial condition geometries. Also, one-dimensional analytical solutions have been developed for first-order rate models in semi-infinite domains (see, e.g., *Lindstrom and Stone*, 1974; *Van Genuchten and Wierenga*, 1976; and *De Smedt and Wierenga*, 1979). Rather than considering a first-order rate process, *Tang and Aral* (1992) integrated a general three-dimensional transport equation over a leaky aquifer thickness and solved the resulting two-dimensional equation analytically. By integrating over the aquifer thickness, they accounted for the effect of diffusive and convective transfer into the aquitard, on the transport of the solute in the main aquifer. *Haggerty and Gorelick* (1995) suggested a multiple-site mass transfer model using a series of first-order equations. They obtained solutions for the specific cases of no flow, analytically in terms of matrix exponential, fast flow, by solving directly for a series of first-order and ordinary linear differential equations, and a semianalytical solution for radial flow to a pumping well.

3.3 Solutions

For an instantaneous point source, the two-dimensional transport of a reactive contaminant in regions of mobile and immobile water can be described by the following equations

$$\frac{\partial C_m}{\partial t} + \beta \frac{\partial C_{im}}{\partial t} + \beta k C_{im} = D_x \frac{\partial^2 C_m}{\partial x^2} + D_y \frac{\partial^2 C_m}{\partial y^2} - u \frac{\partial C_m}{\partial x} - k C_m \tag{3.1}$$

$$\beta \frac{\partial C_{im}}{\partial t} + \beta k C_{im} = \alpha (C_m - C_{im}) - k C_m \tag{3.2}$$

in which C_m is the solute concentration in a high-permeability layer (zone of mobile water) [M/L^3]; C_{im} is the solute concentration in a low-permeability layer (zone of immobile water) [M/L^3]; D_x and D_y are the dispersion coefficients in the x and y directions, respectively, [L^2/T]; u is the average groundwater velocity, assumed in the x direction, [L/T]; k is the decay-rate constant [T^{-1}]; α is a first-order mass transfer rate constant whose expression is shown in equation (3.3) [T^{-1}]; and β is a capacity ratio coefficient which is defined in (3.4a). Equation (1) describes two-dimensional advective-dispersive transport of a reactive solute in the mobile phase, with a distributed source/sink term (second on the left-hand side). The source/sink term is described by a first-order rate expression in (3.2), which accounts in an average sense for the capacity of low-permeability zones (of immobile water) to absorb and release solute mass by molecular diffusion. In Chapter 2, general forms of equations (3.1) and (3.2) were developed by averaging across thicknesses of layers (i.e., in the vertical direction), and they are valid for thin layers and under quasi-steady conditions. A closed-form expression for the mass transfer coefficient α is obtained,

$$\alpha = \frac{3\theta_{im}^{\ 2} D^*}{\theta_m^{\ 2} b_m^{\ 2} (\nu + \beta)} \tag{3.3}$$

in which

$$\beta = \frac{\theta_{im} b_{im}}{\theta_m b_m} \tag{3.4a}$$

$$\nu = \frac{\theta_{im}^{\ 2} D^*}{\theta_m^{\ 2} D_z} \tag{3.4b}$$

where b_{im} and b_m are the thicknesses of thin low-permeability and high-permeability layers, respectively, [L]; D^* is the effective molecular diffusion coefficient [L^2/T]; D_z is the transverse vertical dispersion parameter in the high-permeability layer; and θ_{im} and θ_m are the porosities of the low-permeability and high-permeability layers, respectively. In the following section, we develop solutions to (3.1) and (3.2) in an infinite domain, using the methods of Laplace and Fourier transforms, for the two cases of instantaneous injection of a point source and a continuous injection of a nonpoint source of the contaminant.

3.3.1 Instantaneous Injection of a Point Mass

The initial and boundary conditions, in this case, can be written as

$$C_m(\pm\infty, y, t) = C_m(x, \pm\infty, t) = 0 \tag{3.5a}$$

$$C_m(x, y, 0) = \frac{\Delta M}{B} \delta(x) \delta(y) \tag{3.5b}$$

$$C_{im}(x, y, 0) = 0 \tag{3.5c}$$

in which ΔM is an incremental mass injected over a depth B, at time zero; and $\delta(x)$ and $\delta(y)$ are Dirac delta functions. Taking the Laplace transform of (3.1) and (3.2), and using the initial conditions (3.5b) and (3.5c), one obtains

$$s\overline{C_m} - \frac{\Delta M}{B}\delta(x)\delta(y) + \beta\, s\overline{C_{im}} + \beta\, k\,\overline{C_{im}} + k\,\overline{C_m} = D_x \frac{\partial^2 \overline{C_m}}{\partial x^2} + D_y \frac{\partial^2 \overline{C_m}}{\partial y^2} - u\frac{\partial \overline{C_m}}{\partial x} \tag{3.6}$$

$$\beta\, s\overline{C_{im}} + \beta\, k\,\overline{C_{im}} = \alpha\,(\overline{C_m} - \overline{C_{im}}) \tag{3.7}$$

in which $\bar{f}(x,y,s)$ is the Laplace transform of the function $f(x,y,t)$,

$$\bar{f}(x,y,s) = \int_0^\infty e^{-st} f(x,y,t)\, dt \tag{3.8}$$

Solving (3.7) in terms of $\overline{C_{im}}$, we obtain

$$\overline{C_{im}} = \frac{\alpha}{\alpha + \beta\, k + \beta\, s}\overline{C_m} \tag{3.9}$$

The substitution of (3.9) into (3.6) yields the following partial differential equation in the Laplace transform space:

$$D_x \frac{\partial^2 \overline{C_m}}{\partial x^2} + D_y \frac{\partial^2 \overline{C_m}}{\partial y^2} - u\frac{\partial \overline{C_m}}{\partial x} - \left(s + \frac{(\beta\, s + \beta\, k)\alpha}{\alpha + \beta\, k + \beta\, s} + k \right) \overline{C_m} = -\frac{\Delta M}{B}\delta(x)\delta(y) \tag{3.10}$$

with the boundary conditions:

$$\overline{C_m}(\pm\infty, y, t) = \overline{C_m}(x, \pm\infty, t) = 0 \tag{3.11}$$

Following *Goltz and Roberts* (1986), the solution of (3.10) in the Fourier transform space, after the use of (3.11), is given by

$$\hat{C}_m(p,q,s) = \frac{\Delta M / B}{D_x\, p^2 + D_y\, q^2 + u\, i\, p + N^2} \tag{3.12}$$

where $\hat{C}_m(p,q,s)$ is the Fourier transform of $\overline{C_m}(x,y,s)$,

$$\hat{C}_m(p,q,s) = \int_{-\infty}^{+\infty}\int_{-\infty}^{+\infty} e^{-i(px+qy)}\, \overline{C_m}(x,y,s)\, dx\, dy \tag{3.13}$$

and

$$N^2 = s + (\frac{\alpha}{\beta} + k) + \frac{(-\alpha^2/\beta)}{s + (\frac{\alpha}{\beta} + k)} + (\alpha - \frac{\alpha}{\beta}) \tag{3.14}$$

The inverse Fourier transform of (3.12) can be shown to be (see, *Goltz and Roberts*, 1986)

$$\overline{C_m}(x,y,s) = \frac{\Delta M}{2\pi B\sqrt{D_x D_y}} e^{\frac{u}{2D_x}x} K_0\left\{\sqrt{\left(\frac{u^2}{4D_x} + N^2\right)\left(\frac{y^2}{D_y} + \frac{x^2}{D_x}\right)}\right\} \tag{3.15}$$

where $K_0[x]$ is a zero-order modified Bessel function. Following the method of *Lindstrom* and *Narasimhan* (1973), the inverse Laplace transform of a function, $\bar{f}(s)$, that can be expressed explicitly in terms of the variable z = $s + K + \frac{a}{s+K}$ (i.e., $\bar{f}(s) \equiv \bar{g}(z = s + K + \frac{a}{s+K})$), is given by

$$f(t) = e^{-Kt}\frac{\partial}{\partial t}\int_0^t J_0[2\sqrt{a(t-\tau)\tau}]\, g(\tau)\, d\tau \tag{3.16}$$

in which

$$g(\tau) = L^{-1}{}_z\left\{\bar{g}(z) \equiv \bar{f}(z = s + K + \frac{a}{s+K})\right\} \tag{3.17}$$

where $J_0[x]$ is a zero-order Bessel function and $L^{-1}{}_z$ denotes the inverse Laplace transform with respect to the variable z. The substitution of (3.14) into (3.15) and the use of (3.16) and (3.17), lead to

$$\begin{aligned} C_m(x,y,t) = \frac{\Delta M}{2\pi B\sqrt{D_x D_y}} \exp\left\{\frac{u}{2D_x}x - (\frac{\alpha}{\beta} + k)t\right\} \frac{\partial}{\partial t}\int_0^t \left\{ I_0[2\frac{\alpha}{\sqrt{\beta}}\sqrt{(t-\tau)\tau}\right. \\ \left. \cdot \frac{1}{2\tau}\exp\left\{-\left(\frac{u^2}{4D_x} + (\alpha - \frac{\alpha}{\beta})\right)\tau + \frac{1}{4\tau}\left(\frac{x^2}{D_x} + \frac{y^2}{D_y}\right)\right\} d\tau \end{aligned} \tag{3.18}$$

in which we have used the identity $J_0[ix] = I_0[x]$, and the inverse Laplace transform result (*Roberts and Kaufman*, 1966)

$$L^{-1}{}_z\left\{K_0\left[b\sqrt{d+z}\right]\right\} = \frac{1}{2t}\exp\left\{-\left(dt + \frac{b^2}{4t}\right)\right\} \tag{3.19}$$

By using the Leibnitz rule

$$\frac{\partial}{\partial t}\int_{a(t)}^{b(t)} f(t,\tau)\,d\tau = \int_{a(t)}^{b(t)} \frac{\partial f}{\partial t}\,d\tau + f(t,b(t))\frac{db(t)}{dt} - f(t,a(t))\frac{da(t)}{dt}$$

and the identity $d/dx\{I_0[ax]\} = a\,I_1[ax]$, the integration of (3.18) yields the solution

$$C_m(x,y,t) = \frac{\exp\{-(\alpha + k_m)t\}}{t} G(x,y,t) + \alpha \int_0^t H(t,\tau)\,G(x,y,\tau)\,d\tau \tag{3.20a}$$

in which

$$H(t,\tau) = \frac{I_1\left[2\dfrac{\alpha}{\sqrt{\beta}}\sqrt{(t-\tau)\tau}\right]}{\sqrt{\beta\,(t-\tau)\tau}} \exp\left\{-\frac{\alpha}{\beta}(t-\tau) - \alpha\tau - kt\right\} \tag{3.20b}$$

$$G(x,y,\tau) = \frac{\Delta M}{4\pi B\sqrt{D_x D_y}} \exp\left\{-\frac{1}{4\tau}\left[\frac{(x-u\tau)^2}{D_x} + \frac{y^2}{D_y}\right]\right\} \tag{3.20c}$$

where $I_0[x]$ and $I_1[x]$ are modified Bessel functions of zero and first order, respectively. For inert (nonreactive) constituents, k = 0, and equations (3.20a)-(3.20c) reduce to those suggested by *Harvey and Gorelick* (1995), as a special case of the three-dimensional solution of *Roberts and Goltz* (1986). In the following section, we use the elementary solution (3.20a)-(3.20c) to develop a more general one applicable for a nonpoint source and continuous injection of the solute at the source. In specific, we consider the case of an exponentially-decaying source that is introduced to the water table from a rectangular area.

3.3.2 Instantaneous Injection From a Rectangular-Source Area

Figure 3.1 shows, schematically, the application area of size l_x and l_y in the x and y directions. An incremental solute mass **dM**, introduced at time $t = 0$, over an infinitesimal area $dA = d\xi\, d\eta$ and depth B, can be written as $dM = C_0(\xi,\eta)\, B\, d\xi\, d\eta$, in which $C_0(\xi,\eta)$ is the initial concentration at a point whose coordinates are (ξ,η). The concentration of the mobile solute dC_m at point (x,y) (see, Figure 3.1), produced by dM, can be expressed on the basis of the elementary solution (3.20a)

$$dC_m(x,y,t) = \frac{e^{-(\alpha+k)t}}{t} G(x-\xi, y-\eta, t) + \alpha \int_0^t H(t,\tau)\, G(x-\xi, y-\eta, \tau)\, d\tau \qquad (3.21a)$$

Because of the linearity of equations (3.1) and (3.2), we can use the method of superposition to obtain the contribution of the rectangular source area, shown in Figure 3.1. In this case, we integrate the elementary solution (3.21a) with respect to $d\xi$ and $d\eta$

$$\begin{aligned} C_m(x,y,t) = & \int_{-l_y/2}^{l_y/2} \int_{-l_x/2}^{l_x/2} \frac{e^{-(\alpha+k)t}}{t} G(x-\xi, y-\eta, t)\, d\xi\, d\eta \\ & + \alpha \int_0^t \int_{-l_y/2}^{l_y/2} \int_{-l_x/2}^{l_x/2} H(t,\tau)\, G(x-\xi, y-\eta, \tau)\, d\xi\, d\eta\, d\tau \end{aligned} \qquad (3.21b)$$

in which we have interchanged the order of integration in the second integral, because of the continuity of the integrand with respect to τ. Noting that $H(t,\tau)$ is independent of ξ and η, we can rewrite (3.21b) as

$$\begin{aligned} C_m(x,y,t) = & \frac{e^{-(\alpha+k)t}}{t} \int_{-l_y/2}^{l_y/2} \int_{-l_x/2}^{l_x/2} G(x-\xi, y-\eta, t)\, d\xi\, d\eta \\ & + \alpha \int_0^t H(t,\tau) \left\{ \int_{-l_y/2}^{l_y/2} \int_{-l_x/2}^{l_x/2} G(x-\xi, y-\eta, \tau)\, d\xi\, d\eta \right\} d\tau \end{aligned} \qquad (3.21c)$$

in which, from (3.20c),

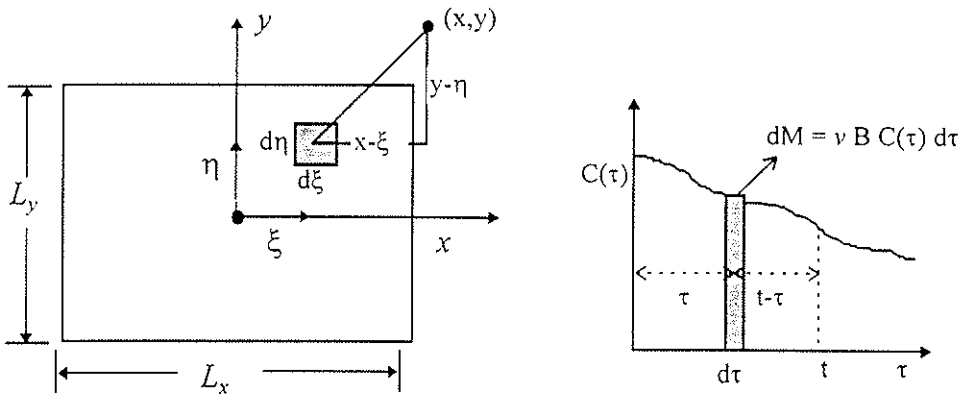

(a) (b)

Figure 3.1 Schematic representation of a contaminant source: (a) rectangular source area; and (b) temporal variation of a contaminant mass at the source.

$$\int_{-l_y/2}^{l_y/2}\int_{-l_x/2}^{l_x/2} G(x-\xi,y-\eta,\tau)\,d\xi\,d\eta = \frac{C_0}{4\pi\sqrt{D_x D_y}}\left\{\int_{-l_x/2}^{l_x/2}\exp\left(-\frac{(x-\xi-u\tau)^2}{4D_x\tau}\right)d\xi\right\} \tag{3.21d}$$

$$\bullet\left\{\int_{-l_y/2}^{l_y/2}\exp\left(-\frac{(y-\eta)^2}{4D_y\tau}\right)d\eta\right\}$$

where C_0 is assumed to be constant. Using the transformations $\xi^* = \frac{\xi-(x-u\tau)}{2\sqrt{D_x\tau}}$ and $\eta^* = \frac{\eta-y}{2\sqrt{D_y\tau}}$, equation (3.21d) can be rewritten as

$$\int_{-l_y/2}^{l_y/2}\int_{-l_x/2}^{l_x/2} G(x-\xi,y-\eta,\tau)\,d\xi\,d\eta = \frac{C_0}{4\pi\sqrt{D_x D_y}}\sqrt{\pi D_x\tau}\;L(x,\tau)\sqrt{\pi D_y\tau}\;F(y,\tau) \tag{3.21e}$$

in which $L(x,\tau)$ and $F(y,\tau)$ are defined below. Finally, the substitution of (3.21e) into (3.21c) yields the solution

$$\frac{C_m(x,y,t)}{C_0} = e^{-(\alpha+k)t}\,L(x,t)\,F(y,t) + \alpha\int_0^\tau H(t,\tau)\,L(x,\tau)\,F(y,\tau)\,d\tau \tag{3.22a}$$

where

$$L(x,\tau) = \frac{1}{2}erf\left(\frac{l_x/2+|x-ut|}{2\sqrt{D_x\tau}}\right) - \frac{1}{2}erf\left(\frac{-l_x/2+|x-ut|}{2\sqrt{D_x t}}\right), \quad if\ |x-ut| > l_x/2$$

$$= \frac{1}{2}erf\left(\frac{l_x/2-(x-ut)}{2\sqrt{D_x t}}\right) + \frac{1}{2}erf\left(\frac{l_x/2+(x-ut)}{2\sqrt{D_x\tau}}\right), \quad if\ |x-ut| \le l_x/2 \tag{3.22b}$$

$$F(y,\tau) = \frac{1}{2}erf\left(\frac{l_y/2+|y|}{2\sqrt{D_y\tau}}\right) - \frac{1}{2}erf\left(\frac{-l_y/2+|y|}{2\sqrt{D_y\tau}}\right), \quad if \quad |y| > l_y/2$$

$$= \frac{1}{2}erf\left(\frac{l_y/2-y}{2\sqrt{D_y\tau}}\right) + \frac{1}{2}erf\left(\frac{l_y/2+y}{2\sqrt{D_y\tau}}\right), \quad if \quad |y| \le l_y/2 \tag{3.22c}$$

Equations (3.22a)-(3.22c) and (3.20b) describe the effect of diffusive sorption and desorption by low-permeability zones, on an advective-dispersive and reactive contaminant plume, whose initial dimensions and concentration are $B \times l_x \times l_y$ and C_0, respectively.

3.3.3 Continuous Injection From a Rectangular-Source Area

For a continuous source of concentration $C_0(\xi,\eta,\tau^*)$, the injection rate of a contaminant mass M, normal to an incremental area $dA = d\xi\, d\eta$ of the source (Figure 3.1), can be written as

$$\frac{dM}{d\tau^*} = v\, C_0(\xi,\eta,\tau^*)\, d\xi\, d\eta \tag{3.23a}$$

in which v is the recharge flux (e.g., accretion to the water table, or recharge to a confined aquifer by leakage) [L/T]. During an infinitesimal time increment $d\tau^*$ (see, Figure 3.1), and assuming a spatially uniform concentration at the source, i.e., $C_0(\xi,\eta,\tau^*) = C_0(\tau^*)$, the incremental contaminant mass dM is given by

$$dM = v\, C_0(\tau^*)\, d\xi\, d\eta\, d\tau^* \tag{3.23b}$$

Because $d\tau^*$ is infinitesimally small, the concentration of the mobile solute can be expressed by the elementary solution

$$dC_m(x,y,t) = \frac{e^{-(\alpha+k)(t-\tau^*)}}{t-\tau^*} G(x-\xi, y-\eta, t-\tau^*) + \alpha \int_0^{t-\tau^*} H(t-\tau^*,\tau)\, G(x-\xi, y-\eta, \tau)\, d\tau \tag{3.24}$$

Once again, because of linearity, we substitute (3.23b) into (3.24) and use the method of superposition to integrate (3.24) with respect to ξ, η, and τ^*. This can be shown to be

$$B\, C_m(x,y,t) = \int_0 e^{-(\alpha+k_m)(t-\tau^*)}\, v\, C_0(\tau^*)\, L(x,t-\tau^*)\, F(y,t-\tau^*)\, d\tau^* + \gamma \int_0 \int_0^{-\tau^*} v\, C_0(\tau^*)\tau\, H(t-\tau^*,\tau)\, L(x,\tau)\, F(y,\tau)\, d\tau\, d\tau^* \tag{3.25a}$$

which upon the use of the linear transformation $\eta = t - \tau^*$, can be expressed as

$$BC_m(x,y,t) = \int_0^t e^{-(\alpha+k_m)\eta}\, \nu C_0(t-\eta)\, L(x,\eta)\, F(y,\eta)\, d\eta + \gamma \int_0^t \int_0^\eta \nu C_0(t-\eta)\tau\, H(\eta,\tau)\, L(x,\tau)\, F(y,\tau)\, d\tau\, d\eta \tag{3.25b}$$

Because of the continuity of the integrand, in the second integral, with respect to τ, following *Lindstrom and Stone* (1974), we can interchange the order of integration and rewrite (3.25b) as

$$BC_m(x,y,t) = \int_0^t e^{-(\alpha+k)\eta}\, \nu C_0(t-\eta)\, L(x,\eta)\, F(y,\eta)\, d\eta + \alpha\, \nu \int_0^t \tau\, L(x,\tau)\, F(y,\tau) \int_\tau^t C_0(t-\eta)\, H(\eta,\tau)\, d\eta\, d\tau \tag{3.25c}$$

If we consider the specific case of $C_0(t) = C_0 e^{-at}$, then the inner integral of the second term is evaluated by parts, after the use of (3.20b), as

$$\int_\tau^t C_0 e^{-a(t-\eta)} H(\eta,\tau)\, d\eta = C_0 \frac{e^{-at+(\frac{\alpha}{\beta}-\alpha)\tau}}{\alpha\tau}\left\{ e^{(a-\frac{\alpha}{\beta}-k)t}\, I_0[2\frac{\alpha}{\sqrt{\beta}}\sqrt{(t-\tau)\tau}] - e^{(a-\frac{\alpha}{\beta}-k)\tau} - (a-\frac{\alpha}{\beta}-k)\int_\tau^t e^{(a-\frac{\alpha}{\beta}-k)\eta} I_0[2\frac{\alpha}{\sqrt{\beta}}\sqrt{(\eta-\tau)\tau}]\, d\eta \right\} \tag{3.25d}$$

The integral on the right-hand side is first transformed using the transformation $\eta^* = \eta - \tau$, and then evaluated using the results *Lindstrom and Stone* (1974),

$$\int_\tau^t e^{(a-\frac{\alpha}{\beta}-k)\eta} I_0[2\frac{\alpha}{\sqrt{\beta}}\sqrt{(\eta-\tau)\tau}]\, d\eta = \frac{e^{(a-\frac{\alpha}{\beta}-k)\tau}}{\frac{\alpha}{\beta}-a+k}\left\{ e^{\frac{\alpha^2\tau}{\beta(\frac{\alpha}{\beta}-a+k)}} - e^{-(\frac{\alpha}{\beta}-a+k)(t-\tau)} \sum_{m=0}^{\infty} \left(\frac{\alpha}{(\frac{\alpha}{\beta}-a+k)\sqrt{\beta}} \sqrt{\frac{\tau}{t-\tau}} \right)^m I_m[2\frac{\alpha}{\sqrt{\beta}}\sqrt{(t-\tau)\tau}] \right\} \tag{3.25e}$$

Finally, we substitute (3.25e) and (3.25d) into (3.25c) to obtain the solution

$$\frac{C(x,y,t)}{C_0} = \frac{v}{B}\int_0 L(x,\tau)\,F(y,\tau)\,H^{\cdot}(t,\tau)\,d\tau \tag{3.26a}$$

where

$$H^{\cdot}(t,\tau) = \exp\left\{-a(t-\tau) - (\alpha + k - \frac{\alpha^2}{(\alpha - \beta\, a + \beta\, k)})\tau\right\} - \left\{e^{-(\frac{\alpha}{\beta}+k)(t-\tau)-(\alpha+k)\tau}\right.$$
$$\left.\bullet\sum_{m=1}^{\infty}\left(\frac{\alpha}{(\frac{\alpha}{\beta} - a + k)\sqrt{\beta}}\sqrt{\frac{\tau}{t-\tau}}\right)^m I_m[2\frac{\alpha}{\sqrt{\beta}}\sqrt{(t-\tau)\tau}]\right\} \tag{3.26b}$$

The solution given by (3.26a) and (3.26b) describes two-dimensional mobile-phase solute concentrations, originating from a rectangular source area, at a fixed rate and exponentially-decaying input concentrations.

3.4 Application and Discussion

The simulation results presented here are obtained by integrating (3.22) and (3.26) numerically, using Romberg method. Because the function $L(x,\tau)$ behaves as a finite pulse in the interval $\tau \in [0,t]$, it is numerically efficient to scan this function with respect to τ before evaluating the integrals in (3.22) and (3.26). Based on observation, we may reduce the integration time interval to $[\max\{0, a_1(t)\}, \min\{t, b_1(t)\}]$, where $a_1(t) = [(x - l_x/2)/u] - (4/u)\sqrt{D_x' t}$; $b_1(t) = [(x + l_x/2)/u] + (4/u)\sqrt{D_x' t}$; and the constant 4, which is multiplied by the square-root expression, is adjustable based on the pulse width; i.e., the value of the longitudinal dispersion parameter D_x. Note that if $b_1(t)$ is negative, the concentration at x is zero, and the contaminant pulse is yet to arrive there at time t.

Figure 3.2 shows the effect of adsorption sites in a low-permeability layer on the dispersion of a solute along the mean flow direction in the high-permeability layer. The relative concentrations are obtained at t = 80 days and y = 0 m, using equation (3.26) and the data: D^* = 1.21×10^{-9} m^2/s; u = 0.1 m/day; α_L = 1.0 cm; α_{TL} = 1 mm; α_{Tv} = 0; θ_{im} = 0.45; θ_m = 0.35; b_m = 15 cm; β = 0.25; L_x = 1.0 m; L_y = 2.0 m; and k = 0.01 day^{-1}. The solute is assumed to be introduced over the application area at a constant rate; i.e., a = 0.0, and over a finite period t_0 = 5 days. Because of linearity of the transport equations, mobile-phase concentrations at t greater than t_0 can be obtained by superposition $C_m(x,y,t)$ - $C_m(x,y,t-t_0)$. Using the above data, the coefficient of mass transfer, in the absence of adsorption, can be predicted using (3.3) and (3.4), α = 0.012 day^{-1}. For simulating linear equilibrium adsorption in the immobile phase, the apparent diffusion parameter used in (3.26) is D^*/R, where R is the retardation factor in the immobile zone. This has the effect of slowing down the rate of mass transfer by reducing the coefficient α. The relative concentration profiles in Figure 3.2 show that retardation in the immobile phase offsets the capacitance effect. The latter is characterized by slow mass exchange between the low- and high-permeability layers that causes a significant decrease in peak mobile-phase concentration and considerable tailing. Note that, from Figure 3.2, at a large retardation factor R = 50, the solute plume is nearly symmetric and showing insignificant tailing with a larger peak concentration. Thus, assuming equilibrium adsorption, the effect of diffusive transfer between the two regions appears to diminish with increasing retardation, which is expected since retardation reduces the apparent diffusion parameter and, consequently, limits the rate of mass transfer. Because the organic carbon fraction in clayey and silt material can be much greater than in sandy material, we will assume that retardation in the latter can be ignored relative to that in the former. Thus, based

on the results of Figure 3.2, and assuming equilibrium adsorption, leachates of organic solutes (e.g., pesticides) that have small distribution coefficients (i.e., least retarded) are likely to show the kind of asymmetric and dispersed behavior that is displayed in Figure 3.2; especially, in aquifers containing a significant volume of material in which diffusion dominates.

In Chapter 2, it was shown on the basis of (3.3) and (3.4), that a dispersive mechanism of a convective nature, under relatively large pore-water velocity u, can influence the interlayer solute mass transfer significantly. The analysis that led to the derivation of the transport equations (3.1) and (3.2), and the explicit expression (3.3) for the coefficient of mass transfer α, remain valid for slowly moving solutes. Although it raises questions about the validity of the linear first-order model (3.2) at large flow velocities (e.g., *Coats and Smith*, 1964), nevertheless, it does not necessarily preclude the fact that u depends on α according to (3.3) and (3.4b), even for large pore-water velocities. The relationship between the coefficient of mass transfer α and the pore-water velocity has been observed in the laboratory and reported in the literature by numerous investigators (*Coats and Smith*, 1964; *Bennet and Goodridge*, 1970; *Baker*, 1977; *Van Genuchten and Wierenga*, 1977; *Rao et al.*, 1980; *De Smedt and Wierenga*, 1984; and *Raven et al.*, 1988). Figure 3.3 shows the effect of mechanical mixing, through vertical transverse dispersivity, on the dispersion of a nonreactive solute in a high-permeability layer (mobile phase), and compares the results to predictions based on the expression of *Parker and Valocchi* (1986), for the mass transfer coefficient $\alpha = 3\theta_{im}^{2} D^{*} / \theta_{m}^{2} b_{m}^{2} \beta$. The effect of vertical transverse dispersion on α in (3.3) is explicit through the coefficient v defined in (3.4b). The results predict relative concentrations along the mean-flow direction at $y = 0$ and $t = 8.0$ days, using the following parameter values: $D^{*} = 1.21 \times 10^{-9}$ m^2/s; $u = 10$ m/day; $\alpha_L = 1.0$ cm; $\alpha_{TL} = 1$ mm; $\alpha_{Tv} =$

0.1 mm; $\theta_{im} = 0.45$; $\theta_m = 0.35$; $b_m = 15$ cm; $\beta = 0.2$; $L_x = 1.0$ m; $L_y = 2.0$ m; and $k = 0.0$ day^{-1}. Also, the solute is assumed to be introduced over the application area at a constant rate; i.e., a = 0.0, and over a finite period $t_0 = 1$ day. Under large pore-water velocities, the characteristic time for vertical transverse dispersion in a high-permeability layer, b_m^2/D_z, is much less than that for molecular diffusion in the low-permeability layer, b_{im}^2/D^*. In effect, $v \rightarrow 0$, and equation (3.3) reduces to the expression of *Parker and Valocchi* (1986). In this case, $\alpha = 0.115$ day^{-1} is relatively small, causing a significant decrease in peak concentration and considerable tailing, as shown by the dotted line in Figure 3.3. In the absence of vertical transverse dispersion, $\alpha_{TV} = 0.0$ cm, we have $D_z = D^*$, $v = 1.65$, and (3.3) predicts $\alpha = 0.012$ day^{-1}, which is an order of magnitude smaller than that predicted on the basis of *Parker and Valocchi* (1986). Consequently, the use of (3.3) in (3.26) predicts a much greater peak concentration and almost a symmetric profile with insignificant tailing, as indicated by the dashed line in Figure 3.3. If $\alpha_{TV} = 0.1$ mm, mechanical dispersion dominates over molecular diffusion in the mobile phase, $D_z = D^* + \alpha_{TV}\, u$ $= 1.28 \times 10^{-8}$ m^2/s, $v = 0.156$; thus, (3.3) predicts $\alpha = 0.065$ day^{-1}. Comparison with the case of zero vertical transverse dispersivity indicates that transverse vertical dispersion (mechanical mixing) reduces peak concentration and increases tailing significantly in the high-permeability layer, as shown by the solid curve in Figure 3.3. In contrast, predictions of mobile concentrations using α based on the expression by *Parker and Valocchi* (1986), exaggerate the capacitance effect.

Figures 3.4 and 3.5 demonstrate the application of equation (3.22) to Borden aquifer data adapted from *Sudicky et al.* (1983). In the experiment, a dilute solution of tracer chloride is injected during a period of one hour at depths between 1 and 1.43 m below the water table. The

initial plume length was reported to be 4 m in length, in the y direction, by 1 m in width, in the x direction, and a vertical thickness of 0.5 m. Because of local heterogeneity, the initial plume separated into two halves after few days of migration from the injection wells, with one-half moving horizontally at an average velocity of 25 cm/day while the other half at a slower rate of 7 cm/day. Figure 3.4 compares measured breakthrough at x = 1.75 m to predictions based on the instantaneous-mass injection solution (3.22), calibrated with the data: $D^* = 0.48 \times 10^{-5}$ cm^2/s; u = 0.07 m/day; α_L = 1.0 cm; α_{TL} = 0.5 mm; α_{Tv} = 0.01 mm; θ_{im} = 0.38; θ_m = 0.38; b_m = 10 cm; β = 0.25; L_x = 1.1 m; L_y = 1.75 m; and k = 0.0 day^{-1} . The value of the effective molecular diffusion above is smaller than that suggested by *Gillham et al.* (1984), and that estimated in Chapter 2, for the fast zone, by fitting theoretical longitudinal variances in the fast zone to measurements. In both cases, vertical transverse and diffusive-type mass transfer, between zones of contrasting permeability, is considered as a possible dispersive mechanism during the early development of the chloride plume. The former applied an advection-diffusion model (essentially, a matrix diffusion model) to estimate the longitudinal variances, while the latter relied on first-order rate models for the calibration. For the typical value of free-solution diffusion coefficient $D = 1.5 \times 10^{-5}$ cm^2/s, the fitted value for the effective diffusion coefficient D^* yielded a tortuosity factor of 0.32. This value is within the range [0.3-0.7] reported by *Bear* (1972). The suggested values for the porosities are based on the average value reported by *Sudicky et al.* (1983), while the values of the dispersivities are typical for granular porous media. Based on the calibrated capacity ratio β = 0.25, the effective coefficient of mass transfer is estimated to be α = 0.01 day^{-1}. Figures 3.5a and 3.5b compare predicted spatial distribution of relative concentrations with measurements, along the mean flow direction, at t = 21 and 121 days and y = 0.0 m. The predictions are made

using the first-order rate model (3.22) and slightly adjusting the initial plume length to 1.4 m. Such adjustment of the initial plume length confirms to the value of 1.5 m suggested by *Gillham et al.* (1984), by fitting the estimated longitudinal variances in the fast zone to the measured ones. The reasonable match between the first-order model (3.22) and observations indicates that, before the plume grows in size and becomes overwhelmed by larger-scale heterogeneities (i.e., stochastic convection), the capacitance effect can be the mechanism responsible, perhaps at the early stages of the development of the plume, for the dispersion of tracer chloride in the Borden aquifer. Although the predictions in Figs. 3.4 and 3.5 are reasons to physically interpret the dispersion mechanism on the basis of diffusive-type transfer, between zones of contrasting permeability, they, however, are based on (3.22), which assumes continuous layers of uniform thicknesses. Unfortunately, this is not the case in general, where heterogeneities manifest themselves also by nonuniform thicknesses of the layers and their spatial discontinuities. Thus, calibrating the initial plume length to larger than what is observed may be a curve-fitting artifact intended to offset the exaggerated diffusive sorption into low-permeability layers by assuming continuous layering.

3.5 Summary and Conclusions

In stratified porous media, the non-Fickian behavior during the early development of a dispersion process can be modeled as a process of transverse mixing between layers of contrasting permeability. It has been shown in Chapter 2 that interlayer diffusive-type mass transfer can be described by a first-order physically rate-limited sorption process, when the time scale of interest is much greater than the characteristic time for molecular diffusion in a typical low-permeability layer and under the condition of small pore-water velocity. In this chapter, two-

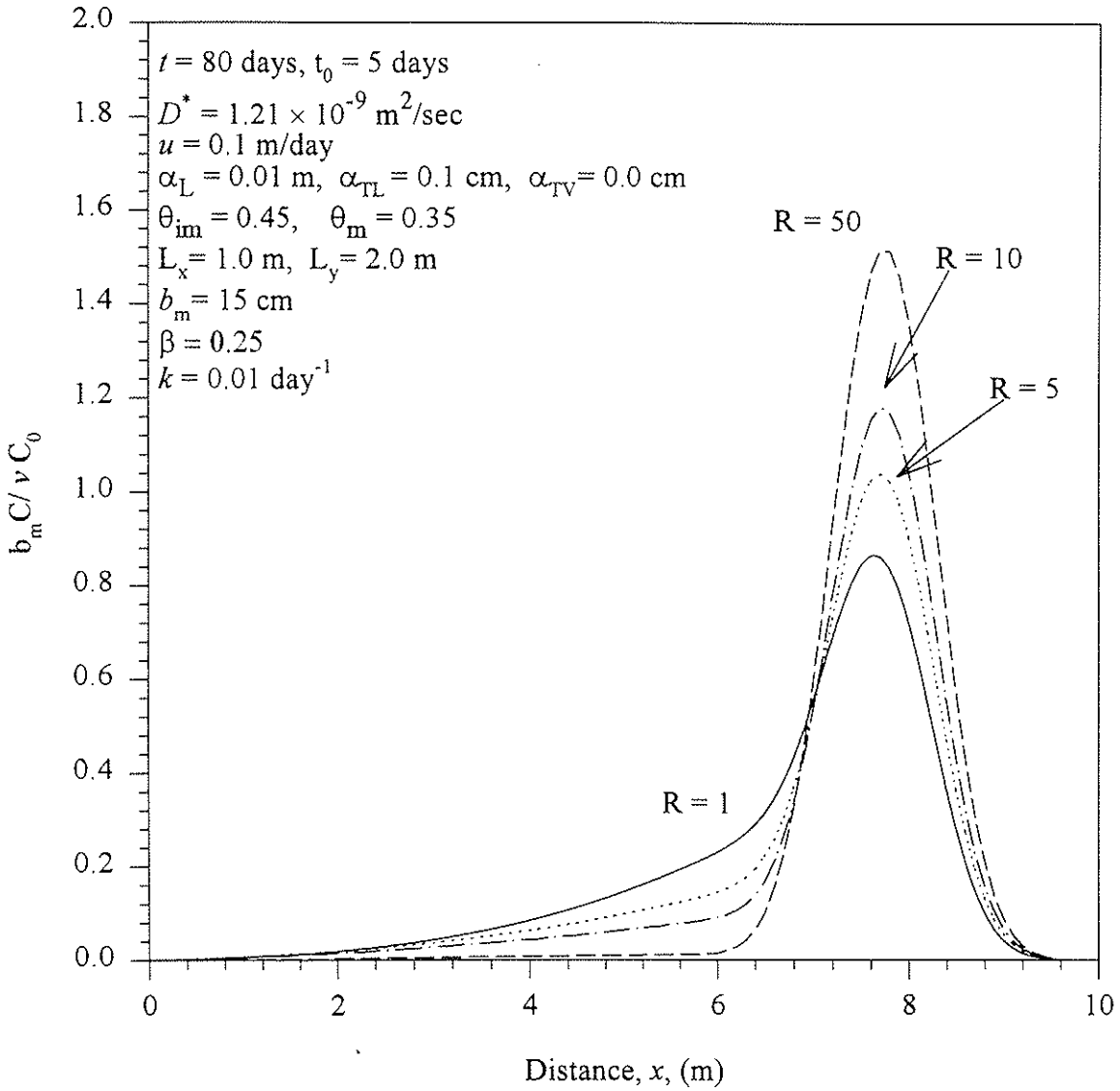

Figure 3.2 Effect of retardation in the immobile phase on relative concentrations in the mobile phase.

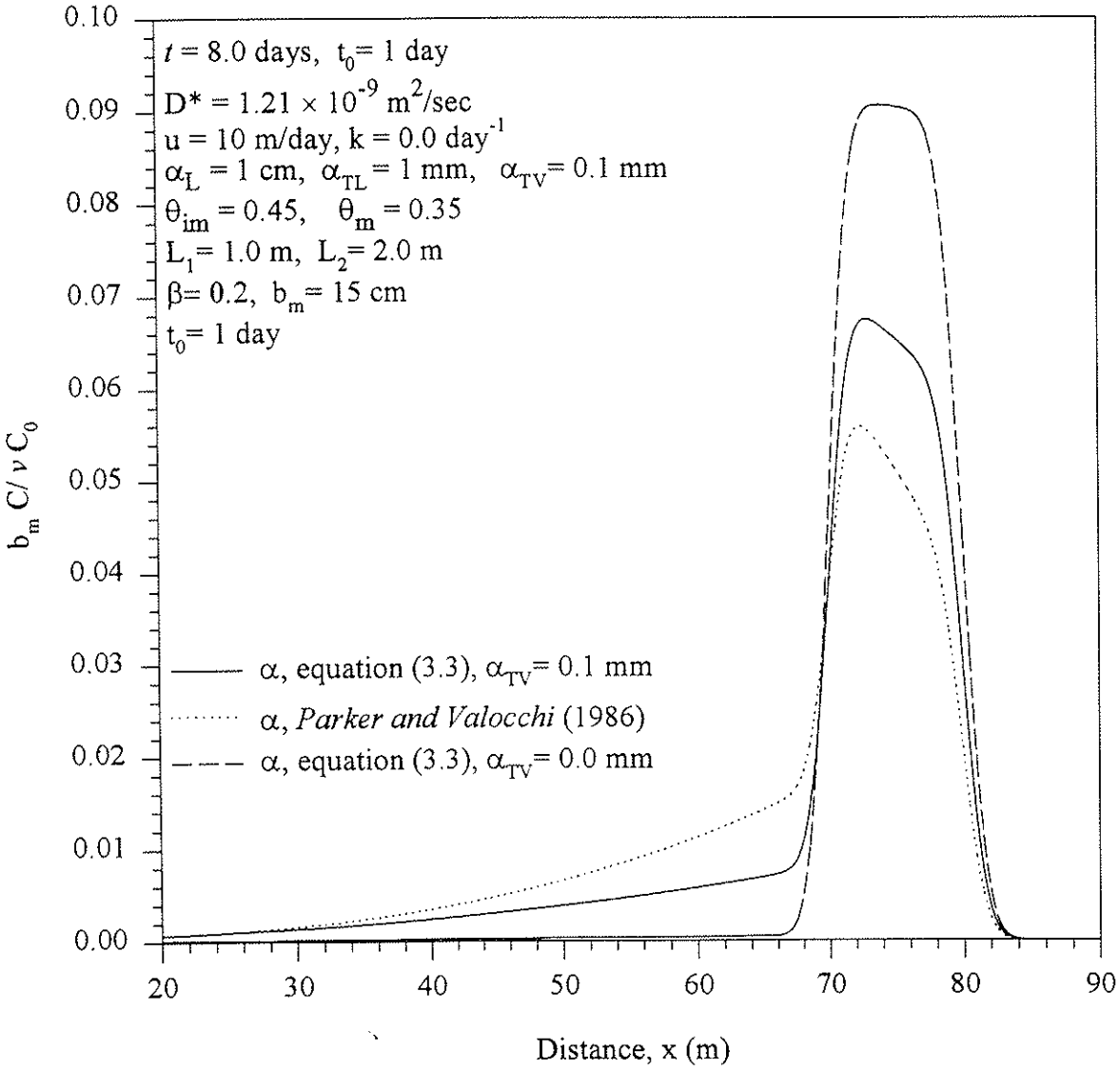

Figure 3.3 Effect of vertical transverse dispersivity on predicted relative concentrations in the mobile phase.

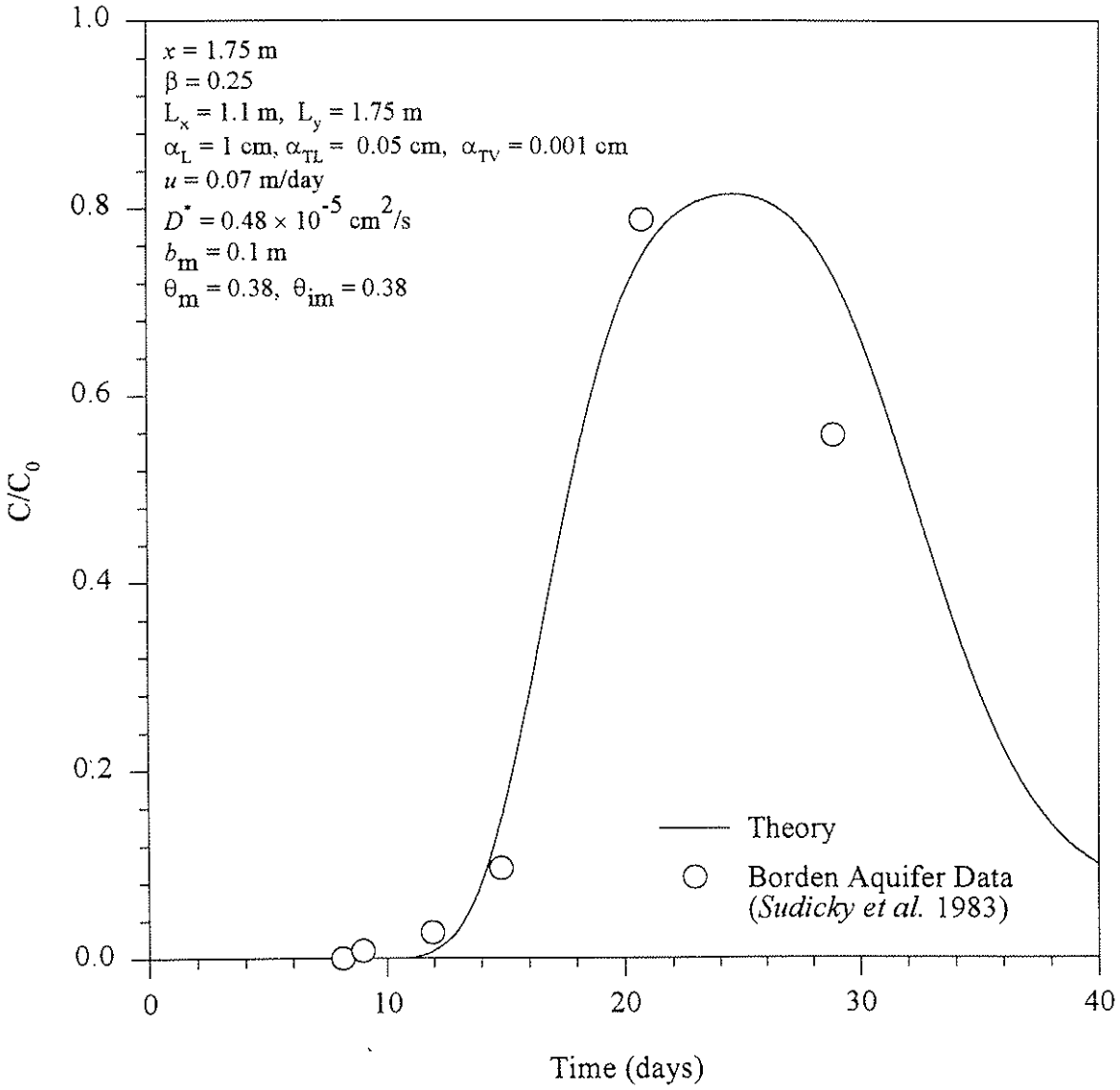

Figure 3.4 Tracer chloride breakthrough at x = 1.75 m: Calibration of first-order rate solution with experimental measurements.

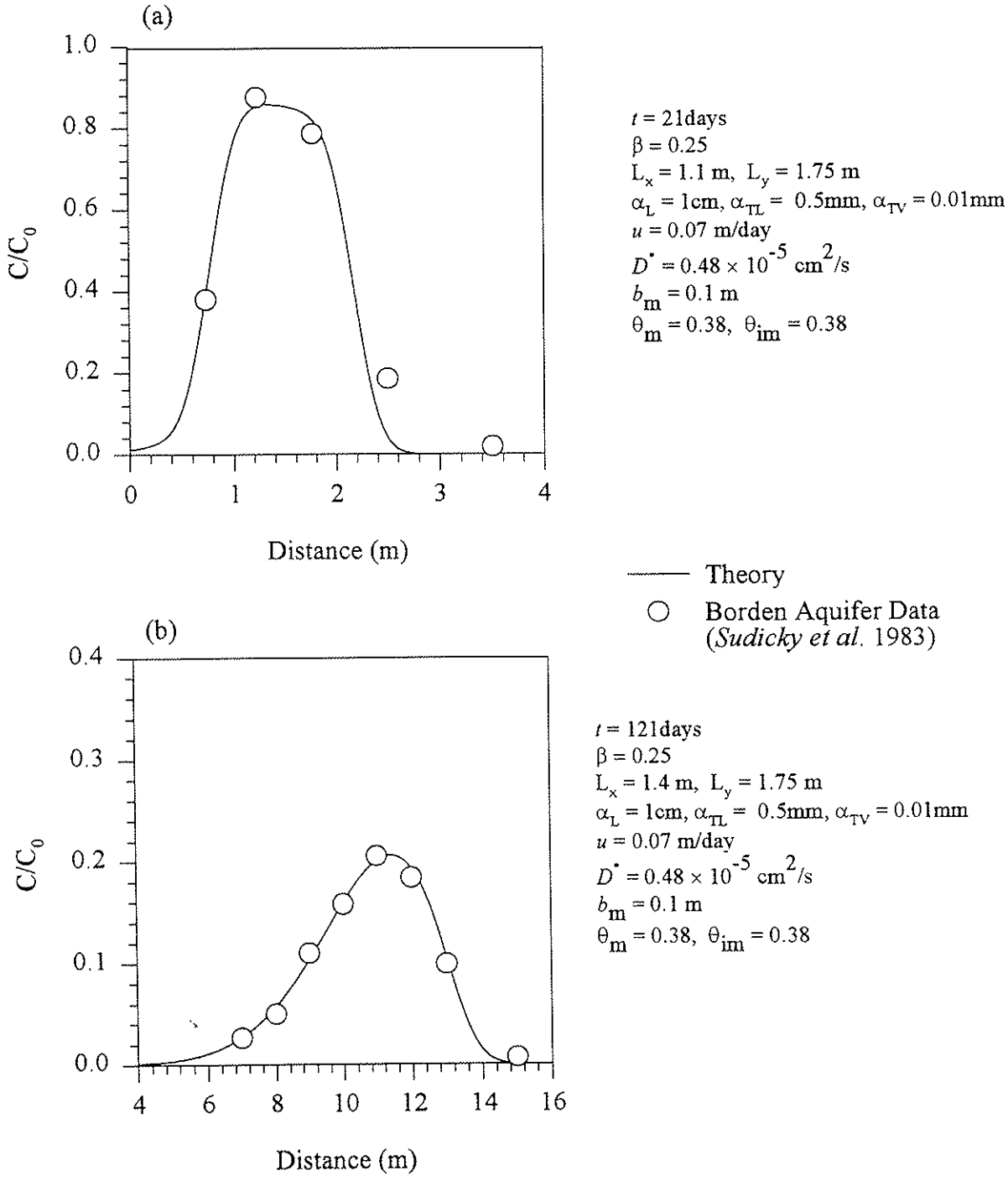

Figure 3.5 Comparison between predictions of tracer chloride relative concentrations and experimental data: (a) t = 21 days and (b) t = 121 days.

dimensional analytical solutions were developed for the first-order rate model in an infinite domain. Solutions were presented for a rectangular source area with (1) an instantaneous release of a contaminant mass, and (2) an exponentially-decaying source concentration, applied at a fixed rate. The solutions simulated the effect of interlayer mass transfer on the dispersion of reactive solutes in the high-permeability layers. Although, the solutions are valid for perfectly stratified porous media, they, nevertheless, are capable of predicting toxic levels introduced at the source with a predetermined rate; e.g., leachate below landfills and pesticides being leached into the water table by return flow and rainfall, at an average annual rate. Application of the theory to the Borden aquifer data indicated that dispersion of a tracer chloride can be interpreted on the basis of interlayer diffusive-mass transfer, rather than by assuming a Fickian behavior with overly estimated longitudinal and lateral dispersivities. With a slight adjustment of the initial plume length, the first-order rate solution predicted reasonably well the measured chloride levels at the Borden site.

Because in natural porous media perfect stratification is seldom the case, the practicality of the solutions developed herein for describing the integral effect of low-permeability layers in a strata, is in question. The ability to define an effective mass transfer coefficient α_{eff}, associated with the bulk formation, and related in some statistical fashion to the spatial variability of α, has the advantage of discriminating between the fraction of a contaminant-plume mass being held in low-permeability zones and the fraction being transported through high-permeability zones. Clearly, the current stochastic approaches, by and large, are deprived of such an advantage. Using moment analysis, *Harvey and Gorelick* (1995) modeled the coefficients α and β as random spatial processes and investigated the effect of their spatial variability on the transport of

contaminant mass and the mean arrival time. Notwithstanding the recent contributions, more research should be directed toward describing the integrated effect of the interlayer mass transfer at the formation scale, where heterogeneity prevails and uncertainty becomes an important factor.

CHAPTER 4

MODELING TRANSPORT OF CONTAMINANTS IN SOILS AND GROUNDWATER

4.1 Abstract

The movement and degradation of pesticides residues in soils and groundwater are complex processes affected by soil physical, (bio)chemical, and hydrogeological properties, climatic conditions, and agricultural practices. This chapter presents a physically-based analytical model suitable for long-term predictions of pesticides concentrations in groundwater. The primary interest is to investigate the impact of soil environment, related physical and (bio)chemical processes, especially, volatilization, crop uptake, and agricultural practices on long-term vulnerability of groundwater to contamination by pesticides. The soil is separated into root and intermediate vadose zones, each with uniform properties. Transport in each soil zone is modeled on the basis of complete mixing, by spatial averaging the related point multiphase-transport partial differential equation (i.e., linear-reservoir models). Transport in the aquifer, however, is modeled by a two-dimensional advection-dispersion transport equation, considering adsorption and first-order decay rate. Vaporization in the soil is accounted for by assuming liquid-vapor phase partitioning using Henry's law, and vapor flux (volatilization) from the soil surface is modeled by diffusion through an air boundary layer. Sorption of liquid-phase solutes by crops is described by a linear relationship that is valid for first-order (passive) crop uptake. The model is applied to five pesticides (Atrazine, Bromacil, Chlordane, Heptachlor, and Lindane), and the potential for pesticides contamination of groundwater is investigated for sandy and clayey soils. Simulation results show that groundwater contamination can be substantially

reduced for clayey soil environments, where bio(chemical) degradation and volatilization are most efficient as natural loss pathways for the pesticides. Also, uptake by crops can be a significant mechanism for attenuating exposure levels in groundwater, especially in a sandy soil environment, and for relatively persisting pesticides. Further, simulations indicate that changing agricultural practices can have a profound effect on the vulnerability of groundwater to mobile and relatively persisting pesticides.

4.2 Introduction

Groundwater vulnerability to contamination has become an important environmental aspect of the use of pesticides in agriculture. In shallow and deep groundwater, a number of pesticides have been detected (e.g., *Cohen et al.*, 1984). Pesticides used for agricultural purposes are leached to the water table through deep percolation by infiltrating rainfall and return flow (excess to evapotranspiration) during irrigation. Vulnerability of groundwater to contamination by pesticides is a long-term process; it emphasizes the need for proper planning to prevent beforehand a contamination problem, or at best to circumvent further deterioration in groundwater quality. In order to evaluate the impact of a land-use decision policy on groundwater, it is neither feasible economically nor practical to conduct extensive and frequent field-scale monitoring of exposure levels of chemicals (i.e., concentrations) in groundwater. It may take decades before pesticides leaching from soils can reach and contaminate nearby drinking-water wells. Given the time frame limitation, a quick decision may be required by policy makers before approving a land-use practice, such as for agricultural purposes. Protection

of groundwater quality benefits considerably from the ability to predict exposure levels of chemicals in the subsurface environment, by using simulation models.

Physically-based transport models provide an efficient tool for predicting exposure levels of contaminants in aquifers. In general, transport models vary from complex distributed parameters to simpler lumped-parameters linear-reservoir models. The former resemble more closely the actual physical system, e.g., heterogeneity, isotropy, etc., but are more difficult to solve than the latter; and they require a detailed set of data to warrant their use. Lumped-parameter models (or linear-reservoir models) are easier to solve since they constitute linear systems and require less data (e.g., *Gelhar and Wilson*, 1974); however, they are based on the restrictive assumption of complete mixing of the system variable, such as a solute mass. *Duffy and Lee* (1992) demonstrated that outflow concentrations calculated on the basis of distributed-parameters and linear-reservoir models were similar, provided that the aquifer length is at least ten times its thickness.

Modeling transport of pesticides in soils is not a new undertaking. *Jury et al.* (1983, 1984) developed a model for multiphase transport of trace organics in soils, and described volatilization by diffusive transfer of volatile pesticides through a stagnant air-boundary layer. Simplified models intended for ranking pesticide potential for groundwater contamination were developed by *Rao et al.* (1985) and *Jury et al.* (1987). The developed ranking indices considered linear, equilibrium liquid-vapor partition, linear, equilibrium adsorption, and (bio)chemical degradation. *Boesten and Van der Linden* (1991) developed a numerical model for calculating nonvolatile pesticides residual levels in the plow layer, and leaching fractions to a shallow water

table. In addition to first-order bio(chemical) degradation, they considered passive crop uptake as a potential loss pathway for the pesticides from the root zone. *Jury and Gruber* (1989) developed a stochastic model for describing the probability distribution of residual mass fraction of a pesticide undergoing first-order degradation, under conditions of soil and climatic variability. *Van Der Zee and Boesten* (1991) incorporated the effect of spatial variability of adsorption, degradation, and soil thickness on the coefficient of variation of the fraction of pesticide dose leached below a depth of 1 m. They considered first-order (passive) crop uptake in their analysis. *Beltman et al.* (1995) composed an analytical model for transport of pesticides in the unsaturated and saturated zones. They coupled expressions developed by *Jury and Gruber* (1989) and *Van der Zee and Boesten* (1991), which describe the fraction of pesticide dose that leaches from the heterogeneous unsaturated zone, to transport in groundwater. However, they ignored volatilization from the soil surface, crop uptake, and dispersion in the aquifer.

This chapter presents analytical modeling and application to pesticides transport in soils and aquifers. The objectives are twofold. First, the development of an analytical simulation model, and second, its application to investigate the impact of crop uptake and volatilization on vulnerability of groundwater to contamination by pesticides under different soil environments and different agricultural practices. The soil is divided into a root zone and an intermediate vadose zone, in each of which complete mixing of the pesticide is assumed. The soil model takes into account processes such as leaching, adsorption, (bio)chemical degradation, crop-roots uptake, and volatilization. Linear, equilibrium liquid-vapor partition is considered based on Henry's Law, and linear, equilibrium adsorption is assumed for sorption and desorption in soil. A

two-dimensional analytical solution for concentrations in groundwater is obtained from an elementary one (Bear, 1979, p. 273), by integration in space and time. The solution considers leaching through soils, advection, dispersion, degradation, and linear-equilibrium adsorption of pesticides in aquifers.

4.3 Basic Solute Transport Equation

Three conceptual models are considered in the current study, each of which corresponds to a given zone: the root zone (upper soil), the intermediate-vadose zone (lower soil), and the saturated zone (aquifer). The migration pathway in soil is distinguished into two different zones because of the variability of soil texture and hydraulic properties, and the relative dominance of different physical, chemical, and biological processes for different zones. For example: (1) soil type may differ from one zone to another; (2) soil geometric and hydraulic properties differ for different zones; (3) average annual soil moisture content varies with depth; (4) most of the water loss due to evaporation, transpiration, and volatilization occurs in the root zone; and (5) water quality parameters such as soil distribution coefficients differ for soils with different fractions of organic carbon.

In the development of the lumped-parameters transport equations, we emphasize the continuity of the mass of a solute in the context of integrated mass balance of the multiphase solute transport in the root and intermediate vadose zones. The one-dimensional transport

equation of a leaching solute existing in liquid, vapor, and adsorbed phases, and undergoing first-order decay, may be written as (*Jury et al.*, 1983):

$$\frac{\partial}{\partial t}(\kappa C_g + \theta C_l + \rho_b C_s) = \frac{\partial}{\partial z}\left(\kappa D_g \frac{\partial C_g}{\partial z}\right) + \frac{\partial}{\partial z}\left(\theta D_s \frac{\partial C_l}{\partial z}\right) - v\frac{\partial C_l}{\partial z} - r_s \qquad (4.1)$$

in which C_g is solute concentration in vapor phase (gm of chemical vapor/m^3 of soil air), C_l is solute concentration in liquid phase (gm of solute /m^3 of soil solution), C_s is adsorbed solute concentration (gm of sorbant/gm of dry soil), κ is volumetric air content, θ is volumetric water content, ρ_b is bulk soil density (gm/m^3), D_g is the soil-gas diffusion coefficient (m^2/day), D_s is porous media dispersion coefficient (m^2/day), v is convective soil moisture flux (m/day), t is time (days), z is soil depth (m), and r_s is the rate coefficient for transformation given by

$$r_s = k(\kappa C_g + \theta C_l + \rho_b C_s) \qquad (4.2)$$

where k is the reaction rate constant (day^{-1}). Since we are concerned with the transport of the solute in the liquid phase, equation (4.1) is rewritten using phase partitioning relationships; the linear-equilibrium sorption isotherm (liquid-sorbed concentrations) and the linear-equilibrium liquid-vapor partitioning known as Henry's law are expressed as

$$C_s = K_d C_l \qquad (4.3)$$

$$C_g = K_H C_l \tag{4.4}$$

where K_d is the distribution coefficient and K_H is the dimensionless Henry's constant (*Jury*, 1991, p. 234), which can be calculated from the saturated vapor density C_g^* (gm/ m^3) and solute solubility C_l^* (gm/ m^3) (*Spencer and Cliath*, 1970),

$$K_H = C_g^* / C_l^* \tag{4.5}$$

In terms of solute concentration in the liquid phase, C_l, equation (4.1) can be rewritten, after the use of (4.2)-(4.4), as

$$\theta R \frac{\partial C_l}{\partial t} = \frac{\partial}{\partial z}\left(\theta D_e \frac{\partial C_l}{\partial z}\right) - v\frac{\partial C_l}{\partial z} - k\theta R C_l \tag{4.6}$$

where D_e is the effective liquid-phase diffusion coefficient given by

$$D_e = (\kappa / \theta) K_H D_g + D_s \tag{4.7}$$

and R is a retardation factor given by

$$R = 1 + (\rho_b K_d + \kappa K_H) / \theta \tag{4.8}$$

Equation (4.6) describes advection and dispersion of a reactive solute in the liquid phase. Note that from (4.7) and (4.8), the effect of volatilization is to increase the dispersion of the solute in water and to decrease its mobility by increasing the retardation factor.

In the next section we develop the integrated balance form of the transport equation (4.6) over each of the crop-root zone as well as the intermediate vadose zone. The simplifying assumptions are: (1) one-dimensional and steady-state downward percolation produced by seasonally-averaged irrigation demand and rainfall processes, both adjusted for possible losses due to evapotranspiration; (2) complete mixing in each zone; and (3) soil texture, hydraulic properties, and organic matter fraction are uniform within each zone; (4) linear-equilibrium sorption isotherm; (5) diffusive solute-vapor movement occurs only in the crop-root zone, and losses from the soil surface to the atmosphere occur through an air boundary layer by vapor diffusion; and (6) passive root uptake.

4.4 Mass Balance in Crop-Root Zone

The root zone or the soil-water zone extends from the ground surface down through the crop roots. Water in this zone exists at less than saturation except temporarily when excessive water reaches the ground surface as from rainfall or irrigation. Almost all of the water lost to evapotranspiration is accounted for in this zone. Leaching of solutes, such as pesticides, in this zone occurs during irrigation and rainfall activities where the infiltrating water mobilizes solute

mass by advection downward to the water table. Volatilization and losses due to root uptake also occur in this zone.

4.4.1 Root Uptake

For passive root uptake (see *Briggs et al.*, 1982, and *Boesten and Van der Linden*, 1991), the rate of uptake of a solute by the crop, r_u, is described by

$$r_u = F S C_l \tag{4.9}$$

in which F is the transpiration stream concentration factor, and S is the rate of water uptake by the crop (day^{-1}). Equation (4.6) modified for crop uptake can be written as

$$\theta R \frac{\partial C_l}{\partial t} = \frac{\partial}{\partial z}\left(\theta D_e \frac{\partial C_l}{\partial z}\right) - v\frac{\partial C_l}{\partial z} - k_r C_l \tag{4.10}$$

in which the effective loss rate k_r is given by

$$k_r = (k\theta R + F S) \tag{4.11}$$

Equation (4.10) describes advective-dispersive transport of a reactive solute subject to passive root uptake. Equation (4.11) describes the net degradation rate in the root zone due to the combined effect of (bio)chemical transformation and root uptake.

(a)

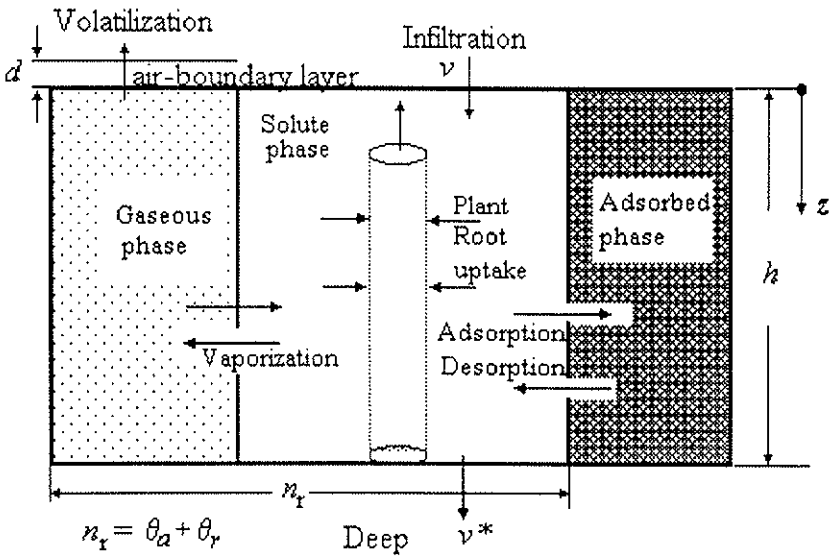

(b)

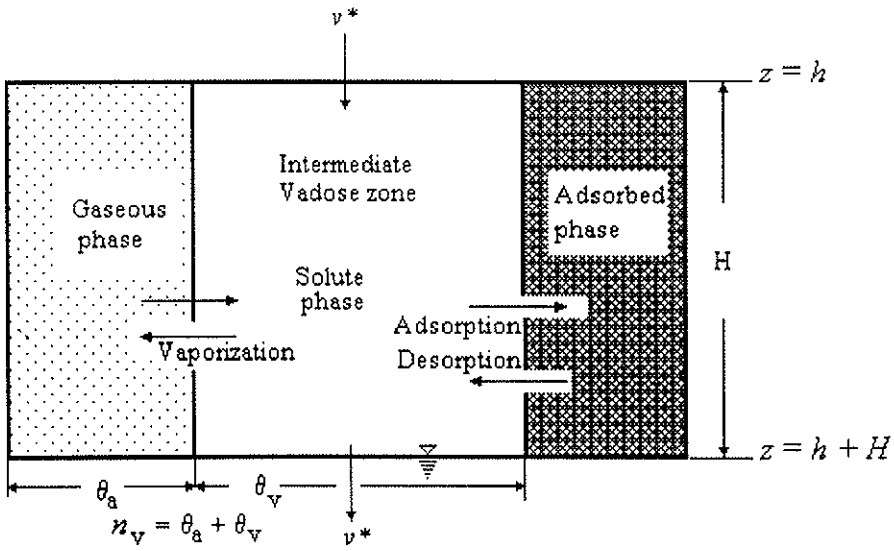

Figure 4.1 Schematic representation of modeled processes in the: (a) root zone; and (b) intermediate vadose zone.

4.4.2 Volatilization

Volatilization whereby chemicals vaporize and escape to the atmosphere may occur through a thin and stagnant layer of air above the soil surface. Following *Jury et al.* (1983), vapor flux at the surface is assumed to diffuse through an air boundary layer of thickness d (m), before entering the atmosphere (Figure 4.1a). Using Fick's law, we may write the vapor-diffusive flux as

$$\kappa D_g \frac{\partial C_g}{\partial z} = \kappa D_g \frac{C_g(0,t) - C_g^{\,a}}{d} \tag{4.12}$$

in which C_g (0,t) is the vapor-phase solute concentration at the soil surface (gm/m^3), and $C_g^{\,a}$ is the concentration above the air boundary layer (gm/m^3). For a well-mixed region of the atmosphere, $C_g^{\,a}$ = 0, and we can rewrite (4.12) in terms of liquid solution concentrations using (4.4),

$$\kappa D_g K_H \frac{\partial C_l}{\partial z} = \sigma C_l(0,t) \tag{4.13}$$

where

$$\sigma = \kappa D_g K_H / d \tag{4.14}$$

Equations (4.13) and (4.14) describe the net rate of loss of vapor concentration from the soil surface to the atmosphere through a thin boundary layer of air.

4.4.3 Integrated Mass-Balance Equation

We start by integrating (4.10) over the depth of the roots h (Figure 1a), from $z = 0$ to $z = h$,

$$\int_0^h \theta R \frac{\partial C_l}{\partial t} dz = \int_0^h \left(\frac{\partial}{\partial z} \left(\theta D_e \frac{\partial C_l}{\partial z} \right) - v \frac{\partial C_l}{\partial z} - k_r C_l \right) dz \tag{4.15}$$

Realizing that the limits of integration are time invariant, and since properties are assumed uniform throughout the root zone, we can simplify (4.15) further,

$$\theta R \frac{d}{dt} \int_0^h C_l(z,t) dz = \left(\theta D_e \frac{\partial C_l(h,t)}{\partial z} - v^* C_l(h,t) \right) - \left(\theta D_e \frac{\partial C_l(0,t)}{\partial z} - v C_l(0,t) \right) - k_r \int_0^h C_l(z,t) dz \tag{4.16}$$

where the net groundwater recharge, i.e., the water flux available for deep percolation below the root zone is given by

$$v^* = v - ET_c \tag{4.17}$$

in which ET_c is the crop evapotranspiration rate (m/day). If we define the average solute concentration in the root zone, $C_r(t)$, as

$$C_r(t) = (1/h)\int_0^h C_l(z,t)\,dz \tag{4.18}$$

then we may approximate (4.13) as follows:

$$\kappa\, D_g K_H \frac{\partial C_l}{\partial z} \approx \sigma\, C_r \tag{4.19}$$

Furthermore, we approximate the solute mass flux at $z = h$ by the relation

$$\theta\, D_s \frac{\partial C_l(h,t)}{\partial z} - v^* C_l(h,t) \approx -v^* C_r \tag{4.20}$$

which is widely used in mixing models (e.g., *Gelhar and Wilson*, 1974, and *Duffy and Gelhar*, 1985). The approximation given by (4.20) is not valid in the most strict sense because it ignores the effect of dispersion. However, it is reasonable for shallow water tables, where the size of an application area is much greater than the depth to the water table, and where convection dominates over the dispersion mechanism. During precipitation and irrigation, we may write the flux boundary condition at the surface as

$$\theta D_s \frac{\partial C_l(0,t)}{\partial z} - \nu C_l(0,t) = -\nu C_0 \tag{4.21}$$

in which C_0 is the concentration of the chemical applied at the surface (gm/m^3). We emphasize that (4.20) and (4.21) are understood as approximations intended for simplifying the analysis. Ignoring dispersion and heterogeneities may lead to serious underestimation of leaching below a given depth in soil (see, e.g., *Beltman et al.*, 1995). The substitution of (4.7) and (4.19-4.21) into (4.16) yields

$$\theta R h \frac{dC_r}{dt} = -\nu^* C_r + \nu C_0 - \sigma C_r - k_r h C_r \tag{4.22}$$

which in turn can be written as

$$\frac{dC_r}{dt} + \beta_r C_r = \alpha_r C_0 \tag{4.23}$$

where

$$\beta_r = \frac{1 + (T_r / \lambda)(\ln(2) + \mu)}{T_r} \tag{4.24}$$

4.4.3.1 Uniform Application

In this case, $C_0(\tau) = C_0$, and (4.28) reduces to

$$C_r(t) = e^{-\beta_r(t-t_0)}C_r(t_0) + \frac{\alpha_r}{\beta_r}C_0(1 - e^{-\beta_r(t-t_0)}) \tag{4.29}$$

in which t_0 coincides with the beginning of a month/season and $t \in [t_0, t_1]$. The first term on the right-hand side represents the contribution of the solute background level in the root-soil profile, while the second term describes the contribution of the soil-surface source.

4.4.3.2 Instantaneous Application

In this case, for a chemical mass M_0, the solute mass flux per area (gm/m^2) applied at the surface is related to the applied chemical mass M_0, through the relationship

$$v\,C_0(\tau) = M_0\delta(\tau - t_0) \tag{4.30}$$

in which $\delta(t)$ is the Dirac-delta function. In (4.30), it is assumed that M_0 is totally mobilized in the liquid phase, initially. If we substitute (4.30) into (4.28) and evaluate the integral, we obtain

$$C_r(t) = e^{-\beta_r(t-t_0)}C_r(t_0) + \frac{M_0}{\theta_r h R_r}e^{-\beta_r(t-t_0)} \tag{4.31}$$

Equation (4.31) describes on an average basis the residual concentrations of an applied chemical mass at the soil surface and initially contaminated profile in the root zone.

4.5 Mass Balance in Intermediate-Vadose Zone

The intermediate vadose zone extends from the bottom of the root zone to the water table. No loss of water to the atmosphere is expected from this zone. Almost all the water that enters this zone below the root zone percolates downward to the water table. Leachate concentration entering this zone is equal to the average concentration of the solute in the root zone. We integrate (4.6) over the intermediate-zone depth (Figure 4.1b), from $z = h$ to $z = h+H$:

$$\int_h^{H+h} \theta R \frac{\partial C_l}{\partial t} dz = \int_h^{H+h} \left(\frac{\partial}{\partial z} \left(\theta D_e \frac{\partial C_l}{\partial z} \right) - v \frac{\partial C_l}{\partial z} - \theta k R C_l \right) dz \tag{4.32}$$

The evaluation of (4.32) yields

$$\theta R \frac{d}{dt} \int_h^{H+h} C_l(z,t) dz = \left(\theta D_e \frac{\partial C_l(H+h,t)}{\partial z} - v^* C_l(H+h,t) \right) - \left(\theta D_e \frac{\partial C_l(h,t)}{\partial z} - v^* C_l(h,t) \right) \tag{4.33}$$

$$- \theta k R \int_h^{H+h} C_l(z,t) dz$$

in which θ, R, and k are assumed uniform. Similarly, if we define the average solute concentration in the intermediate-vadose zone C_u as

$$C_u(t) = (1/H) \int_h^{H+h} C_l(z,t)\, dz \tag{4.34}$$

and assume emission to the water table follows the boundary flux equation:

$$\theta D_s \frac{\partial C_l(H+h,t)}{\partial z} - v^* C_l(H+h,t) \approx - v^* C_u \tag{4.35}$$

Then, substituting (4.20), (4.34), and (4.35) into (4.33) yields

$$\theta R H \frac{dC_u}{dt} = -v^* C_u + v^* C_r - \theta k R H C_u \tag{4.36}$$

In compact form, (4.36) is rewritten as

$$\frac{dC_u}{dt} + \beta_u C_u = \alpha_u C_r \tag{4.37}$$

in which

$$\beta_u = \frac{1+\ln(2)(T_u/\lambda)}{T_u} \tag{4.38}$$

$$\alpha_u = 1/T_u \tag{4.39}$$

where

$$T_u = H R_u / (v^*/\theta_u) \tag{4.40}$$

θ_u and R_u are the moisture content and retardation factor in the intermediate vadose zone, respectively. In arriving at (4.36), we have ignored diffusive flux of solute vapor from the intermediate vadose zone to the root zone ($\kappa D_g \partial/\partial z\ C_g(h,t) = \kappa D_g \partial/\partial z\ C_g(h+H,t) = 0$), which implies underestimation of vapor losses by volatilization. The volatilization rate from the soil surface increases, because the upward diffusive movement (Fick's law) of solute vapor from the intermediate vadose zone tends to augment reduced vapor concentrations in the root zone.

Equation (4.37) is also a first-order and linear differential equation that relates the spatially-averaged solute concentration in the intermediate-vadose zone to leaching, first-order reaction, and linear-equilibrium adsorption. The solution is given by

$$C_u(t) = C_u(t_0) e^{-\beta_u (t-t_0)} + \int_{t_0}^{t} e^{-\beta_u (t-\tau)} \alpha_u(\tau) C_r(\tau) d\tau \tag{4.41}$$

$$C_u(t) = C_u(t_0)e^{-\beta_u(t-t_0)} + \int_{t_0}^{t} e^{-\beta_u(t-\tau)}\alpha_u(\tau)C_r(\tau)d\tau \qquad (4.41)$$

Similarly, assuming monthly/seasonally-averaged leaching rate and moisture content, explicit forms can be obtained for the two cases discussed earlier.

4.5.1 Uniform Application

The substitution of (4.29) for $C_r(t)$ into (4.41) yields the following solution

$$\begin{aligned} C_u(t) &= e^{-\beta_u(t-t_0)}C_u(t_0) + \frac{\alpha_u}{\beta_u-\beta_r}\left(C_r(t_0)-\frac{\alpha_r}{\beta_r}C_0\right)e^{-\beta_u(t-t_0)}(e^{(\beta_u-\beta_r)(t-t_0)}-1) \\ &\quad + \frac{\alpha_r\alpha_u}{\beta_r\beta_u}C_0(1-e^{-\beta_u(t-t_0)}) \end{aligned} \qquad (4.42)$$

The first term on the right-hand side represents the contribution of the solute background level in the intermediate-vadose-soil profile, whereas the second term describes the contribution of solute emissions from the overlying crop-root zone.

4.5.2 Instantaneous Application

In this case, we substitute (4.31) into (4.41), and the result is given by

$$C_u(t) = e^{-\beta_u(t-t_0)}C_u(t_0) + \alpha_u\left(C_r(t_0)+\frac{M_0}{\theta_r h R_r}\right)\frac{e^{-\beta_r(t-t_0)}-e^{-\beta_u(t-t_0)}}{\beta_u-\beta_r} \qquad (4.43)$$

In the next section we develop a two-dimensional groundwater transport model that considers the solute emissions to a water table, described by (4.42) and (4.43), as the primary source of contamination.

4.6 Solute Transport in Ground Water

In ground water, the two-dimensional advection-dispersion of a reactive solute may be described by the following partial differential equation (*Bear*, 1979)

$$R\frac{\partial C}{\partial t} = D_{xx}\frac{\partial^2 C}{\partial x^2} + D_{yy}\frac{\partial^2 C}{\partial y^2} - u\frac{\partial C}{\partial x} - k_a C \tag{4.44}$$

where C is the concentration of the contaminant in groundwater (gm/m^3); D_{xx} is the hydrodynamic dispersion coefficient along the x axis (m^2/day), D_{yy} is the hydrodynamic dispersion coefficient along the y axis (m^2/day); and u is the average linear pore-water velocity along the x axis. D_{xx} and D_{yy} can be expressed in terms of two components (*Freeze and Cherry*, 1979)

$$D_{xx} = d^* + \alpha_L u \tag{4.45}$$

$$D_{yy} = d^* + \alpha_T u \tag{4.46}$$

in which d^* is the molecular diffusion coefficient multiplied by the tortuosity (m^2/day); α_L is the longitudinal dispersivity (m) along the mean flow direction; and α_T is the transverse dispersivity (m). Equation (4.44) can describe also advection-dispersion in a heterogeneous aquifer with a spatially variable hydraulic conductivity. In this case (4.44) is understood in a macroscopic sense, and the dispersion parameters in (4.45) and (4.46) are modified to account for macrodispersivities that are functions of the mean and variance of log conductivity, its integral scale, local dispersivities, the mean hydraulic gradient, and the mean specific discharge (*Gelhar and Axness*, 1983). The use of constant macrodispersions in (4.44) is only valid after large displacement of the contaminant plume where it has grown sufficiently in size, which is greater than several integral scales of the log hydraulic conductivity field.

If we define

$$C^*(x,y,t) = e^{\frac{k_a}{R}t} C(x,y,t) \tag{4.47}$$

then (4.44) can be reduced to the following advection-dispersion and adsorption partial differential equation:

$$R\frac{\partial C^*}{\partial t} = D_{xx}\frac{\partial^2 C^*}{\partial x^2} + D_{yy}\frac{\partial^2 C^*}{\partial y^2} - u\frac{\partial C^*}{\partial x} \tag{4.48}$$

in which

$$R = \left(1 + \frac{\rho_b k_d}{n}\right) \tag{4.49}$$

The solution of (4.48) in an infinite domain for an instantaneous injection of solute mass per depth, M, at time $t = 0$, and assuming zero initial concentration, $C(x,y,0) = 0$, is given by *(Bear, 1979)*

$$C^*(x,y,t) = \frac{M}{4\pi\sqrt{D'_{xx}D'_{yy}}\,t}\exp\left\{-\left(\frac{(x-u't)^2}{4D'_{xx}t}+\frac{y^2}{4D'_{yy}t}\right)\right\} \tag{4.50}$$

where $D'_{xx} = D_{xx}/R$, $D'_{yy} = D_{yy}/R$, $u' = u/R$, and $k'_a = k_a/R$. The solution of (4.44) for the instantaneous injection of solute mass M is obtained by substituting the elementary solution (4.50) into (4.47):

$$C(x,y,t) = \frac{M}{4\pi\sqrt{D'_{xx}D'_{yy}}\,t}\exp\left\{-\left(\frac{(x-u't)^2}{4D'_{xx}t}+\frac{y^2}{4D'_{yy}t}+k'_a t\right)\right\} \tag{4.51}$$

The solute mass injected, per unit depth B of aquifer, from an incremental area dA = dξ dη (see, Figure 4.2) at the interface between the intermediate-vadose zone and the water table, during time interval [τ , τ + dτ] is

$$dM = \frac{v^*(\tau)}{n\ B}C_u(\tau)\,n\,d\zeta\,d\eta\,d\tau \tag{4.52}$$

and the corresponding increment of solute concentration is

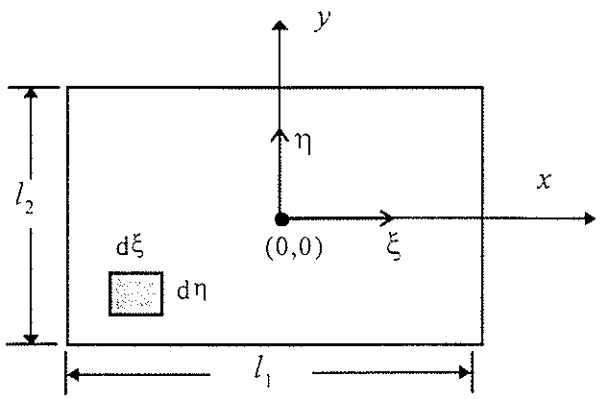

Figure 4.2 Schematic representation of application, related geometry, and hypothetical drinking water well.

$$dC(x,y,t) = \frac{v^*(\tau)\,C_u(\tau)}{4\pi\,B\sqrt{D'_{xx}D'_{yy}}\,(t-\tau)}\,e^{-\left(\frac{(x-u'(t-\tau))^2}{4D'_{xx}(t-\tau)}+\frac{y^2}{4D'_{yy}(t-\tau)}+k'_a(t-\tau)\right)}\,d\xi\,d\eta\,d\tau \tag{4.53}$$

in which $d\tau$ is understood to be infinitesimally small so that the solution (4.51), which is valid for instantaneous injection of solute mass dM, can be applied. For a nonpoint source, dM is not only a function of space (ξ,η), but also a function of time, and its variation in time is the result of the dependence of the concentration in the intermediate-vadose zone on time, and the temporal variation of the leaching process below the root zone. If the pesticide is applied over an area of size $L_1 \times L_2$ (Figure 4.3), then the solution of (4.44) can be obtained using the principle of superposition, i.e., integrating (4.53) over the application area (Figure 4.2) and in time,

$$C(x,y,t) = \int_0^t \int_{-L_2/2}^{L_2/2} \int_{-L_1/2}^{L_1/2} \frac{v^*(\tau)C_u(\tau)}{B}\,\frac{e^{-\left(\frac{(x-\xi-u'(t-\tau))^2}{4D'_{xx}(t-\tau)}+\frac{(y-\eta)^2}{4D'_{yy}(t-\tau)}+k'_a(t-\tau)\right)}}{4\pi\sqrt{D'_{xx}D'_{yy}}\,(t-\tau)}\,d\xi\,d\eta\,d\tau \tag{4.54}$$

Since the terms that contain the dummy variables ξ and η are separable, (4.54) can be written as

$$C(x,y,t) = \int_0^t \frac{v^*(\tau)\,C_u(\tau)}{4\pi B\sqrt{D'_{xx}D'_{yy}}\,(t-\tau)}\,e^{-(k'_a)(t-\tau)}\left\{\int_{-L_1/2}^{-L_1/2} e^{-\frac{(x-\xi-u'(t-\tau))^2}{4D'_{xx}(t-\tau)}}\,d\xi \cdot \int_{-L_2/2}^{-L_2/2} e^{-\frac{(y-\eta)^2}{4D'_{yy}(t-\tau)}}\,d\eta\right\}d\tau \tag{4.55}$$

Upon the use of the transformations $\xi^* = [\xi - (x - u'(t-\tau)]/(2[D'_{xx}(t-\tau)]^{1/2})$ and $\eta^* = (\eta - y)/(2[D'_{yy}(t-\tau)]^{1/2})$, the integrals with respect to ξ and η can be evaluated to yield

$$C(x,y,t) = (1/B)\int_0^t v^*(\tau)\, C_n(\tau)\, e^{-(k_n')(t-\tau)} G(\tau;x,t)\, F(\tau;y,t)\, d\tau \qquad (4.56)$$

in which

$$G(\tau;x,t) = \frac{1}{2} erf\left(\frac{l_1/2 + |x - u'(t-\tau)|}{2\sqrt{D'_{xx}(t-\tau)}}\right) - \frac{1}{2} erf\left(\frac{-l_1/2 + |x - u'(t-\tau)|}{2\sqrt{D'_{xx}(t-\tau)}}\right),$$

$$if\ |x - u'(t-\tau)| > l_1/2$$

$$= \frac{1}{2} erf\left(\frac{l_1/2 - (x - u'(t-\tau))}{2\sqrt{D'_{xx}(t-\tau)}}\right) + \frac{1}{2} erf\left(\frac{l_1/2 + (x - u'(t-\tau))}{2\sqrt{D'_{xx}(t-\tau)}}\right), \qquad (4.57)$$

$$if\ |x - u'(t-\tau)| \le l_1/2$$

and

$$F(\tau;y,t) = \frac{1}{2} erf\left(\frac{l_2/2 + |y|}{2\sqrt{D'_{yy}(t-\tau)}}\right) - \frac{1}{2} erf\left(\frac{-l_2/2 + |y|}{2\sqrt{D'_{yy}(t-\tau)}}\right), \quad if \quad |y| > l_2/2$$

$$= \frac{1}{2} erf\left(\frac{l_2/2 - y}{2\sqrt{D'_{yy}(t-\tau)}}\right) + \frac{1}{2} erf\left(\frac{l_2/2 + y}{2\sqrt{D'_{yy}(t-\tau)}}\right), \quad if \quad |y| \le l_2/2 \qquad (4.58)$$

Equations (4.56-4.58) describe analytically the mobility, transformation, and spreading characteristics of the residual mass of a chemical in groundwater, after leaching through the soil.

For the monthly/seasonal variations of input variables such as moisture content, groundwater recharge, evapotranspiration, application of, e.g., pesticides and herbicides, and volatilization, (4.56) can be written on a monthly/seasonal basis as

$$C(x,y,t) = (1/B)\sum_{s=1}^{N} v^*_s \int_{t_{s-1}}^{t_s} C_u(\tau)\, e^{-k'_u(t-\tau)} G(\tau;x,t)\, F(\tau;y,t)\, d\tau \qquad (4.59)$$

where $t_N = t$.

4.7 Application

Table 4.1 shows selected chemical properties of the pesticides Atrazine, Chlordane, Heptachlor, Bromacil, and Lindane. By comparing the values of the chemical organic C partition coefficient, degradation half-life, and the dimensionless Henry's constant (Table 4.1), it is clear that the five selected pesticides differ significantly with respect to their mobility dictated by the organic C partition coefficient, persistence which is a function of degradation half-life, and volatilization, whereby a chemical evaporates and escapes from the soil surface, which depends on the value of K_H. For example, Atrazine is expected to be highly mobile with very low persistence in the soil, because of its relatively low organic C partition coefficient and low half-life. The application area is assumed to be 200 m × 200 m (4 ha) and the application rate for each pesticide is assumed to be 3.4 kg/ha (assumed a worst case scenario by *Varshney et al.*, 1993), once a year at the beginning of the growing season of the crop, e.g., maize. Two growing scenarios are considered, (May 1- September 30) and (March 1- July 31). Two types of soils are investigated, sand and clay. They differ significantly with respect to their vulnerability to

Table 4.1. Organic C Partition Coefficients, Degradation Half-Lives, and Henry's Constants for Five Pesticides.

Pesticide	K_{oc} (cm^3/g)	$t_{1/2}$ (days)	K_H
Atrazine*	160	71	2.5×10^{-7}
Chlordane*	38000	3500	2.2×10^{-4}
Heptachlor*	24000	2000	1.45×10^{-1}
Bromacil*	72	350	3.7×10^{-8}
Lindane*	1300	266	1.3×10^{-4}

Source: *Jury et al.* (1984) and *Rao et al.* (1985).

* Application rate is 3.4 kg/ha, applied once a year at the beginning of the growing season.

Table 4.2. Typical Values of Properties for Sandy and Clayey Soils.

Property	Sandy Soil	Clayey Soil
Bulk density g/cm^3	1.7	1.5
Average water content	0.22	0.35
Residual water content ★	0.045	0.07
Organic C fraction	0.005	0.03
Porosity	0.4	0.5

★ Residual water content is used for the root zone during the growing season (May-September).

Table 4.3. Geohydrologic Data.

Property	Value
Thickness of root zone (m)	1
Thickness of intermediate-vadose zone (m)	8
Thickness of aquifer (m)	10
Groundwater Darcian velocity (m/yr)	50
Longitudinal dispersivity (m)	5
Transverse dispersivity (m)	0.1
Effective molecular diffusion (cm^2/sec)	10^{-5}
Gaseous diffusion coefficient (cm^2/day)	4320*
Air-boundary layer thickness (cm)	5*

*Suggested by *Jury et al.* (1983).

Table 4.4. Meteorological and Crop Data.

Property	Value	Property	Value
Average precipitation (m) (May - Sep.) *1	0.0216	Average surface runoff (m) (May - Sep.) *3	0
Average precipitation (m) (Mar. - Jul.) *1	0.102	Average surface runoff (m) (Mar - Jul.) *4	0.038m (clay)
			0.024m (sand)
Average precipitation (m) (Oct. - Apr.) *1	0.4	Average surface runoff (m) (Oct. - Apr.) *4	0.15m (sand)
			0.22m (clay)
		(Aug. - Feb.) *4	0.13m (sand)
Average precipitation (m) (Aug. - Feb.) *1	0.32	Reduction factor (γ)	0, 0.5, 0.8
Average potential ET (m) (May-Sep.) *2	0.885	Average leaf area index (cm2/cm2)	
		(maize crop) *5	2.4
Average potential ET (m) (Mar-Jul.) *2	0.765	Transpiration stream concentration factor *5	1

* 1 Average values in Davis based on 1917-1972 recorded data (*Cayan and Wear*, 1977).

* 2 Based on average values for reference ET in Davis (*Pruitt et al.*, 1987).

* 3 Assumed.

* 4 Calculated using the SCS method, assuming normal antecedent moisture conditions.

* 5 Adapted from *Boesten and van der Linden* (1991), averaged over the growing season.

groundwater contamination (e.g., *Jury and Gruber*, 1989), and typical values for their properties are displayed in Table 4.2. Table 4.3 shows geometric and geohydrologic data used for the simulations. Organic carbon fraction is neglected in the intermediate vadose zone and in the aquifer; hence, mobility of a pesticide is only affected in the root zone because of retardation there. The aquifer is assumed to be of alluvial origin and characterized, predominantly, by sand and gravel layers. The average depth of the root zone is assumed to be 1 m, which is typical to corn crops. The climatic data with respect to averaged precipitation and reference evapotranspiration are typical to the Sacramento Valley in California (see Table 4.4). For calculating the rate of water uptake by the crop, S, we use the relationship suggested by *Boesten and van der Linden* (1991),

$$S = (\gamma / h) \quad ET_p \, (1 - e^{-0.6 I}) \qquad (4.60)$$

in which γ is a reduction factor assumed here a constant; ET_p is the potential ET; and I is leaf area index (cm^2cm^{-2}). In a more realistic manner, *Feddes et al.* (1976) considered the variation of the reduction factor γ as a function of matric suction, for modeling the effect of roots uptake on moisture distribution in soil. In the simulations (Figures. 4.4-4.7), we ignore the fraction of deep percolation (below the root zone) produced by water in excess to irrigation demand. That is, future predictions are based on irrigation rates that meet estimated crop evapotranspiration ET_c (see, *Pruitt et al.*, 1987). Predictions for the pesticides levels in groundwater are made at a hypothetical drinking-water well located at a distance 200 m down gradient from the center of the application area (x = 200 m, y = 0 m). Figure 4.3 shows a schematic representation of the

the application area (x = 200 m, y = 0 m). Figure 4.3 shows a schematic representation of the soil-aquifer system with related geometry used in the simulations. Simulated groundwater concentrations shown in Figures 4.4-4.7 correspond to the agricultural practice: a growing season (May-September) of duration of 153 days (0.42 yr) with average precipitation of 0.0216 m/153 days, and a wet season (October-April) of duration 212 days (0.58 yr) with average precipitation of 0.4 m/212 days. Emissions of pesticides to groundwater predominantly occur during the wet season, where leaching below the root zone is most significant due to greater than the annual average of the precipitation.

The results displayed in Figures 4.4-4.8 are based on instantaneous injection of the given pesticide mass at the beginning of the growing season. Thus, we use equations (4.31), (4.43), and (4.59), in which the integral is evaluated using the Romberg method. For efficient numerical evaluation of the integral, we note that, for a fixed x and t, the function $G(\tau;x,t)$ behaves as a finite pulse contained in the interval $[a_1(t), b_1(t)]$, where

$$a_1(t) = t - \left[(x + l_1/2)/u'\right] - (4/u')\sqrt{D'_x t}, \quad \text{and} \quad b_1(t) = t - \left[(x - l_1/2)/u'\right] + (4/u')\sqrt{D'_x t}$$

Therefore, rather than integrating from t_{s-1} to t_s in (4.59), we instead integrate from $\max\left[t_{s-1}, a_1(t)\right]$ to $\min\left[t_s, b_1(t)\right]$. Note that for large x and small t, evaluating the integral is redundant and $b_1(t)$ can be negative, implying that the contaminant pulse is yet to arrive at x and the concentration is zero there.

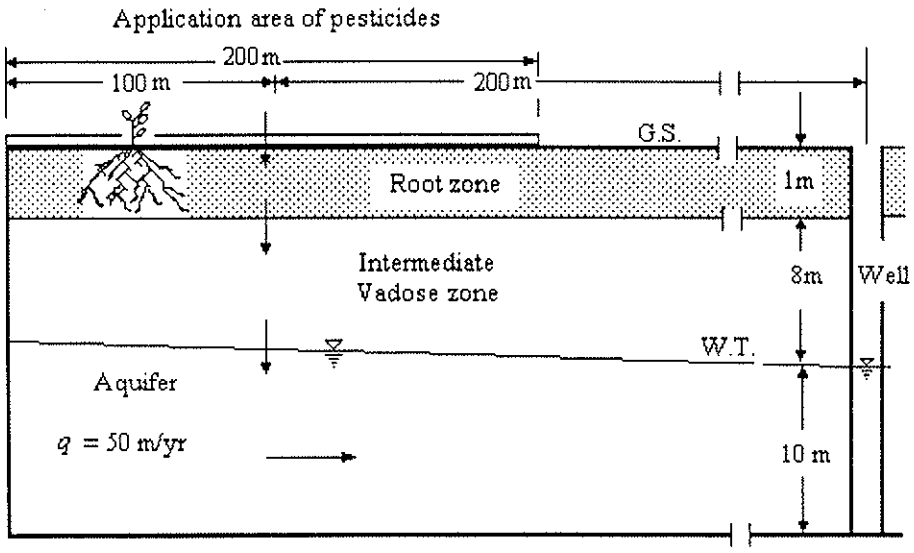

Figure 4.3 Schematic representation of application area, related geometry, and hypothetical drinking water well.

4.8 Discussion

4.8.1 Effect of Crop-Root Uptake

Figure 4.4 shows predicted Atrazine concentrations for sandy and clayey soils, assuming agricultural practices are maintained throughout the prediction period. For both soils, the predicted Atrazine concentrations at the drinking-water well showed very low exposure levels (in ppb) and rather a strong stationary-periodic behavior (unsteady in the regular sense) after two years. Such a behavior represents the kind of temporal variability which is a manifestation of the combined effect of the high degradation rate of Atrazine and the seasonal effect of the leaching mechanism produced by the net infiltration below the root zone. Transport through a clayey soil resulted in much lower Atrazine concentrations, by an order of magnitude (Figure 4.4b), when compared to exposure levels predicted on the basis of a sandy soil (Figure 4.4a). The greater the organic carbon fraction, the greater the retardation Atrazine encounters due to adsorption in the root zone. Whereas, increasing the retardation results in relatively greater residence time, T_r, i.e., holding up the pesticide for a longer time in the root zone. Because such a condition favors relatively greater losses of adsorbate by degradation, the net result is concentrations being emitted to the water table via a clayey soil that show much smaller predicted exposure levels in the well (Figure 4.4a), when compared to the case when emissions to the water table occur through a sandy soil (Figure 4.4b). It is imperative in this effort to realize that in addition to degradation, persistence of pesticides in the soil may be significantly reduced due to volatilization and crop-root uptake, especially for longer residence times such as in a clayey soil (also, refer to equations (4.24), (4.26), and (4.27)). However, for less volatile pesticides like

Atrazine ($K_H = 2.5 \times 10^{-7}$), low exposure levels in groundwater are a manifestation of low persistence due to bio(chemical) degradation, rather than volatilization and root uptake. Low concentrations of Atrazine in the root zone, due to degradation, result in reduced passive uptake by crops, because of the linear dependence of the latter on the soluble concentrations, as equation (4.9) indicates. As mentioned earlier, the strong temporal variability of Atrazine residual levels in groundwater, albeit being periodic because of the seasonally-averaged climatic input data (recall, two seasons are considered here), is attributed to the combined effect of high degradation rate and seasonal variations of the leaching process. The effect of soil type on leaching is accounted for in this effort, indirectly, by allowing for surface runoff calculated by the SCS method (see, e.g., *Chow et al.*, 1988, p. 147). Such an approximation is somewhat stringent; however, intended for distinguishing the relative behavior of a given pesticide in different soil environments, rather than predicting absolutely the effect of hydraulic properties of the soil on the prediction process. Nevertheless, a lower infiltration rate in a clayey soil, as indicated by greater estimate of surface runoff (Table 4.4), results in lower persistence of Atrazine in the root zone, because of greater residence time and reduced residual concentrations due to greater degradation. Subsequently, the effect of crop-root uptake on the predicted concentrations in groundwater is marginalized (Figure 4.4b). In contrast, Figure 4.4a shows in a more resolute manner the sensitivity of predicted Atrazine concentrations with respect to crop uptake, when the soil environment is predominantly sand. Prediction based on $\gamma = 0.5$ shows reductions in Atrazine levels as large as 12.5 % if root uptake is taken into consideration as a viable loss pathway from a sandy soil.

Figure 4.5 shows predicted exposure levels of Bromacil in the drinking well for the two cases of sandy and clayey soils. Because of the low organic C partition coefficient and relatively large half-life of the pesticide Bromacil (Table 4.1), it is highly mobile and somewhat persistent in soils and, furthermore, nonvolatile due to its negligibly-small dimensionless Henry's constant ($K_H = 3.7 \times 10^{-8}$). Altogether, these characteristics favor greater residual concentrations in the root zone; thus, rendering Bromacil a good candidate among the selected pesticides to provide a greater insight into the effect of crop uptake, ultimately, on the predicted concentrations in groundwater. In contrast to the behavior of Atrazine, predicted Bromacil concentrations in groundwater show a gradual buildup toward steady-state periodic levels that are greater by two orders of magnitude, after 10 years from the beginning of the agricultural practices. It is clear that in a sandy soil environment the cumulative effect of root uptake has a profound effect on the predicted Bromacil levels in the drinking-water well, after approximately 3 years (Figure 4.5b). For $\gamma = 0.5$ and 0.8, the predicted steady-state concentrations are 38% and 50%, respectively, smaller than the values predicted when crop uptake is not accounted for. In the case of a clayey soil, the predicted concentrations are smaller by an order of magnitude than in the case of a sandy soil, and the effect of crop uptake is relatively less remarkable with concentrations reduced by as much as 13% and 18% for $\gamma = 0.5$ and 0.8, respectively (Figure 4.5a).

4.8.2 Effect of Volatilization

Heptachlor is much less mobile and slowly degradable when compared to Atrazine and Bromacil, because of its greater organic C partition coefficient (greater retardation) and greater half-life; however, it is highly volatile due to its high dimensionless Henry's number ($K_H =$

0.145). Figure 4.6 shows predicted Heptachlor concentrations for sandy and clayey soil environments. In both soils, predicted exposure levels in the hypothetical drinking well show a continuous buildup toward steady levels, with the temporal variability being smothered by the high persistence and buildup of the concentrations. Due to the reduced leaching capacity and greater retardation, the longer residence time in a clayey soil favors greater losses by volatilization; subsequently, much smaller exposure levels of the highly volatile Heptachlor in groundwater, by less than half the levels predicted on the basis of a sandy soil. Further, the estimated concentrations in Figure 4.6 show no sensitivity with respect to root uptake, even for the extreme case of $\gamma = 1$. This is a direct consequence of losses by volatilization which lead to lower concentrations, hence, negligible passive root uptake.

Notwithstanding the relative similarity between Heptachlor and Chlordane with respect to mobility and degradation, Heptachlor shows much smaller predicted concentrations in groundwater due to its greater susceptibility to volatilization than Chlordane, as shown in Figure 4.7. The relatively nonvolatile Lindane shows predicted concentrations greater than Chlordane up to 5 years, before leveling off, but with a temporally variable pattern, because of the relatively low persistence of the latter in soils (i.e., greater degradation). It is worth emphasizing that increased losses by volatilization due to upward movement of water which is instigated by evaporation from the soil surface, is not modeled here, especially in an inactive (nongrowing) season characterized by drier climate. Because of the upward movement of water, solute accumulates at the interface between the soil surface and the air boundary layer; thus, leading to

CHAPTER 5

STOCHASTIC ANALYSIS OF CONTAMINANT TRANSPORT IN SOIL AND GROUNDWATER

5.1 Abstract

In this chapter, we represent chemical and physical transport processes in a stochastic way, because of the heterogeneity in the field conditions and imperfect representation of the actual processes. The pesticides transport model, which was developed in Chapter 4, is integrated with the Monte Carlo method to obtain the probability density function, mean, and standard deviation of the concentrations in groundwater. The distribution coefficient, which is used to calculate the retardation factor for equilibrium adsorption, is assumed to be normally distributed, and the precipitation is modeled by fitting an ARIMA model to an observed time series. Consequently, the results of the analysis are also probability distribution functions for the concentrations of contaminants, which are useful representations for environmental quality regulations and management. The case study involves modeling transport of the herbicide Simazine, which is widely used for weed control, in a subsurface environment typical to the area of Fresno, California. Although this case study involves great complexity, the results are expected to predict typical long-term Simazine concentrations in groundwater. The results show that: (1) the predicted concentration probability distributions are non-Gaussian (nonsymmetric or skewed), exhibiting values in the same range of magnitude as the field-measured values; (2) long-term predictions of Simazine concentrations are characterized by a quasi-steady state of dynamic equilibrium, where seasonal variations are dominated by the driving rainfall/infiltration

processes; (3) predictions made on the basis of averaged values of the properties may lead to a substantial underestimation or overestimation of the dominant (ensemble-average or mean) behavior of the contaminant levels in groundwater; and (4) on the basis of an application area of size 200 m × 200 m (4 hectares), it is expected that under the application practice of 2.34 kg/ha of Simazine, in the late fall and winter, exposure levels in groundwater will not increase dramatically in the zone most affected by Simazine concentrations. However, this may not be the conclusion for greater application areas, or when a preferential flow mechanism becomes significant. When preferential flow dominates, the long-term buildup in Simazine concentrations may significantly exceed predictions that ignore such a mechanism.

5.2 Problem

5.2.1 Introduction to the Problem

There has been much interest in the assessment of contaminant levels of organic chemicals in the Fresno basin and its evolution in time. Currently, the groundwater of the basin exhibits widespread contamination of dibromochloro-propane (DBCP) and, to a lesser extent, of Simazine. The specific site is an area intensely pumped to which large amounts of groundwater flow converge. Fresno is located in the southeast part of the San Joaquin Valley in California. The use of Simazine for weed control in vineyards has been a practice for the last two decades. As a consequence, Simazine has contaminated the groundwater in specific sites. Pesticides have been detected in groundwater in many locations of the United States. For example, in California, widespread contamination in the eastern part of the San Joaquin Valley is resulting from the application of the soil fumigant DBCP (*Cohen*, 1986). The use of DBCP was suspended in 1979, but the product has been persistent in groundwater.

5.2.2 Hydrogeological Conditions

The Fresno area comprises about 1,400 mi^2 lying west of the foothills of the Sierra Nevada, in the eastern San Joaquin Valley. Alluvial fans are the dominant geomorphic features in the area. The deposits of quaternary age may be of a different nature: older alluvium, lacustrine and marsh deposits, younger alluvium, flood-basin deposits, and sand dunes. Even though clay layers confine the older alluvium sediments, an unconfined water body underlies most of the Fresno area. The Fresno area is underlaid by alluvial and Pleistocene nonmarine deposits derived from the weathering of Sierra Nevada granites. These deposits are highly permeable, medium to coarse-grained sands with low organic carbon (*Domagalski and Dubrovsky*, 1991). Leaching conditions pose the highest risk for sandy soils exposed to pesticide soil application and flood or sprinkler irrigation. The intensive application of Simazine in this area, combined with fairly-permeable soil conditions, may create a region with higher vulnerability to long-term groundwater contamination .

Depth to the water table varies from 9 m, near the eastern boundary of the area of interest, to about 35 m near the southwestern boundary (as of the Spring, 1991). Depth to the water table beneath much of the area, where DBCP and Simazine were present in the groundwater, ranged from 9 to 24 m and averaged about 15 m in the Spring, 1991 (*Franz*, 1994). It has been observed that, in a regional sense, groundwater levels in the area of study are nearly stable on the long term.

5.2.3 Pesticides in the Study Area

A total of 13,523,120 pounds of active ingredients were applied in Fresno County during 1986. That corresponds to 16 percent of the total use in the State. Pesticide application in the Central Valley accounts for about 10 percent of the total application in the United States (Domagalski and Dubrovsky, 1991). About 190,377 pounds of this product were applied in 1986 in the San Joaquin Valley. Domagalski and Dubrovsky (1991) studied the fate and transport of pesticides in the Valley by integrating geologic, hydrologic, and geochemical information. Their analysis is based on the Central Valley RASA study, started in 1979 and whose phase II was completed in 1990. Simazine is used in vineyards and orchards in the area of interest and its application peaks in the late Fall and Winter, during the rainy season. The herbicide was not detected in some of the areas of highest application south and west of the city of Fresno. Hypotheses explaining such observations include a deeper water table and limited hydraulic conductivity; however, the information is not conclusive since well screenings and depths are unknown. Table 5.1 displays typical values of the parameters and properties that are used in the simulations reported in this chapter. Some of the values can be found in the literature while others are assumed, although they are typical values. The results presented later on are based on months grouped into four seasons, according to periods of high and low precipitation. The reader is referred to Bonilla (1996) for further information on the study area, soil properties, geohydrology, and chemical properties of Simazine.

Table 5.1. Typical Values for Parameters Used in the Case Study.

Parameter	Value	Units
Chemical	Simazine	
Henry's constant (dimensionless)	0.0001	
Gass diffusion coefficient in free air	158	m2/yr
Soil distribution coefficient in the root zone	0.7	cm3/gm
Soil distribution coefficient in the vadose zone	0.3	cm3/gm
Average moisture content in the root zone, season 1	0.3	
Average moisture content in the vadose zone, season 1	0.3	
Average moisture content in the root zone, season 2	0.15	
Average moisture content in the vadose zone, season 2	0.15	
Average moisture content in the root zone, season 3	0.065	
Average moisture content in the vadose zone, season 3	0.045	
Average moisture content in the root zone, season 4	0.22	
Average moisture content in the vadose zone, season 4	0.22	
Aquifer porosity	0.38	
Soil porosity	0.4	
Bulk density, root zone	1.4	g/cm3
First-order decay coefficient, root zone	5.6	1/yr
Bulk density, vadose zone	1.5	g/cm3
First-order decay coefficient, vadose zone	2.08	1/yr
Bulk density, aquifer	1.6	g/cm3
Aquifer distribution coefficient	0	m3/gm
First-order decay coefficient, aquifer	0.69	1/yr
Coefficient of molecular diffusion	0.032	m2/yr
Longitudinal dispersivity, aquifer	5	m
Transverse dispersivity, aquifer	0.1	m
Average depth of the root zone	1.3	m
Average depth of the vadose zone	8.5	m
Average thickness of the aquifer	60	m
Average Darcy's velocity in the aquifer	50	m/yr
Number of forecasting time points	6	
Dimensions of the field: L1, L2	200	m
Mass of applied pesticide, season 1	0.12	g/m2
Mass of applied pesticide, season 2	0	g/m2
Mass of applied pesticide, season 3	0	g/m2
Mass of applied pesticide, season 4	0.12	g/m2
Transpiration-stream concentration factor	1	
Initial concentration in the root zone	0	g/m3
Initial concentration in the vadose zone	0	g/m3
Time length, season 1	0.3	yr
Average rainfall (runoff) during season 1	0.91(0.1)	m/yr
Time length, season 2	0.2	yr
Average rainfall (runoff) during season 2	0.18(0.01)	m/yr
Time length, season 3	0.2	yr
Average rainfall (runoff) during season 3	0.03(0.00)	m/yr
Time length, season 4	0.3	yr
Average rainfall (runoff) during season 4	0.6(0.07)	m/yr

5.3 Modeling Precipitation in Fresno

Monthly precipitation time series were used to analyze the sensitivity of the system to climatic variations. It is important to notice that the average annual precipitation in the vicinity of Fresno is less than 10 inches. Because peak applications for Simazine are during late fall and winter, the herbicide is likely to show fluctuations and buildup of its exposure levels in the soil and groundwater due to the variable precipitation. A hypothetical case was added to analyze the effect of different rainfall regimes in the otherwise same scenario. It is important to realize that by seasonally aggregating the precipitation data, some information is lost by averaging out the variability. This smoothing effect is a good approximation, only when the residence time of the pesticide is of the same order of magnitude or bigger than the aggregation level of the precipitation data. If we are interested in modeling preferential flow, it is important to de-aggregate to that time interval (i.e., increase the time resolution). The effect of such de-aggregation will be seen later in the results section.

Figure 5.1 shows monthly averages of the mean and standard deviation of the precipitation in the Fresno area. An autoregressive integrated moving average model (ARIMA) was fitted to a historical record of monthly precipitation, which is typical to the Fresno area, for the years 1948-1994 (Figure 5.2). The best fitted model for the Fresno case is an ARIMA(0,0,1) $\times (0,1,1)_{12}$ (e.g., see *Shumway*, 1988, p. 140, on ARIMA models) with parameters:

$\theta_1 = -0.1264$ (simple moving average)

$\Theta_1 = 0.8601$ (seasonal moving average)

$\sigma_w = 0.1644$ (residual variance)

$AIC_1 = -0.79$ (goodness criterion)

$$(1-B^{12})X_t = (1-\theta_1 B)(1-\Theta_1 B^{12})w_t \qquad (5.1)$$

or in a form suitable for forecasting:

$$X_t = X_{t-12} + w_t - \Theta_1 w_{t-12} - \theta_1 w_{t-1} + \theta_1 \Theta_1 w_{t-13} \qquad (5.2)$$

in which X represents the logarithm of the monthly precipitation and w represents white noise with standard deviation σ_w. Alternative models fitted to the same time series are ARIMA$(1,0,1) \times (0,1,1)_{12}$, ARIMA$(1,0,1) \times (1,1,1)_{12}$, and ARIMA$(0,0,1) \times (1,1,1)_{12}$.

Figure 5.3 shows the autocorrelation (ACF) and partial autocorrelation (PACF) of the transformed series, obtained after taking the logarithm of the monthly precipitation. Figure 5.4 shows the ACF and PACF of the residual series, after fitting the ARIMA model to the transformed series. As expected, the ARIMA model transforms the initial time series to white noise, as we observe the residuals ACF and PACF do not have significant peaks.

The random independent sequences of rainfall were generated as follows (*Bonilla*, 1996): (1) using the sequence for generating Gaussian deviates, a long sequence (generally of 1,000 numbers) of Gaussian deviates or white noise is generated; (2) using equation 5.2, and initializing the values of X at the monthly mean, a sequence of monthly rainfall is generated; (3) the first 100 values of this sequence are discarded (not considered in order to eliminate initial-value effects), and the synthesized series is used in the transport model per one Monte Carlo simulation; and (4) using a different seed for the generation of Gaussian deviates (ensures independence), the process is repeated.

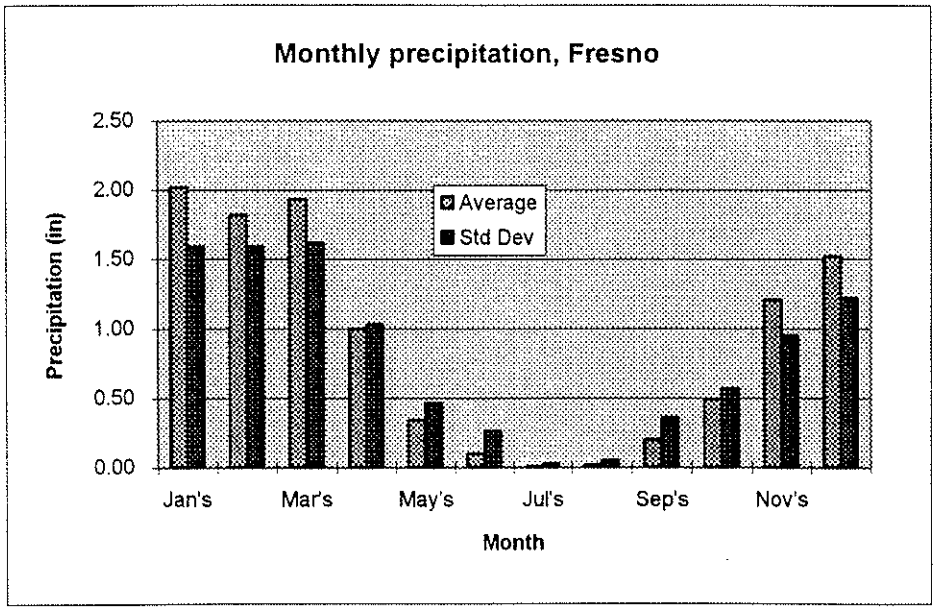

Figure 5.1 Averaged monthly precipitation, Fresno air terminal. Based on record years 1948-94.

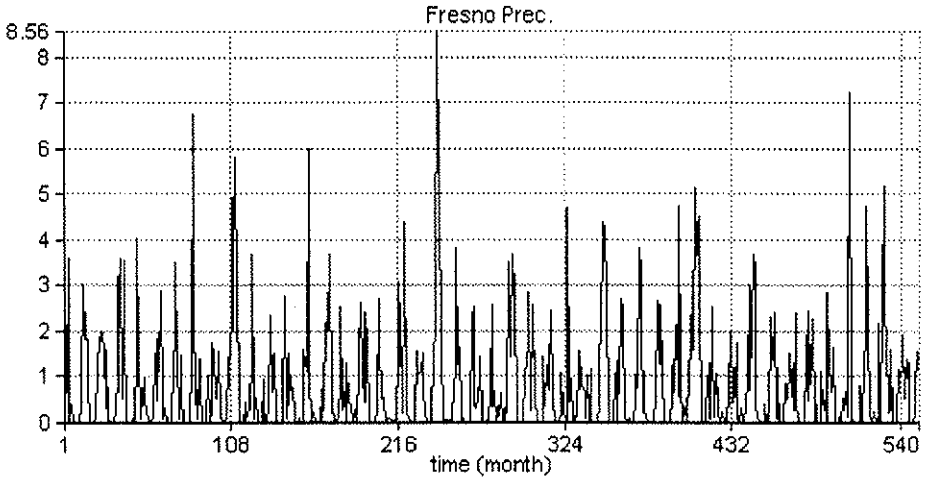

Figure 5.2 Historical time series, monthly rainfall, Fresno air terminal.

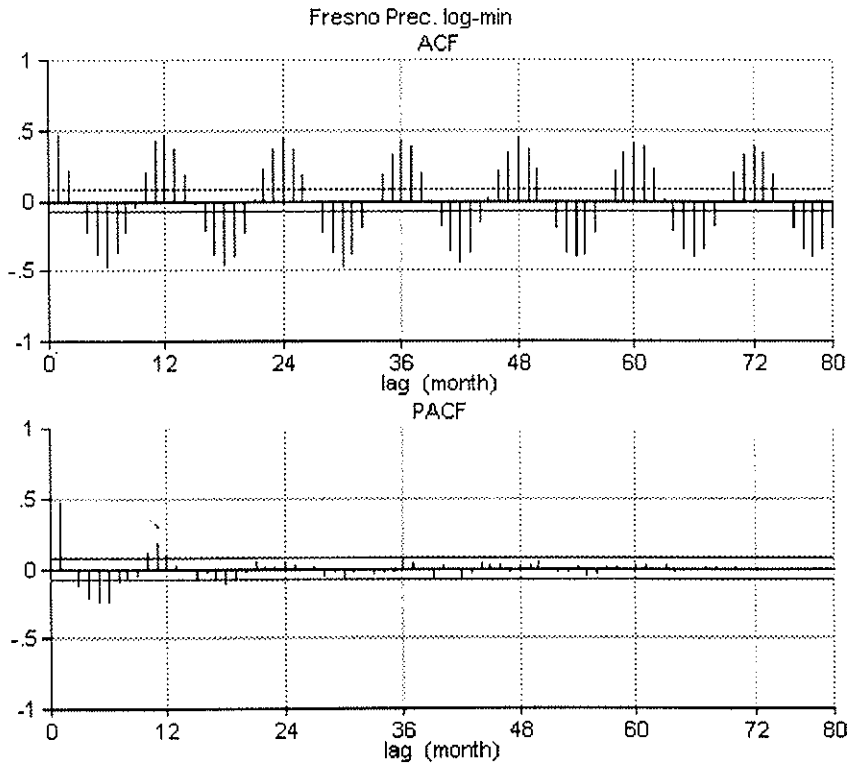

Figure 5.3 Historical time series, monthly rainfall, Fresno air terminal: ACF and PACF of the rainfall logarithm.

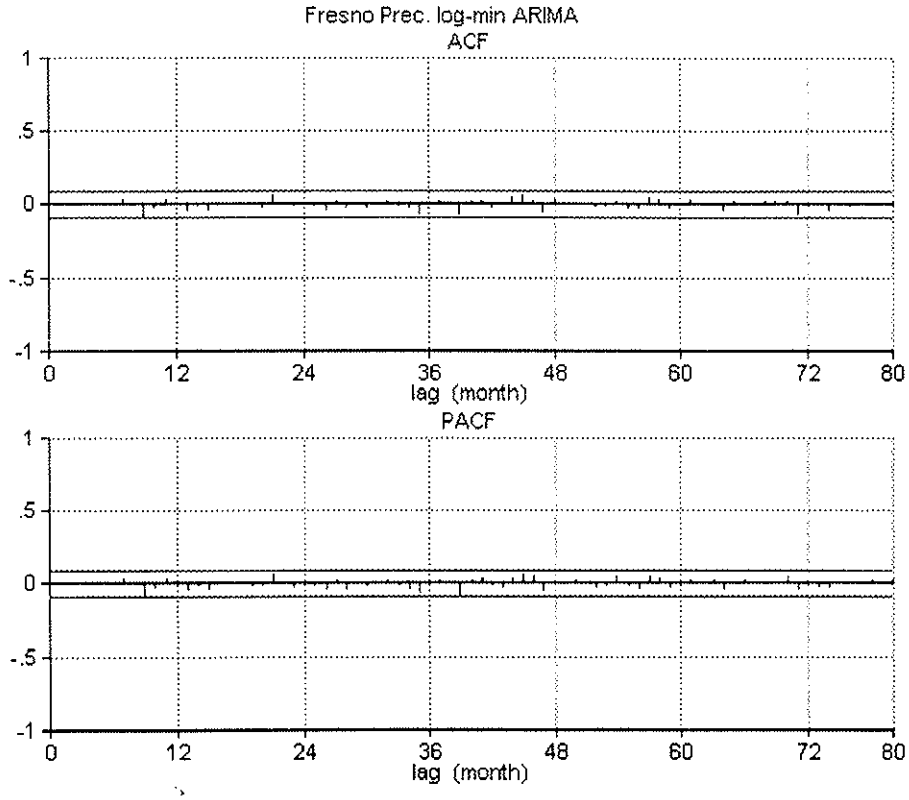

Figure 5.4 Historical time series, monthly rainfall, Fresno air terminal: ACF and PACF of the residuals after fitting the ARIMA model.

5.4 Results and Discussion

In the stochastic analysis, we consider the randomness of the input variables or parameters, each at a time; that is, if one parameter is random, the others are held fixed and assumed their field averages. The random input variables are the retardation factor, for equilibrium adsorption, and the precipitation. A preferential flow condition is tested in an average sense, by assuming water flux to occur during a period smaller than the duration of one season. The total applied mass of the pesticide is assumed to be mobilized completely and instantaneously by the infiltrating water; hence, we use equations (4.31), (4.43), and (4.59) to predict Simazine concentrations per Monte Carlo (M.C.) simulation. Table 5.2 includes the assumed variability for the chemical parameters. In the case of climatic variability, the seasonal aggregation (average of three months per season) of the monthly series will also average out some of the monthly variability. This effect can be minimized by grouping the months with most similar rainfall conditions in the seasonal aggregation. For most of the cases, it was possible to obtain convergence in the output distributions (for concentrations) after 1,000 M.C. simulations. The marginal improvement achieved by increasing the number of simulations up to 5,000 was not significant. One thousand simulations took, on average, 1 hour and 15 minutes in a Pentium/100 (Tti).

Table 5.2. Statistical Properties.

Parameter	Mean	Coef. of variation
Soil distribution coefficient in root zone (cm^{3}/g)	0.7	40%
Soil distribution coefficient in vadose zone (cm^{3}/g)	0.3	35%
Soil distribution coefficient in aquifer (cm^{3}/g)	0.12	25%
Decay coefficient in root zone (1/yr)	5.6	60%
Decay coefficient in vadose zone (1/yr)	2.08	50%
Decay coefficient in aquifer (1/yr)	0.69	40%
Depth of root zone (m)	1.5	-
Depth of intermediate-vadose zone (m)	8.5	-
Mass of applied pesticide (kg/ha)	2.34	-

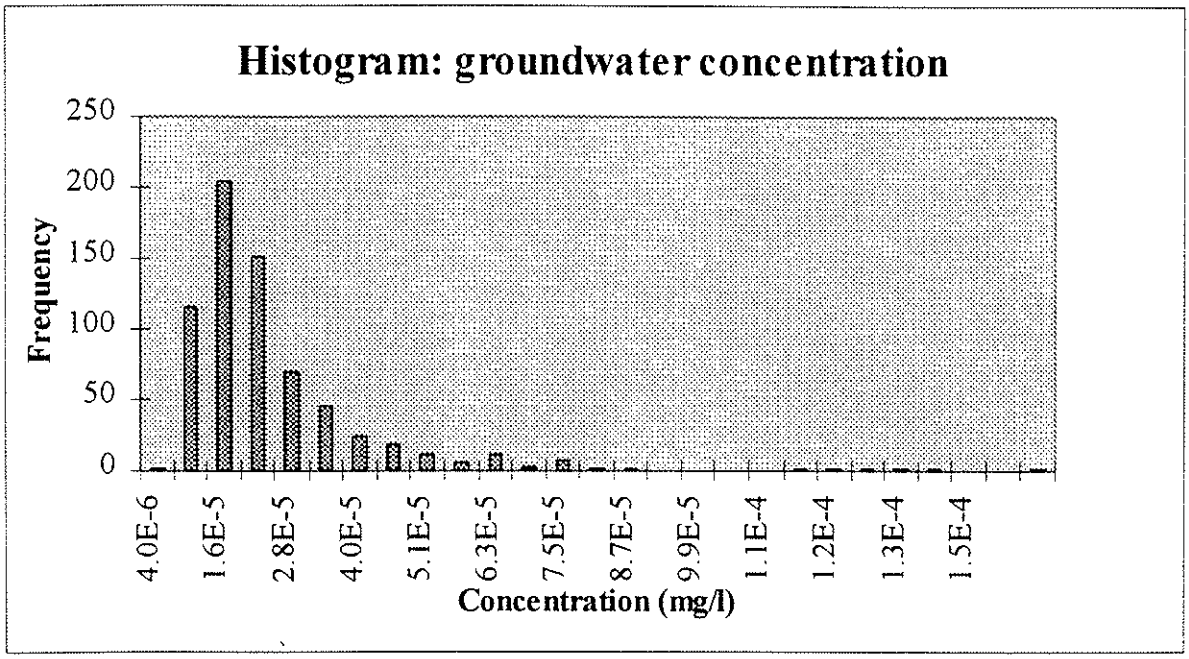

Figure 5.5 Concentration histogram as a result of variable adsorption parameter.

5.4.1 Effect of Variable Adsorption

When partition coefficients are considered random with Gaussian distributions, the predicted Simazine concentrations exhibited a skewed distribution, as shown in Figure 5.5. Because the partition coefficient attains only positive values, generated negative values are discarded. This operation, however, may not preserve normality under certain values of the coefficient of variation for the parameter. Lognormally-distributed parameters would have been an alternative to avoid negative values; however, experimental results suggest that the parameters' variability may be described by a Gaussian distribution. Figures 5.6 and 5.7 show the confidence intervals for predictions of Simazine concentrations as a function of time, thus, highlighting the importance of considering the variability and unknown nature of adsorption process in the assessment of subsurface water contamination. The calculated probability density function for the predicted Simazine concentrations is clearly not Gaussian; it is skewed in favor of smaller concentrations (Figure 5.5). Figures 5.6 and 5.7 show that standard deviations, which are measures of uncertainty of the mean of the concentrations, are on the order of the magnitude of the means (note that the ensemble mean is calculated from the sample average of the Monte Carlo simulations). Thus, it appears that spatial variability of adsorption leads to a significant uncertainty in the predicted mean of Simazine concentrations. The oscillating behavior of the estimated standard deviations reflects the seasonal effect of net infiltration below the root zone, especially during seasons of high precipitation. Such oscillating pattern is less pronounced in groundwater; however, the standard deviations of the predicted concentrations remain significant (Figure 5.7).

A shortcoming in the results is that excess irrigation water, which infiltrates below the root zone and recharges the water table, is not accounted for in the analysis. Because we are making predictions, future irrigation demand is assumed to be equal to the predicted evapotranspiration. Certainly, this assumption may severely underestimate the role of leaching on the emissions of Simazine to the water table. The net result is overestimation of the residence time and degradation in the soil and, consequently, the underestimation of Simazine concentrations in the vadose zone and groundwater.

5.4.2 Effect of Climatic Variations

The effect of variable rainfall may be appreciated in Figures 5.8 and 5.9. It is important to notice that for a product like Simazine, with peak application in the late fall and winter, the impact of rainfall variation will be more accentuated than for products applied in the spring and summer, a case in which irrigation dominates and the variations are expected to be smaller because of evpotranspiration. Figure 5.10 compares the mean concentrations (M.C.) to predicted concentrations that are based on seasonally-averaged precipitation (i.e., mean parameters; this is equivalent to first-order approximation, in which the mean is assumed to be independent of the variability). Notice that averaging precipitation results in overestimating, in most part, the mean (M.C.) concentrations in groundwater. Hence, accounting for the temporal variability of the precipitation may be crucial for the assessment of exposure levels of pesticides in groundwater.

5.4.3 Effect of Preferential Flow

Preferential flow effects are assessed, assuming we know the mean residence time when preferential flow is dominating. For this purpose, the amount of pesticide is mixed during a

season of length of one month. Figures 5.11 and 5.12 show how the dose of Simazine reaching the water table may increase by a factor of, at least, three (Cu and Su denote the mean and standard deviation of concentrations in the vadose zone, respectively, and Cg and Sg denote the mean and standard deviation of concentrations in groundwater, respectively). Figure 5.12 compares the mean concentrations (M.C.) in groundwater, which are based on synthesizing random and independent sequences of seasonally-aggregated precipitation, to the predicted concentrations that are based on the preferential flow scenario. We should emphasize that preferential flow is not accounted for herein on a firm physical background. Rather, preferential flow is accounted, in an average sense, by assuming that mixing in soil occurs during a one-month period, which is shorter than the duration of one season (approximately, 3 months). In this case, the residence time in the soil is smaller, a condition which favors smaller losses by degradation. Thus, the net effect is increased Simazine concentrations in groundwater, as Figure 5.12 indicates. Thus, ignoring preferential flow may lead to gross underestimation of the exposure levels of pesticides in groundwater.

5.5 Summary and Conclusions

A stochastic methodology, using Monte Carlo simulations, is presented for the assessment of long-term exposure levels of pesticides in soils and groundwater. The presented results are useful for regulatory agencies, environmental risk assessment in subsurface water, and quantitative support for existing pesticide management strategies. The presented approach showed several advantages: (1) flexibility to accommodate field information at adequate spatial and time scales; (2) flexibility in representing water balance and water residence times in the

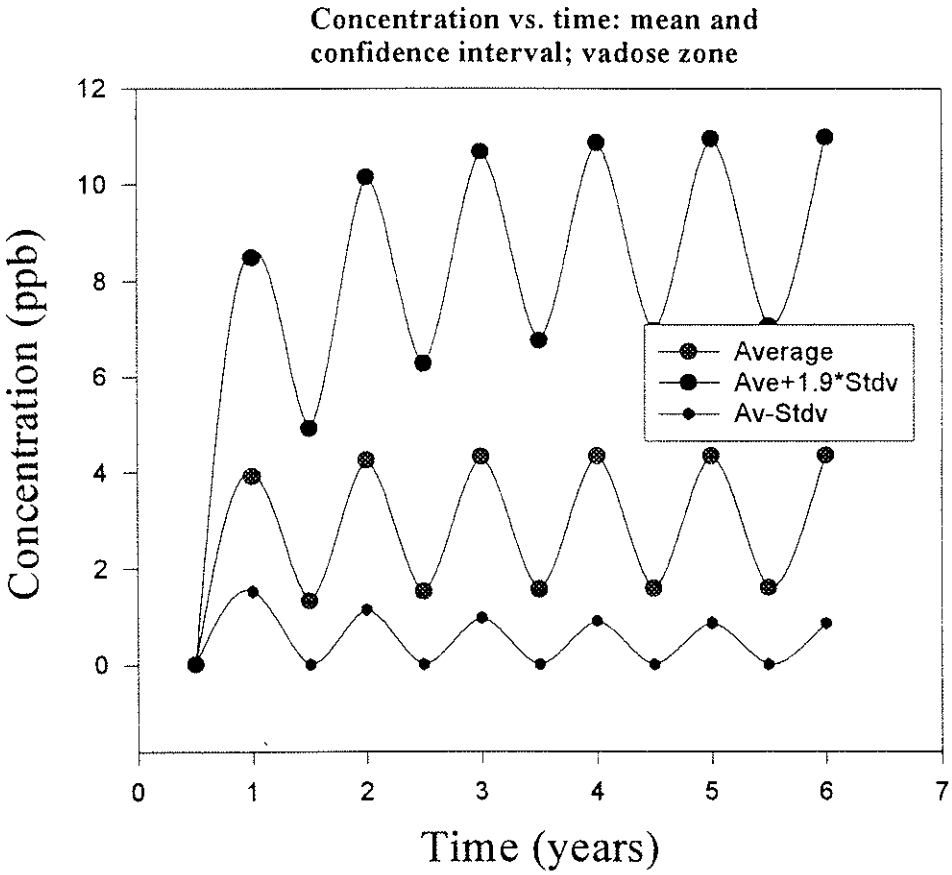

Figure 5.6 Mean and standard deviation of simazine concentrations in the vadose zone (random adsorption).

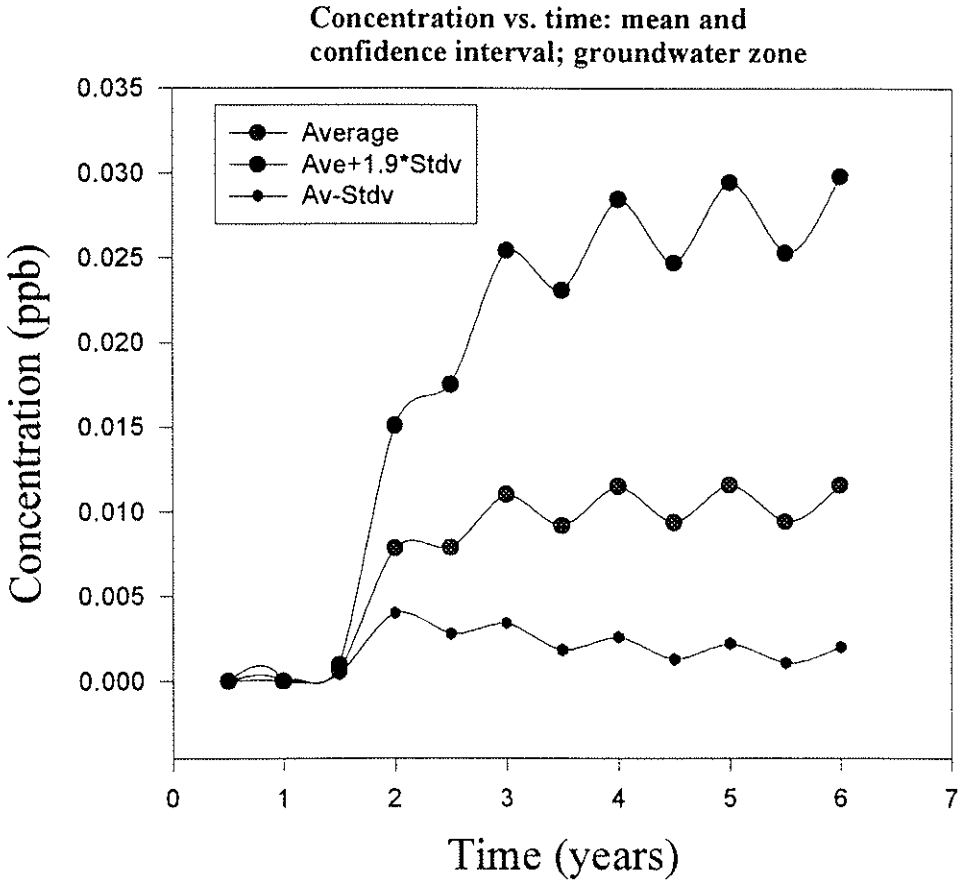

Figure 5.7 Mean and standard deviation of simazine concentrations in groundwater (random adsorption).

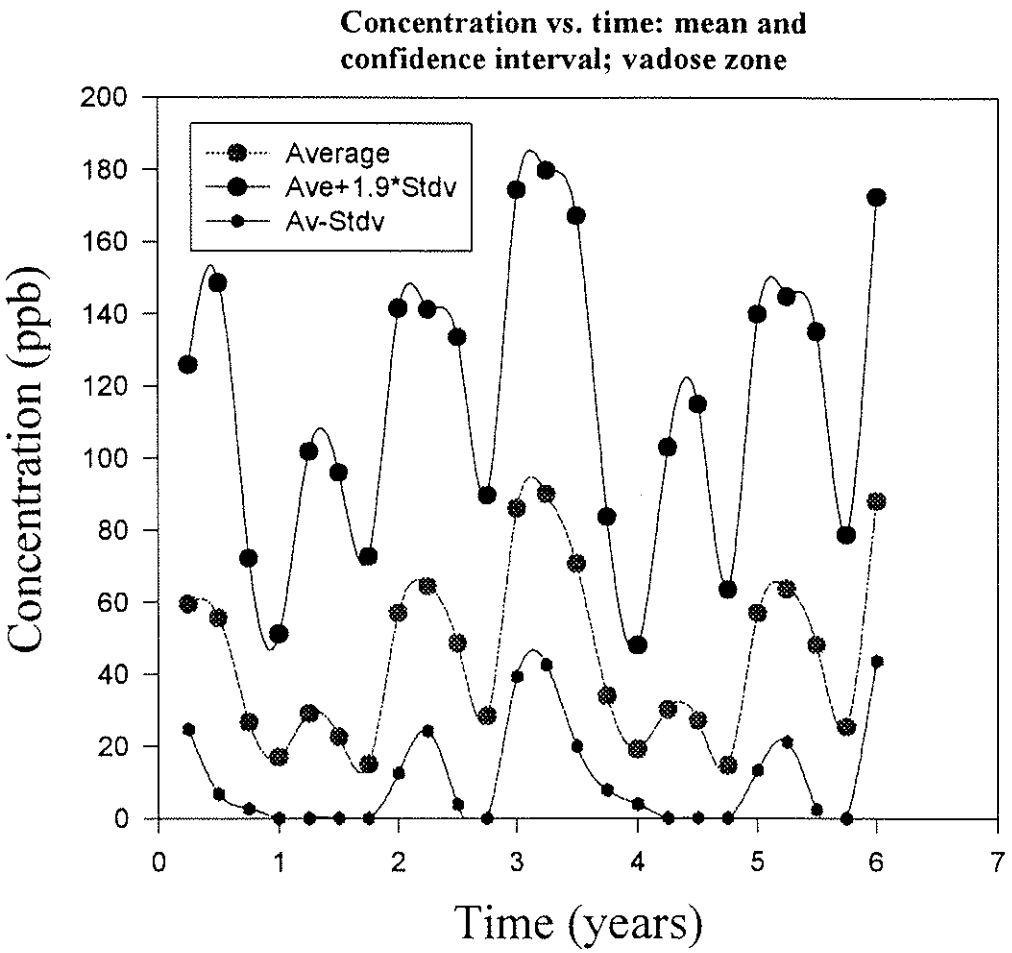

Figure 5.8 Mean and standard deviation of simazine concentrations in the vadose zone due to climatic variability.

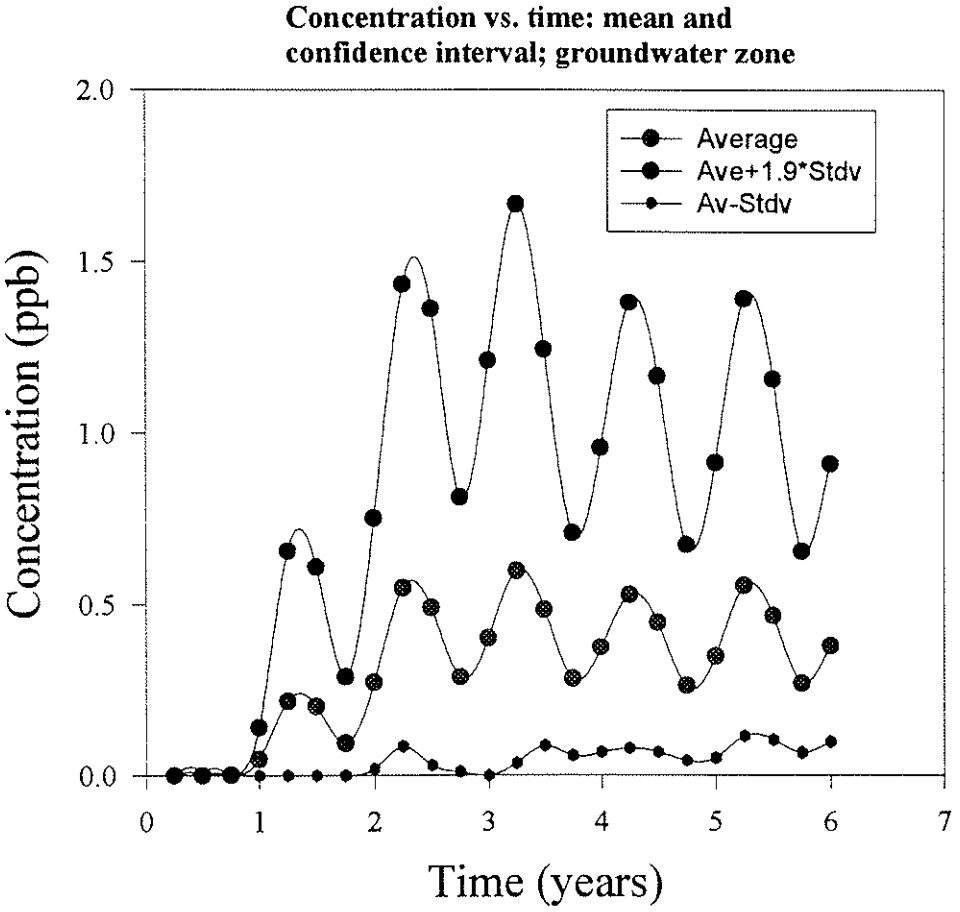

Figure 5.9 Mean and standard deviation of simazine concentrations in groundwater due to climatic variability.

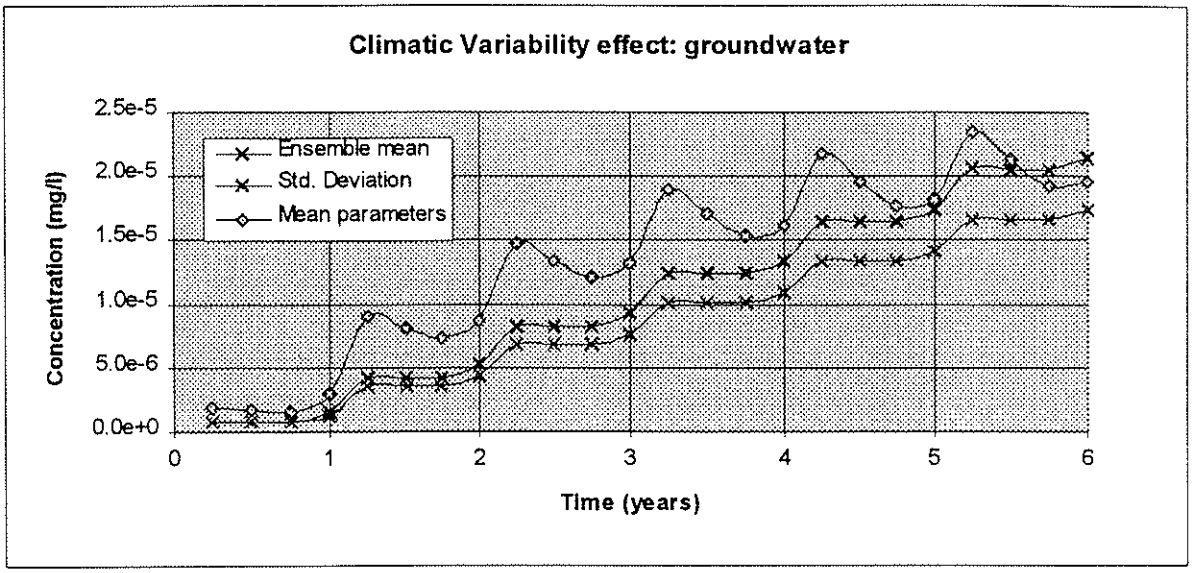

Figure 5.10 Mean concentrations in groundwater based on Monte Carlo simulations (ensemble average) and based on average input parameters (first-order approximation), and standard deviations due to climatic variations.

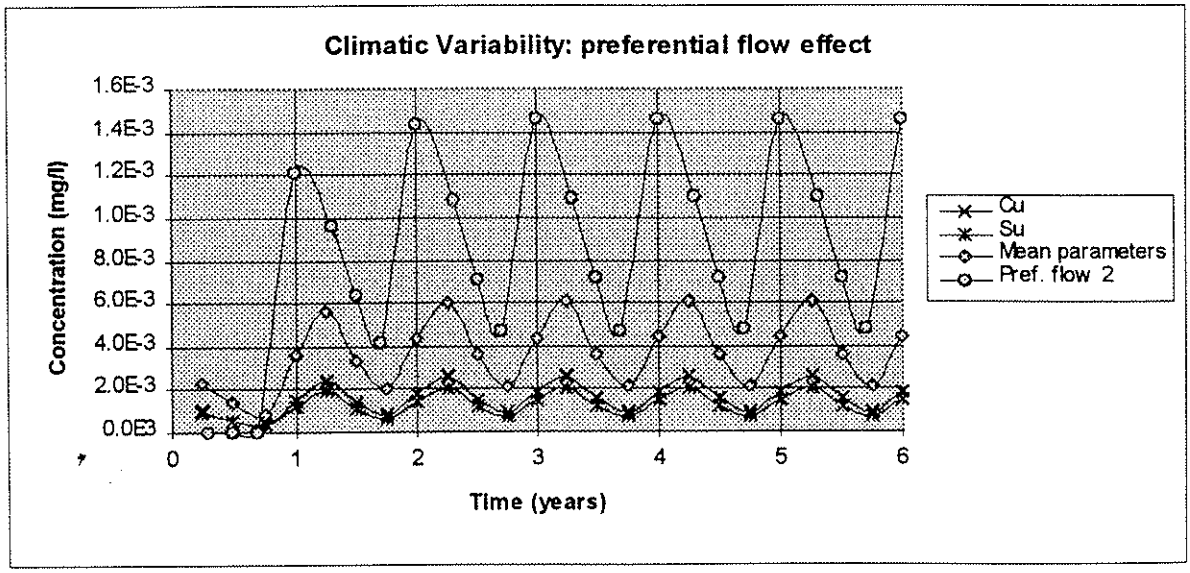

Figure 5.11 Effects of preferential flow on simazine concentrations in the vadose zone.

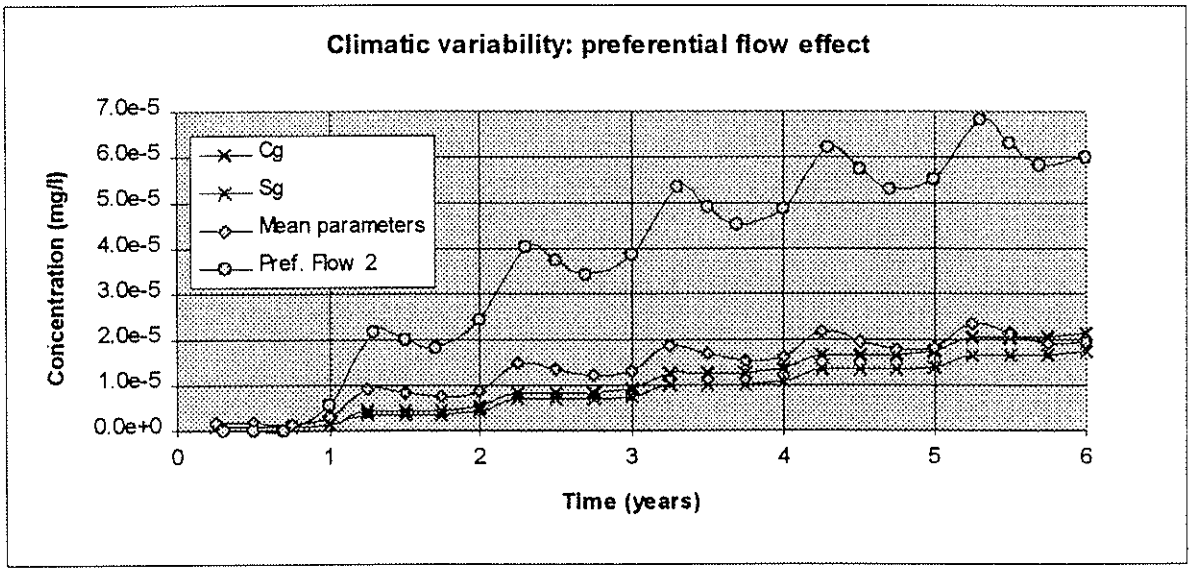

Figure 5.12 Effects of preferential flow on simazine concentrations in groundwater.

system; and (3) the representation of the output as probability density functions for the predicted contaminant concentrations.

The incorporation of uncertainty in the adsorption parameter and precipitation, for the prediction of concentrations, showed to be important in a heterogeneous environment that is subject to climatic variability. The estimated wide confidence intervals (relative to the mean), using Monte Carlo simulations, indicated how the Simazine concentrations in the soil and groundwater are significantly influenced by temporal and spatial variations of the input parameters. Even for sites with similar soil and groundwater characteristics, the climatic variability may play an important role in the mass of contaminant present in the groundwater.

Some of the limitations of this approach are: (1) mixing models do not consider dispersion in the root and vadose zones (this may be a reasonable assumption under rapid infiltration and when the horizontal scale is much larger than the vertical scale in soils); and (2) the approach ignores variations at small-time scales and it is not expected to give accurate results in such cases (assumption of total mixing).

When comparing point equations that require numerical approaches (e.g., Richards equation) with spatially averaged schemes (e.g., mixing models here), we may appreciate the advantages at the computational level and in the practical aspects of the assessment process: (1) executing a numerical simulation at the regional scale involves a rather complex task in parameters' estimation; (2) even when parameters are estimated for the numerically-rigorous models, incorporation of random parameters brings about new difficulties such as convergence and time requirements; and (3) the present approach may be easily incorporated to a smaller

database or geographical information system (GIS), and be refined as more information becomes available.

The model was applied to data that are typical to the Fresno area in California. The results showed: (1) the predicted concentration probability distributions were not Gaussian (asymmetric or skewed) and exhibited values in the same range of values of field-measured values (*Bonilla*, 1996); (2) a quasi-steady state, or a dynamic equilibrium, for the long-term predictions of Simazine concentrations, where seasonal variations are dominated by the driving rainfall/infiltration processes; (3) the predictions made on the basis of averaged values of the properties, lead to a substantial underestimation, and later overestimation, of the dominant (mean) behavior of the contaminant levels in groundwater; and (4) on the basis of application to an area of size 200 m × 200 m (4 hectares (ha)), it is expected that under the application practice of 2.34 kg/ha of Simazine, in the fall and winter seasons, exposure levels in groundwater will not increase to alarming levels in the zone most affected by Simazine concentrations. However, this may not be the conclusion for greater application areas and for a significant preferential flow mechanism. When preferential flow dominates, the long-term buildup in Simazine concentrations may significantly exceed the levels predicted by models that ignore such a mechanism.

CHAPTER 6

RECOMMENDATIONS AND IMPLICATIONS

Acknowledging the assumptions on which the research results are based, we make the following recommendations, to improve prediction capabilities and to suggest scientific and practical guidelines, with the objective of protecting groundwater beforehand from hazardous chemicals:

1. Modeling techniques for aquifer decontamination by pumping may consider equations (2.45)-(2.50) as governing transport equations for reactive solutes in aquifers that contain a significant volume of low-permeability material.
2. Pump-and-treat remediation strategies are often prolonged by the fact that part of the contaminant plume is sorbed into layers of stagnant water and released back slowly into regions that are accessible to flow. Hence, prolonged but less vigorous pumping may be needed.
3. Future research should also explore the development of an effective rate coefficient of mass transfer, which describes, on average, the global capacitance effect of low-permeability zones of an entire formation. The rational approach is a stochastic one, which relates the formation-scale or effective mass transfer rate coefficient to the smaller-scale ones that are estimated on the basis of local measurements and equations (2.45)-(2.48). Aquifer remediation by pumping will benefit considerably from models that consider the spatial variability of mass transfer rate coefficients.

4. Crop-root uptake and volatilization of pesticides from soil surface are important natural loss pathways; hence, they must be accounted for in prediction models.
5. Growing crops on a clayey/silty soil environment poses less risk to groundwater quality than a sandy soil environment. The former is less conductive and favors more losses of the pesticides by (bio)chemical degradation and volatilization.
6. The role of crop-root uptake as a natural loss pathway highlights the role of agro-forestry systems when it comes to the problem of groundwater salinity.
7. (Bio)chemically degradable, volatile, and immobile pesticides (e.g., Atrazine and Heptachlor) are least threatening to long-term groundwater quality; hence, they are recommended, especially, when the soil environment is predominantly sand. On the other hand, groundwater is vulnerable on a long-term basis to persisting (slowly degradable and nonvolatile) and mobile pesticides (e.g., Bromacil and Lindane) that are applied on a continuous annual basis. Therefore, it is recommended to use the same farm to grow, intermittently, different crops that require less threatening pesticides. This allows more time for the relatively persisting pesticides to degrade naturally to acceptable levels before they are applied again.
8. In shallow-water table aquifers, rapid infiltration and continuous application may increase vulnerability of groundwater to mobile pesticides (e.g., Atrazine and Bromacil). In this case, one of the following actions may be recommended: (1) installing drains to intercept the leachate; and (2) changing the agricultural practice, whenever possible, by growing during a wet season. In the latter action, increasing portions of consumption by crops can be met by the infiltrating rain; thus, reducing the net infiltration below the root zone and allowing more

time for losses by degradation, volatilization, and root uptake. The net effect is reduced emission of the pesticides to the water table.

9. Because some pesticides undergo natural decay, increasing their residence time in the soil favors more losses. Increasing the residence time, besides installing drains, can also be achieved by lowering the water table below agricultural fields via pumping, and storing the water or recharging it back to the aquifer, somewhere else.
10. The spatial variability of the retardation factor, the decay rate coefficient, and the temporal variability of the precipitation, must be accounted for when making predictions using transport models. Predictions made on the basis of average values of the properties, may lead to a substantial underestimation or overestimation of the actual dominant (ensemble mean) behavior of the contaminant levels in groundwater. Transport models that ignore the mechanism of preferential flow may seriously underestimate exposure levels of chemicals in groundwater, especially during periods of high precipitation. Future research should develop more physically-based concepts for describing preferential flow, as it occurs under field conditions.

REFERENCES

Baker, L. E. 1977. Effects of dispersion and dead-end pore volume in miscible flooding. Soc. Petrol. Eng. J., 7, 219-227.

Bear, J. 1972. Dynamics of Fluids in Porous Media. Elsevier, New york, 764 p.

Bear, J. 1977. On the aquifer's integrated balance equations. Adv. in Water Resour., 1(1), 15-24.

Bear, J. 1979. Hydraulics of Groundwater. McGraw-Hill Inc., 567 p.

Beltman, W. H. J., J. J. T. I. Boesten, and S. E. A. T. M. Van der Zee. 1995. Analytical modelling of pesticide transport from the soil surface to a drinking water well. J. Hydrol., 169, 209-228.

Bennet, A., and F. Goodridge. 1970. Hydrodynamics and mass transfer studies in packed adsorption columns: 1. Axial liquid dispersion. Trans. Int. Chem. Eng., 48, 232-244.

Boesten, J. J. T. I., and A. M. A. Van der Linden. 1991. Modeling the influence of sorption and transformation on pesticide leaching and persistence. J. Environ. Qual., 20, 425-435.

Bond, W. J., and P. J. Wierenga. 1990. Immobile water during solute transport in unsaturated sand columns. Water Resour. Res., 26(10), 2475-2481.

Bonilla, F. A. 1996. *Assessment of pesticide exposure levels in soil and groundwater at the regional scale*. M.S. thesis, Hydrologic Sciences, Department of Land, Air and Water Resources, University of California, Davis, California.

Briggs, G. G., R. H. Bromilow, and A. A. Evans. 1982. Relationship between lipophilicity and root uptake and translocation of non-ionised chemicals by Barley. Pestic. Sci , 13, 495-504.

Carnahan, C. L., and J. S. Remer. 1984. Nonequilibrium and equilibrium sorption with a linear sorption isotherm during mass transport through an infinite porous medium: Some analytical solutions. J. Hydrol., 73, 227-258.

Cayan, D. R., and B. C. Weare. 1977. Some aspects of recent climatic variability in Davis, California. Contributions in atmospheric science No. 14, University of California-Davis.

Chow, V. T., Maidment, D. R., and Mays, L.W. 1988. Applied Hydrology. McGraw-Hill, Inc.

Coats, K. H., and B. D. Smith. 1964. Dead-end pore volume and dispersion in porous media. Soc. Pet. Eng. J., 73-84.

Cohen, S. Z., S. M. Creeger, R. F. Carsel, and C. G. Enfield. 1984. Potential for pesticide contamination of groundwater resulting from agricultural uses. Page 297-325 in R. F. Kruger and J. N. Sieber (eds.), Treatment and disposal of pesticide wastes. ACS Symposium Series No. 259, American Chemical Association, Washington, DC.

Cohen, D.B., 1986. Groundwater contamination by toxic substances: A California assessment. in Garner, W.Y., and others, ds., Evaluation of pesticides in ground water: American Chemical Society Symposium Series 315, p. 499-529.

Dagan, G. 1984. Solute transport in heterogeneous porous formations. J. Fluid Mech. , 145, 151-177.

De Smedt, F., and P. J. Wierenga. 1984. Solute transfer through columns of glass beads. Water Resour. Res., 20, 225-232.